HOKKAIDO UNIVERSITY

Title	Advanced jig separation for resources recycling: effects of particle geometry on separation efficiency and development of continuous-type jig using restraining wall
Author(s)	Phengsaart, Theerayut
Citation	北海道大学. 博士(工学) 甲第13801号
Issue Date	2019-09-25
DOI	10.14943/doctoral.k13801
Doc URL	http://hdl.handle.net/2115/79290
Type	theses (doctoral)
File Information	Theerayut_Phengsaart.pdf

Instructions for use

Hokkaido University Collection of Scholarly and Academic Papers : HUSCAP

Doctoral Thesis

Advanced Jig Separation for Resources Recycling: Effects of Particle Geometry on Separation Efficiency and Development of Continuous-type Jig Using Restraining Wall

A dissertation submitted in partial fulfillment of the requirements for the degree of Doctorate in Engineering

by

THEERAYUT PHENGSAART

Laboratory of Mineral Processing and Resources Recycling,
Division of Sustainable Resources Engineering,
Graduate School of Engineering,
Hokkaido University, Japan
September 2019

Abstract

There are two common types of plastic recycling: (1) material recycling wherein plastics are recovered and reused, and (2) thermal recycling whereby plastics are used as fuel for power generation. Among the two, material recycling is a more sustainable and profitable approach, but different types of plastics must be separated to obtain very high purities. Most separation techniques for recycling were modified from techniques developed for mineral processing. Among of these techniques, jig separation, one of the oldest techniques that separates particles based on density differences, that is widely used in mineral processing especially in coal cleaning because of its simplicity, low cost, and high efficiency, was also applied for resources recycling. However, there is a critical challenge in the use of jig separation for secondary resources because of the wide variety of shapes formed after crushing, which is very different from the more uniform and sphere-like particles traditionally treated in mineral processing. In jig separation, the separation efficiency is dependent on particle motion, which is also a function of geometrical properties like size and shape. This means that understanding the effects of particle shape is important in the design of suitable jig separation process. This study investigated the effects of particle shape (disk-like plastics and rod-like metals wires) on the jig separation and identified the reasons why the particles shape affects to their behaviors and jig separation efficiency. Moreover, novel methods to estimate the jig separation efficiency using shape factors were proposed and modified waveform and shape separation methods to improve jig separation efficiency were developed. Finally, a discharge system for continuous jig separation of plastics using a restraining wall was developed.

Chapter 1 describes the background and objectives of the study.

In Chapter 2, previous studies on “the effects of particle geometry on physical separation” and “the application of gravity separation for coal cleaning and resources recycling” are reviewed.

In Chapter 3, effects of particle geometry (size and shape) on jig separation efficiency of crushed plastics are investigated. The shape factors (flatness ratio etc.) and settling velocity of crushed plastics containing various size and shape were measured and the results showed that particles are more disk-like at coarser size fraction while the fine fraction is dominated by sphere-like particles. The results of jig separation of mixed plastics showed that separation efficiency was higher for the mixture of light, disk-like particles and heavy, sphere-like particles that was in line with the results of settling velocity experiments. These results indicate that settling velocity and jig separation are affected by both size and shape.

In Chapter 4, empirical equation to calculate settling velocity of non-spherical particles using

flatness ratio and projection area was developed, and a modified concentration criterion (CC_s) is proposed to estimate jig separation efficiency of non-spherical particles. The experimental results showed that sharpness index decreased with increasing CC_s calculated from the velocity of non-spherical particles. This result indicates that CC_s can be used to estimate jig separation efficiency of non-spherical particles. Based on the CC_s proposed here it was hypothesized that separation efficiency of the mixture of light, sphere-like particles and heavy, disk-like particles will be improved when the water rising velocity increase. This hypothesis was confirmed by the jig separation of the mixed plastic samples.

In Chapter 5, separation of rod-like and sphere-like particles are discussed. Jig separation was applied to separate plastics and metals including copper (Cu) wires obtained from a recycling plant. The results showed that separation efficiency was low because of Cu wire entanglement that prevents particle motion in the separation chamber. The results of model experiments showed that the separation efficiency decreased with increasing the amount and length of Cu wires. To limit the effects of wire entanglement, two methods of shape separation were investigated. In addition, estimation of jig separation efficiency using the entanglement factor of rod-like particles is proposed.

In Chapter 6, discharge systems for continuous jig separation of plastics are discussed. The purity of bottom layer products becomes lower when the heavy particles ratio in feed is low, because entrainment of light particles by a screw-extractor occurs. To suppress the entrainment, a new discharge system using a vertical restraining wall was developed. The restraining wall was installed to separate a chamber into two and particles can transfer from one to another through the channel under the wall. The results showed that purity of bottom layer products was improved with a restraining wall.

Finally, Chapter 7 gives the general conclusions of this study.

Table of Contents

CHAPTER 1 – GENERAL INTRODUCTION

1.1 Background

Increasing demand for mineral resources and higher waste generation due to rapid population growth are fast becoming critical problems of majority of countries around the world. One of the most important approach to address these concerns is recycling because it not only lessens our dependence on natural mineral resources but also reduces the volume of wastes for disposal. The United Nations, for example, included recycling as a key strategy in their sustainable development goals (SDGs) (United Nations Department of Public Information, 2019). Among of the generated wastes, plastic is one of big amount waste rather than traditional materials like glass, metals and wood, especially when compared in volume-based due to their low specific gravity (SG) (Tsiamis et al., 2018).

Plastics are unique because their physical properties like toughness, hardness or flexibility can be engineered by either using various types of organic molecules or combining plastic resins with other types of materials like graphite or fiber glass. Plastics are found in cars, electronics, home appliances, and packaging materials to name a few. Because of its flexibility and favorable properties, the total global production of plastics has grown from around 1.5 million tons in 1950 to 348 million tons in 2017. The world consumption has also been increasing yearly at a rate of 5% with the largest increase reported in Asia especially in China, which is the world leader in terms of plastic production due to the country's low production costs (PlasticsEurope, 2018; Statista, 2019).

In contrast, the Japanese consumption as well as waste generation of plastics have gradually decreased for the past 20 years because of the enactment of recycling laws for "containers and packaging", "home appliances" (i.e., air conditioners, televisions, refrigerators, and washing machines), "automobiles", and "small home appliances" (i.e., personal computers, mobile phones, digital cameras and clocks, game consoles, music players, and hair dryers) in 1995, 1998, 2002, and 2012, respectively (Ministry of the Environment of Japan, 2014; Plastic Waste Management Institute of Japan, 2018).

There are two common types of plastic recycling: (1) material recycling wherein plastics are recovered and reused, and (2) thermal recycling whereby plastics are used as fuel for power generation. Thermal recycling is more widely used to manage plastic wastes than material recycling. Because plastics are primarily composed of carbon, they are good sources of energy for electric power generation plants. Some plastics like polyvinyl chloride (PVC), however, are unsuitable for thermal recycling because they contain additives that have adverse effects to the refractory materials used in boilers like chloride (Cl^-) and should be separated prior to thermal recycling (Kikuchi et al., 2008,

Kuwayama et al., 2011). Although more profitable and sustainable, applications of material recycling to plastic wastes remain limited because of the challenges and difficulties of efficiently separating the various types of plastics to generate products with very high purities. This means that plastic-plastic separation techniques should be developed or improved for both thermal and material recycling (Choi et al., 2018).

Recently, the Japanese government is planning to increase the material recycling ratio for combustible materials like plastics and reduce the amounts that end up for thermal recovery. For example, the Ministry of Environment of Japan supported verification tests to improve material recycling including plastic-plastic separation from automobile shredded residue (ASR) (Ministry of Environment of Japan, 2018).

In 2016, for example, about 9 million tons (roughly 84% of the total amount of plastic wastes) was recycled in Japan, 58 and 23% of which went to thermal and material recycling, respectively while the remaining 19% were disposed to landfills (Plastic Waste Management Institute of Japan, 2018). They are treated domestically for material and thermal recycling or exported to other countries for recycling. In 2016, for example, about half of the world's plastic wastes including Japan were exported for recycling and most of them ended up in China (about 7 million tons of plastic wastes). Since 2017, however, China has banned the importation of 24 kinds of foreign wastes including plastics (Reuter, 2018a). Because China is no longer the main player in the global recycling of plastic wastes, big waste exporters such as the US, UK, and Japan are scrambling to find alternative ways to manage their plastic wastes. One alternative is the offloading of their plastic wastes to developing nations in South East Asia but in recent years, Malaysia, Vietnam and Thailand have also started the cancellation of importation and processing licenses of plastic wastes (Reuter, 2018b). These recent bans mean that plastic waste exporting countries have to develop recycling systems of their own and limit their reliance on other developed and also developing countries.

In recent years, several studies have utilized mineral processing techniques to separate mixed-plastic wastes into their individual components (e.g., gravity separation (Ferrara et al., 2000; Hori et al., 2009a, 2009b; Ito et al., 2010; Kuwayama et al., 2011; Pita and Castilho, 2016; Tsunekawa et al., 2005, 2012), dense medium separation (Ferrara et al., 2000; Richard et al., 2011; Pongstabodee et al., 2008), electrical separation (Dodbiba et al., 2003, 2005; Gente et al., 2003), flotation (Burat et al., 2009; Dodbiba et al., 2002; Fraunholcz, 2004; Güney et al., 2015; Marques and Tenório, 2000; Pita and Castilho, 2017; Pongstabodee et al., 2008; Saisinchai, 2014; Shent et al., 1999; Shibata et al., 1996; Takoungsakdakun and Pongstabodee, 2007; Wang et al., 2014, 2015)).

Among of these techniques, jig separation, one of the oldest techniques that separates particles based on density differences, that is widely used in mineral processing especially in coal cleaning

because of its simplicity, low cost, and high efficiency, was also applied for resources recycling.

In recent years, rapid development in science and technology as well as the growing appetite of consumer for many electronic devices as lifestyle products have caused a surge in demands for natural resources (e.g., metals) and generation of wastes, which poses serious problems to the future of our modern society. Among the many types of wastes, generation of waste electrical and electronic equipment (WEEE) is one of the fastest growing worldwide. Every year, 20-50 million tons of WEEE are generated and is estimated to increase annually at a rate of around 3-5% (three time faster than other forms of municipal solid waste (MSW)), which could be attributed to the reduction of average lifetimes of many electronic products (Huang et al., 2009; Tesfaye et al., 2017; Tuncuk et al, 2012). Because of this, recycling of WEEE that contain various valuable materials using techniques like physical separation (e.g., gravity separation and flotation) and hydrometallurgy have become important industries in many developing and developed countries (Havlik et al, 2014; Lambert et al, 2015; Mäkinen et al, 2015; Tesfaye et al., 2017; Tuncuk et al, 2012).

However, there is a critical challenge in the use of jig separation for secondary resources because of the wide variety of shapes formed after crushing, which is very different from the more uniform and sphere-like particles traditionally treated in coal cleaning and mineral processing (Beunder, 2000). Since fine grinding (-100 μm) is typically required to liberate chalcopyrite from its ores prior to flotation, so the bulk of material for processing have sphere-like shapes. In contrast, wastes especially those containing plastics are commonly crushed to obtain coarse particles (mm to cm), so the material for processing is a mixture of different types of plastics with a variety of shapes (Beunder, 2000). For examples, waste electrical and electronic equipment (WEEE) contains particles with shapes ranging from rod-like (e.g., wires) to blade-like (e.g., large, flattened wires, wood and metallic plates) and disk-like (e.g., plastics and metallic plates) to sphere-like (e.g., plastics and ceramics) (Jeon et al., 2018a, 2018b, 2019). In jig separation, the separation efficiency is dependent on particle motion, which is also a function of geometrical properties like size and shape. This means that understanding the effects of particle shape is important in the design of suitable jig separation process.

This study investigated the effects of particle shape (disk-like plastics and rod-like metals wires) on the jig separation and identified the reasons why the particles shape affects to their behaviors and jig separation efficiency. Moreover, novel methods to estimate the jig separation efficiency using shape factors were proposed and modified waveform and shape separation methods to improve jig separation efficiency were developed. Finally, a discharge system for continuous jig separation of plastics using a restraining wall was developed.

1.2 Outline of the dissertation

This dissertation is composed of seven chapters. The key contents of each chapter are outlined as

follows:

Chapter 1 describes the general introduction including background, statement of the problem and outline of the dissertation.

Chapter 2 reviews previous studies on “the effects of particle geometry on physical separation” and “the application of gravity separation for coal cleaning and resources recycling”.

Chapter 3 investigated the effects of particle geometry on jig separation efficiency of crushed plastics.

Chapter 4 proposes the improvement of jig efficiency by modified water pulsation and novel methods to estimate the of separation efficiency and settling velocity of crushed plastics using geometrical parameters.

Chapter 5 proposes the improvement of jig efficiency by shape separation and novel methods to estimate the of separation efficiency using the entanglement factor.

Chapter 6 discusses the discharge systems for continuous jig separation of plastics.

Chapter 7 gives the general conclusion of the dissertation.

References

Beunder, E.M., 2000. Influence of shape on particle behaviour in recycling techniques. Thesis (PhD), Delft University of Technology, Netherlands.

Burat, F., Güney, A., Olgaç Kangal, M., 2009. Selective separation of virgin and post-consumer polymers (PET and PVC) by flotation method. Waste Manag. 29, 1807–1813. https://doi.org/10.1016/j.wasman.2008.12.018

Choi, C., Choi, H.J., Rhee S.W., 2018. Current status and improvements on management of plastic waste in Korea, J. Korean Inst. Resources Recycling. 27, 3-15. https://doi.org/10.7844/kirr.2018.27.4.3

Dodbiba, G., Haruki, N., Shibayama, A., Miyazaki, T., Fujita, T., 2002. Combination of sink–float separation and flotation technique for purification of shredded PET-bottle from PE or PP flakes. Int. J. Miner. Process. 65, 11–29. https://doi.org/10.1016/S0301-7516(01)00056-4

Dodbiba, G., Shibayama, A., Sadaki, J., Fujita, T., 2003. Combination of triboelectrostatic separation and air tabling for sorting plastics from a multi-component plastic mixture. Mater. Trans. 44, 2427–2435. https://doi.org/10.2320/matertrans.44.2427

Dodbiba, G., Sadaki, J., Okaya, K., Shibayama, A., Fujita, T., 2005. The use of air tabling and triboelectric separation for separating a mixture of three plastics. Miner. Eng. 18, 1350–1360. https://doi.org/10.1016/j.mineng.2005.02.015

Ferrara, G., Bevilacqua, P., De Lorenzi, L., Zanin, M., 2000. The influence of particle shape on the dynamic dense medium separation of plastics. Int. J. Miner. Process. 59, 225–235. https://doi.org/10.1016/S0301-7516(99)00078-2

Fraunholcz, N., 2004. Separation of waste plastics by froth flotation—a review, part I. Miner. Eng. 17, 261–268. https://doi.org/10.1016/j.mineng.2003.10.028

Gente, V., La Marca, F., Lucci, F., Massacci, P., 2003. Electrical separation of plastics coming from special waste. Waste Manag. 23, 951–958. https://doi.org/10.1016/S0956-053X(03)00088-6

Güney, A., Özdilek, C., Kangal, M.O., Burat, F., 2015. Flotation characterization of PET and PVC in the presence of different plasticizers. Sep. Purif. Technol. 151, 47–56. https://doi.org/10.1016/j.seppur.2015.07.027

Havlik, T., Orac, D., Berwanger, M., Maul, A., 2014. The effect of mechanical–physical pretreatment on hydrometallurgical extraction of copper and tin in residue from printed circuit boards from used consumer equipment. Miner. Eng. 65, 163–171. https://doi.org/10.1016/j.mineng.2014.06.004

Hori, K., Tsunekawa, M., Hiroyoshi, N., Ito, M., 2009a. Optimum water pulsation of jig separation for crushed plastic particles. Int. J. Miner. Process. 92, 103–108. https://doi.org/10.1016/j.minpro.2009.01.001

Hori, K., Tsunekawa, M., Ueda, M., Hiroyoshi, N., Ito, M., Okada, H., 2009b. Development of a new gravity separator for plastics —a hybrid-jig—. Mater. Trans. 50, 2844–2847. https://doi.org/10.2320/matertrans.M-M2009825

Huang, K., Guo, J., Xu, Z., 2009. Recycling of waste printed circuit boards: A review of current technologies and treatment status in China. J. Hazard. Mater. 164, 399–408. https://doi.org/10.1016/j.jhazmat.2008.08.051

Ito, M., Tsunekawa, M., Ishida, E., Kawai, K., Takahashi, T., Abe, N., Hiroyoshi, N., 2010. Reverse jig separation of shredded floating plastics — separation of polypropylene and high density polyethylene. Int. J. Miner. Process. 97, 96–99. https://doi.org/10.1016/j.minpro.2010.08.007

Jeon, S., Tabelin, C.B., Takahashi, H., Park, I., Ito, M., Hiroyoshi, N., 2018a. Interference of coexisting copper and aluminum on the ammonium thiosulfate leaching of gold from printed circuit boards of waste mobile phones. Waste Manage. 81, 148-156. https://doi.org/10.1016/j.wasman.2018.09.041

Jeon, S., Ito, M., Tabelin, C.B., Pongsumrankul, R., Kitajima, N., Park, I., Hiroyoshi, N., 2018b. Gold recovery from shredder light fraction of E-waste recycling plant by flotation-ammonium

thiosulfate leaching. Waste Manage. 77, 195-202. https://doi.org/10.1016/j.wasman.2018.04.039

Jeon, S., Ito, M., Tabelin, C.B., Pongsumrankul, R., Tanaka, S., Kitajima, N., Saito, A., Park, I., Hiroyoshi, N., 2019. A physical separation scheme to improve ammonium thiosulfate leaching of gold by separation of base metals in crushed mobile phones. Miner. Eng. 138, 168-177. https://doi.org/10.1016/j.mineng.2019.04.025

Kikuchi, R., Kukacka, J., Raschman, R., 2008. Grouping of mixed waste plastics according to chlorine content. Sep. Purif. Technol. 61, 75–81. https://doi.org/10.1016/j.seppur.2007.10.001

Kuwayama, Y., Ito, M., Hiroyoshi, N., Tsunekawa, M., 2011. Jig separation of crushed automobile shredded residue and its evaluation by float and sink analysis. J. Mater. Cycles. Waste Manag. 13, 240–246. https://doi.org/10.1007/s10163-011-0008-y

Lambert, F., Gaydardzhiev, S., Léonard, G., Lewis, G., Bareel, P.F., Bastin, D., 2015. Copper leaching from waste electric cables by biohydrometallurgy. Miner. Eng. 76, 38–46. https://doi.org/10.1016/j.mineng.2014.12.029

Mäkinen, J., Bachér, J., Kaartinen, T., Wahlström, M., Salminen, J., 2015. The effect of flotation and parameters for bioleaching of printed circuit boards. Miner. Eng. 75, 26–31. https://doi.org/10.1016/j.mineng.2015.01.009

Marques, G.A., Tenório, J.A.S., 2000. Use of froth flotation to separate PVC/PET mixtures. Waste Manag. 20, 265–269. https://doi.org/10.1016/S0956-053X(99)00333-5

Ministry of the Environment of Japan, 2014. History and current state of waste management in Japan. https://www.env.go.jp/en/recycle/smcs/attach/hcswm.pdf (accessed 25 December 2017)

Ministry of the Environment of Japan, 2018. Promotion of 3R of ASR. http://www.env.go.jp/recycle/car/material5.html (accessed 31 August 2018).

Pita, F., Castilho, A., 2016. Influence of shape and size of the particles on jigging separation of plastics mixture. Waste. Manage. 48, 89-94. https://doi.org/10.1016/j.wasman.2015.10.034.

Pita, F., Castilho, A., 2017. Separation of plastics by froth flotation. The role of size, shape and density of the particles. Waste Manag. 60, 91–99. https://doi.org/10.1016/j.wasman.2016.07.041

PlasticsEurope, 2018. Plastics - the Facts 2018. An Analysis of European Plastics Production, Demand and Waste Data, https://www.plasticseurope.org/application/files/6315/4510/9658/Plastics_the_facts_2018_AF_web.pdf. (accessed 15 May 2019).

Plastic Waste Management Institute of Japan, 2018. Current status of production, disposal, recycling, and disposal of plastic products. http://www.pwmi.or.jp/pdf/panf2.pdf. (accessed 7 March 2019).

Pongstabodee, S., Kunachitpimol, N., Damronglerd, S., 2008. Combination of three-stage sink–float method and selective flotation technique for separation of mixed post-consumer plastic waste. Waste Manag. 28, 475–483. https://doi.org/10.1016/j.wasman.2007.03.005

Reuter, 2018a. China's plastic recyclers go abroad as import ban bites. https://www.reuters.com/article/us-china-pollution-waste/chinas-plastic-recyclers-go-abroad-as-import-ban-bites-idUSKBN1JM0L9 (accessed 05 December 2018).

Reuter, 2018b. Thailand to ban imports of high-tech trash, plastic waste. https://uk.reuters.com/article/uk-thailand-environment-waste/thailand-to-ban-imports-of-high-tech-trash-plastic-waste-idUKKBN1L10RN (accessed 05 December 2018).

Richard, M.G., Mario, M., Javier, T., Susana, T., 2011. Optimization of the recovery of plastics for recycling by density media separation cyclones. Resour. Conserv. Recycl. 55, 472–482. https://doi.org/10.1016/j.resconrec.2010.12.010po

Saisinchai, S., 2014. Separation of PVC from PET/PVC mixtures using flotation by calcium lignosulfonate depressant. Eng. J. 18, 45–54. https://doi.org/10.4186/ej.2014.18.1.45

Shent, H., Pugh, R.J., Forssberg, E., 1999. A review of plastics waste recycling and the flotation of plastics. Resour. Conserv. Recycl. 25, 85–109. https://doi.org/10.1016/S0921-3449(98)00017-2

Shibata, J., Matsumoto, S., Yamamoto, H., Kusaka, E., Pradip, 1996. Flotation separation of plastics using selective depressants. Int. J. Miner. Process. 48, 127–134. https://doi.org/10.1016/S0301-7516(96)00021-X

Statista, 2019. Global Plastic Production from 1950 to 2017 (In Million Metric Tons). https://www.statista.com/statistics/282732/global-production-of-plastics-since-1950. (accessed 15 May 2019).

Takoungsakdakun, T., Pongstabodee, S., 2007. Separation of mixed post-consumer PET–POM–PVC plastic waste using selective flotation. Sep. Purif. Technol. 54, 248–252. https://doi.org/10.1016/j.seppur.2006.09.011

Tesfayea, F., Lindberga, D., Hamuyunib, J., Taskinenb, F., Hupa, L., 2017. Improving urban mining practices for optimal recovery of resources from e-waste. Miner. Eng. 111, 209–221. https://doi.org/10.1016/j.mineng.2017.06.018

Tsiamis, D.A., Torres, M., Castaldi, M.J., 2018. Role of plastics in decoupling municipal solid waste and economic growth in the U.S. Waste Manag. 77, 147–155. https://doi.org/10.1016/j.wasman.2018.05.003

Tsunekawa, M., Naoi, B., Ogawa, S., Hori, K., Hiroyoshi, N., Ito, M., Hirajima, T., 2005. Jig separation of plastics from scrapped copy machines. Int. J. Miner. Process. 76, 67–74. https://doi.org/10.1016/j.minpro.2004.12.001

Tsunekawa, M., Kobayashi, R., Hori, K., Okada, H., Abe, N., Hiroyoshi, N., Ito, M., 2012. Newly developed discharge device for jig separation of plastics to recover higher grade bottom layer product. Int. J. Miner. Process. 114–117, 27–29. https://doi.org/10.1016/j.minpro.2012.09.003

Tuncuk, A., Stazi, V., Akcil, A., Yazici, E.Y., Deveci, H., 2012. Aqueous metal recovery techniques from e-scrap: Hydrometallurgy in recycling. Miner. Eng. 25, 28–37. https://doi.org/10.1016/j.mineng.2011.09.019

United Nations Department of Public Information, 2019. Sustainable development goals. https://sustainabledevelopment.un.org/?menu=1300 (accessed 23 February 2019)

Wang, H., Wang, C., Fu, J., Gu, G., 2014. Flotability and flotation separation of polymer materials modulated by wetting agents. Waste Manag. 34, 309–315. https://doi.org/10.1016/j.wasman.2013.11.007

Wang, C., Wang, H., Fu, J., Liu, Y., 2015. Flotation separation of waste plastics for recycling—A review. Waste Manag. 41, 28–38. https://doi.org/10.1016/j.wasman.2015.03.027

CHAPTER 2 – THE LITERATURE REVIEWS ON "THE EFFECTS OF PARTICLE GEOMETRY ON PHYSICAL SEPARATION" AND "THE APPLICATION OF GRAVITY SEPARATION FOR COAL CLEANING AND RESOURCES RECYCLING"

2.1 Introduction

As described in the general introduction (chapter 1), for the future development of existing recycling technologies, a better understanding of the difference between physical separation especially gravity separation of primary and secondary resources is imperative. In this chapter, quantitative expressions of "the effects of particle geometry on physical separation" and "the application of gravity separation for coal cleaning and resources recycling" are reviewed.

2.2 The effects of particle geometry on physical separation: a review

Most physical separation techniques applied for resources recycling were originally designed for mineral processing. In these techniques, materials are separated based on the differences in their density, magnetic susceptibility, electrical properties, and surface wettability (Barton, 1979). A big difference between the materials processed in mineral processing and resources recycling is in their geometrical properties (i.e., size and shape). In this section, quantitative expressions of particle shapes, effects of shape in physical separation and current shape separation methods are reviewed.

2.2.1 Particle diameter and geometrical shape descriptors

The particle size of an ideal particle like a sphere, the particle size is easily defined by the geometrical diameter (D) while for non-spherical particles, their sizes are defined by statistical diameters (e.g., Feret's and Martin's diameters), which are usually measured using two or three-dimensional image analysis (Masuda et al., 2006). Equivalent diameters, defined as diameters of spheres that have the same geometrical or physical properties as those of non-spherical particles, are also used (Yang, 2013). Examples of equivalent particle diameters are summarized in Table 2-1.

Table 2-1. Examples of equivalent particle diameters (Masuda et al., 2006; Yang, 2013).

Equivalent diameter	Definition
Equivalent projection area diameter (D_a)	diameter of a sphere that has the same projected area as the particle viewed in a direction perpendicular to the plane of the greatest stability of the particle
Equivalent volume diameter (D_V or D^*) $D_V \text{ or } D^* = \left(\frac{6V_P}{\pi}\right)^{1/3}$ (2-1) where V_P is volume of particle (m^3)	diameter of a sphere that has the same volume as a particle
Equivalent surface diameter (D_S) $D_S = \left(\frac{S_P}{\pi}\right)^{1/2}$ (2-2) where S_p is surface area of particle (m^2)	diameter of a sphere that has the same surface as a particle
Equivalent surface-volume diameter (D_{SV}) $D_{SV} = \left(\frac{6V_P}{S_P}\right) = \frac{D_V^3}{D_S^2}$ (2-3)	diameter of a sphere that has the same external-surface-area-to-volume ratio as a particle
Sieve diameter (D_A) $D_A = \frac{1}{2}(a_1 + a_2) \text{ or } \sqrt{a_1 a_2}$ (2-4) where a_1 and a_2 are opening of sieves (m)	diameter equal to the diameter of a sphere passing through the same sieve aperture as a particle
Stokes diameter (D_{st}) $D_{st} = \sqrt{\frac{18\mu v_\infty}{(\rho_P - \rho_F)g}}$ (2-5) where μ is viscosity of fluid (Pa·s), v_∞ is terminal velocity of particle (m/s), ρ_P is density of particle (kg/m^3), ρ_F is density of fluid (kg/m^3), and g is gravitational acceleration (m/s^2)	diameter of a sphere that has the same gravitational settling velocity in Stokes' law regime as a particle

The other important geometrical property of particles is shape (Stückrath et al., 2006). Three different descriptors of particle shape are described below:

Sphericity (ψ) is the "whole-particle" or three-dimensional equivalent of the two-dimensional property known as circularity. This is usually viewed with reference to the sphere (Mgangira and

Komba, 2014; Wadell, 1932).

Wadell defined the operational sphericity as the ratio of the particle surface area to the area of a sphere that has the same volume (Mgangira and Komba, 2014; Wadell, 1932). Wadell's operational sphericity is given by;

$$\psi = \left(\frac{V_P}{V_{cs}}\right)^{1/3} \tag{2-6}$$

where V_P is the particle volume and V_{cs} is the volume of the smallest circumscribing sphere. This equation may be approximated as;

$$\psi = \frac{SIL}{L^3} = \left(\frac{SI}{L^2}\right)^{1/3} \tag{2-7}$$

where *S*, *I* and *L* are the short, intermediate, and long axis dimensions of the particle, respectively (Krumbein, 1940). A sphere has a sphericity of one while particles that have other shapes have sphericities of less than one (Krumbein, 1940; Mora and Kwan, 2000).

Another shape factor that is frequently used is the aspect ratio (AR), which is defined as the ratio of the length of the minimum and the maximum axis (Bouwman et al., 2004; Stückrath et al., 2006).

$$AR = \frac{S}{L} \tag{2-8}$$

Aspect ratio contains only two-dimensional information of particle shape. To describe particles in three-dimensions, Zingg (1935) developed a more versatile shape classification scheme that uses the particle dimensions along the three principal axes, termed flatness ratio ($\emptyset_{Flat}$) and elongation ratio ($\emptyset_{Elong}$);

$$\emptyset_{Flat} = \frac{S}{I} \tag{2-9}$$

$$\emptyset_{Elong} = \frac{I}{L} \tag{2-10}$$

Based on the flatness ratio and elongation ratios, particles are classified into four types: sphere-like, disk-like, rod-like, and blade-like (Arasan et al., 2011; Lees, 1964; Mgangira and Komba, 2014). Fig. 2-1(a) shows the Zingg diagram (Zingg, 1935) superimposed with curves of operational sphericity. The Zingg diagram is one of the best way to describe geometrical aspects of particle shape, but it still does not deal adequately with the hydrodynamic aspects of particle shape (Sneed and Folk, 1958).

Sneed and Folk measured the distribution of pebbles in the lower Colorado river and developed a different sphericity index, the maximum projection sphericity, which could explain the hydrodynamic behaviors of particles in a fluid (Sneed and Folk, 1958). The maximum projection sphericity of a particle is given by the equation;

$$\psi = \left(\frac{S^2}{IL}\right)^{1/3} \tag{2-11}$$

Sneed-Folk diagram with the curves of maximum projection sphericity is shown in Fig. 2-1(b). It classifies particles into sphere-like, disk-like, and rod-like based on the particle dimensions along the three axes a triangular diagram (Arasan et al., 2011; Graham and Midgley, 2000; Lewis and McConchie, 1994).

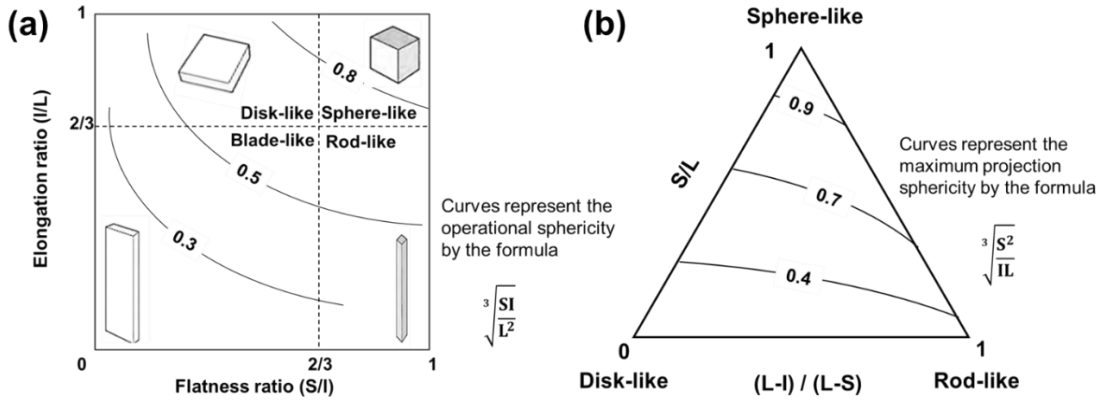

Figure 2-1. (a) Zingg diagram with the curves of operational sphericity and (b) Sneed-Folk diagram with the curves of maximum projection sphericity (Lewis and McConchie, 1994; Sneed and Folk, 1958; Zingg, 1935).

Roundness is the local aspect of shape that is commonly determined on a two-dimensional cross section or projection area of a particle, which distinguishes whether it is round or angular (Stückrath et al., 2006). Wentworth first defined roundness as (Wentworth, 1919):

$$Roundness = \frac{r_i}{R} \tag{2-12}$$

where r_i is the radius of curvature of the sharpest corner and R is the radius of the smallest circumscribing sphere (Fig. 2-2). Wadell defined the Wadell roundness index by (Wadell, 1932):

$$Roundness = \frac{\sum_{i=1}^{n}\left(\frac{r_i}{R}\right)}{n} \tag{2-13}$$

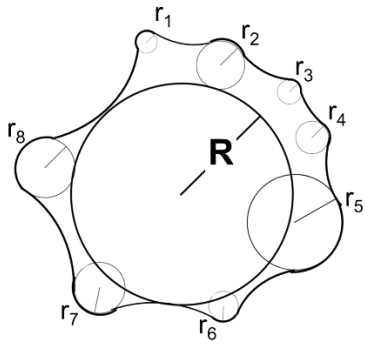

Figure 2-2. A two-dimensional particle showing the definitions of the radius of curvature of corners (r_1, r_2, and etc.) and the radius of the smallest circumscribing sphere (R) (Krumbein, 1940).

Roughness is the shape factor that distinguishes smooth and rough surface of the particles (Stückrath et al., 2006). Many experiments have shown that roughness do not affect the hydraulic falling behavior of edged objects (Bouwman et al., 2004; Stückrath et al., 2006).

The above mentioned descriptors are all static shape factors. There are dynamic shape factors that are more useful in physical separation, which is generally defined as (Kousaka et al., 1981; Ohya, 1997);

$$Dynamic\ shape\ factor = \frac{actual\ \ forced\ to\ particle}{forced\ to\ sphere\ having\ same\ volume} \tag{2-14}$$

In the following chapters, effects of particle size and shape during physical separation are discussed in detail.

2.2.2 Particle movement in a fluid

In physical separation, particles are treated and separated in a fluid like water and air (Brozek and Surowiak, 2007; Concha, 2014). Settling of a single spherical particle in a liquid has a terminal velocity (v_∞^*). When the particle reaches the terminal velocity, gravitational, buoyancy, and drag forces (F_G, F_B, and F_D, respectively) are in equilibrium and described by Eq. (2-15) and Fig. 2-3;

$$F_G - F_B = F_D \tag{2-15}$$

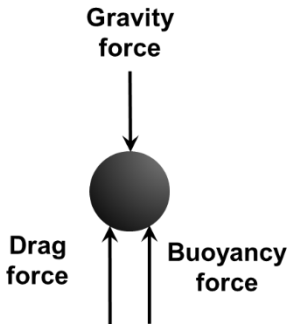

Figure 2-3. Force balance of the gravitational, bouyancy, and drag forces on a settling particle.

A particle that has a density greater than water will settle down due to its submerged weight that is different between gravity and buoyancy force. The direction of the drag force of the fluid acting on the particle is opposite to that of the settling velocity vector. The Eq. (2-15) can be revised as;

$$Submerged\ weight = Drag\ force \tag{2-16}$$

The gravitational, buoyancy, and drag forces can be written into Eqs. (2-17), (2-18), and (2-19), respectively.

$$F_G = m_P g = V_P \rho_P g \tag{2-17}$$

$$F_B = m_F g = V_P \rho_F g \tag{2-18}$$

$$F_D = \frac{C_D}{8} \pi d^2 v_\infty^{*2} \rho_F \tag{2-19}$$

where m_P is the mass of the particle, m_F is the mass of fluid, and C_D is the drag coefficient.

Substituting Eqs. (2-17), (2-18), and (2-19), into Eq.(2-15):

$$\frac{\pi D^3}{6}(\rho_P - \rho_F) g = \frac{C_D}{8} \pi d^2 v_\infty^{*2} \rho_F \tag{2-20}$$

So, the terminal settling velocity of a sphere is

$$v_\infty^* = \sqrt{\frac{4}{3}\frac{(\rho_P - \rho_F)}{\rho_F}\frac{gD}{C_D}} \tag{2-21}$$

The value of drag coefficient depends on the fluid flow regime that can be expressed by $C_D = f(Re_P)$ where Re_P is the Particle Reynolds number (Loth, 2008).

$$Re_P = \frac{v_\infty^* D \rho_F}{\mu} \tag{2-22}$$

In a laminar, creeping flow, or Stokes' law regime ($Re_P < 0.1$); $C_D = \frac{24}{Re_p}$, so that (Loth, 2008; Yang, 2013);

$$v_\infty^* = \frac{\rho_P - \rho_F}{18}\frac{gD^2}{\mu} \tag{2-23}$$

In a turbulent or Newton's law regime ($Re_p > 500$); $C_D = 0.445$, so the terminal velocity of a spherical particle is given by;

$$v_\infty^* = \sqrt{\frac{3(\rho_P - \rho_F)}{\rho_F} gD} \tag{2-24}$$

And in an intermediate or transition regime ($0.1 < Re_p < 500$); $C_D = f(Re_p)$ and $v_\infty^* = f(C_D)$. Turton and Levenspiel (1986) approximated the C_D at this regime as;

$$C_D = \frac{24}{Re_p}\left(1 + 0.173Re_p^{0.657}\right) + \frac{0.413}{1 + 1.63 \times 10^4 Re_p^{-1.09}} \tag{2-25}$$

However, the above equations are suitable only for a sphere. Particle movement especially settling velocity in fluids is strongly influenced by differences in shapes, so the separation efficiency is affected as well (Barton, 1979; Gabitto and Tsouris, 2008). The terminal velocities of non-spherical particles are dependent on their orientation (Yang, 2013). Actually, non-spherical particles have lower terminal velocities than spherical particles during settling in fluids (Arasan et al., 2011; Brozek and Surowiak, 2007). Moreover, non-spherical particles that have disk-like shape do not drop straight down like a sphere but tend to waft into a zig-zag pattern, like a falling leaf. Because of these reasons, some corrections are needed for the drag force of non-spherical particles.

Dynamic shape factor is further sub-classified by fluid flow regime as Stokes shape factor, Newton's shape factor, and intermediate regime shape factor (Loth, 2008) (Lau and Chuah, 2013) [. Previous studies mostly dealt with isometric particles such as cubes and cylinders but for anisometric and irregularly shaped, a particles satisfactory method to correct the drag coefficient is still not available (Yang, 2013). Almost all corrections of the drag coefficient can be expressed by $C_D = f(Re, \emptyset)$, where $\emptyset$ is the shape factor based on sphericity or dynamic shape factor (Gabitto and Tsouris, 2008; Hölzer and Sommerfeld, 2008; Lau and Chuah, 2013).

$$\emptyset = \frac{v_\infty}{v_\infty^*} \tag{2-26}$$

where v_∞ is the terminal settling velocity of the particle and v_∞^* is the terminal settling velocity of a

spherical particle that has the same volume. For example, Hölzer and Sommerfeld (2008) suggested that the correlation formula for the drag coefficient of non-spherical particle by shape factor be based on sphericity:

$$C_D = \frac{8}{Re}\frac{1}{\sqrt{\emptyset_{\parallel}}} + \frac{16}{Re}\frac{1}{\sqrt{\emptyset}} + \frac{3}{\sqrt{Re}}\frac{1}{\emptyset^{3/4}} + 0.4210^{0.4(-\log\emptyset)^2}\frac{1}{\emptyset_{\perp}} \quad (2\text{-}27)$$

where $\emptyset_{//}$ is the lengthwise shape factor and $\emptyset_{\perp}$ crosswire shape factor.

This formula shows that non-spherical particles ($\emptyset < 1$) have higher C_D than spherical particles ($\emptyset = 1$). Due to the higher C_D, a non-spherical particle has a higher drag force and slower settling velocity when compared with a spherical particle when the density of the particle is higher than the fluid. For particles that have density less than the fluid, they rise up against gravitational force, so a non-spherical particle has higher velocity than a spherical particle (Yang, 2013).

In the case of particle movement in flowing fluid, the direction of the drag force is the same as the flow direction. In fluids flowing in the horizontal direction, a non-spherical particle moves faster than a spherical particle because of the stronger drag force on the former than the latter. In the centrifugal separation, however, drag force has direction opposite to the centrifugal force, so spherical particles are forced by centrifugal force and recovered into the underflow product while non-spherical particles are influenced by drag force and recovered into the overflow (Gupta and Yan, 2006; Wills and Napier-Munn, 2006)

2.2.3 Effects of particle shape in separation processes

2.2.3.1 Screening and size classification

Screening and size classification are processes to separate particles into the desired size fractions for feeding to the next separation stage (Wills and Napier-Munn, 2006). In the screening of non-spherical particles, the probability of passage is a function not only of the particle size but also of the particle orientation relative to the screen opening (Beunder, 2000; Koyanaka et al., 1995; Yamamoto et al., 2009). The non-spherical particle can pass through the screen if it has at least one orientation smaller than the screen aperture (Koyanaka et al., 1995; Yamamoto et al., 2009). The probability of passage is affected by particle shape, especially for rod-like particles. The rod-like particle will pass through the screen aperture in the case of (a), (b), and (c) but not in (d) in Fig. 2-4 (Beunder, 2000).

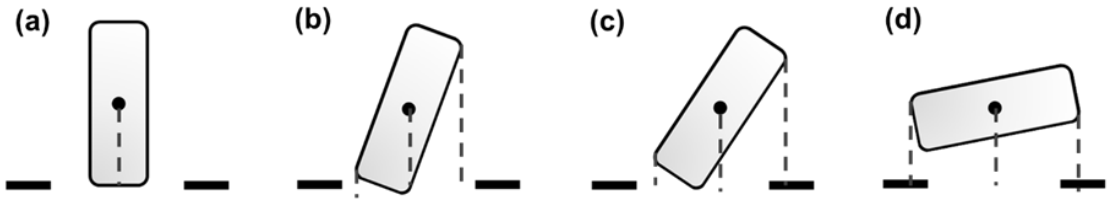

Figure 2-4. Examples of rod-shaped particle orientations during screening: (a, b, and c) orientation that can pass through the screen (d) orientation that cannot pass through the screen through the screen (Beunder, 2000).

The probability of passage of a rod-like particle depends on its length (Beunder, 2000). Because the screen is not perfectly flat, the vertical movement of the screen can make the particles roll on the screen (Beunder, 2000; Beunder and Rem, 1999). During this rolling, the particles can turn over on the screen and pass through if their center of mass and edge are within the opening as shown in Fig. 2-5 (Beunder, 2000; Beunder and Rem, 1999).

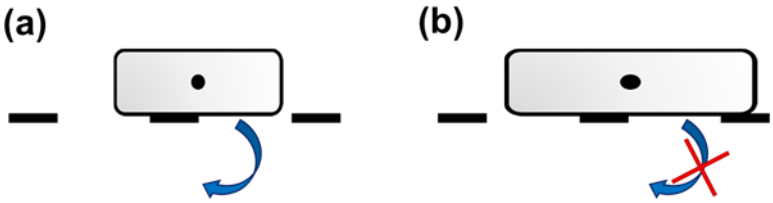

Figure 2-5. (a) Particles with a length less than or equal to twice the mesh size may turn over the edge of the mesh, whereas (b) longer particles cannot (Beunder and Rem, 1999).

The sieving behavior of rod-like particles at different elongation ratio was also investigated by numerical simulation. The motion of rod-like particles was simulated under vertical and horizontal vibrations. In the both case, sieving rate decreased and longer residence time were needed when the particle was longer (Endoh et al., 1984; Yamane et al., 2012). A rod-like particle that has high ductility could entangle on the screen and disk-like particles cover the opening of the screen. Smaller particles cannot pass through the screen when these phenomena occur (Beunder, 2000).

For particles too fine to be screened, methods using the differences in particle velocities in a fluid is often employed (Endoh, 2001; Wills and Napier-Munn, 2006). The cyclone is a continuous classifier that uses centrifugal force to classify particles in a fluid (Wills and Napier-Munn, 2006). Hydrocyclone apply hydrodynamic fields for particles, which depends on dynamic properties of particles orientation (Endoh et al, 1992). As described in the previous section, a non-spherical particle is more strongly affected by the drag force than a spherical particle. Because of this, disk-like particles could be recovered as overflow product even though they are relatively coarse (Kashiwaya et al., 2012; Wills

and Napier-Munn, 2006).

2.2.3.2 Gravity separation

Gravity separation is a technique that separates materials based on differences in their densities and their movement in fluids relative to each other. The concentration criterion (CC) is one indicator used in gravity separation, which is defined as (Wills and Napier-Munn, 2006):

$$CC = \frac{\rho_H - \rho_F}{\rho_L - \rho_F} \tag{2-28}$$

where ρ_H and ρ_L are the densities of heavy and light particles (kg/m^3), respectively.

When the CC value is more than 2.5, separation becomes easier but if this value is less than 1.25, separation of particles is not possible (Wills and Napier-Munn, 2006). As the values of CC approaches 1.25, separation requires coarser particles. Fig. 2-6 shows the limit size curve of gravity separation from concentration criterion (CC) (Gupta and Yan, 2006).

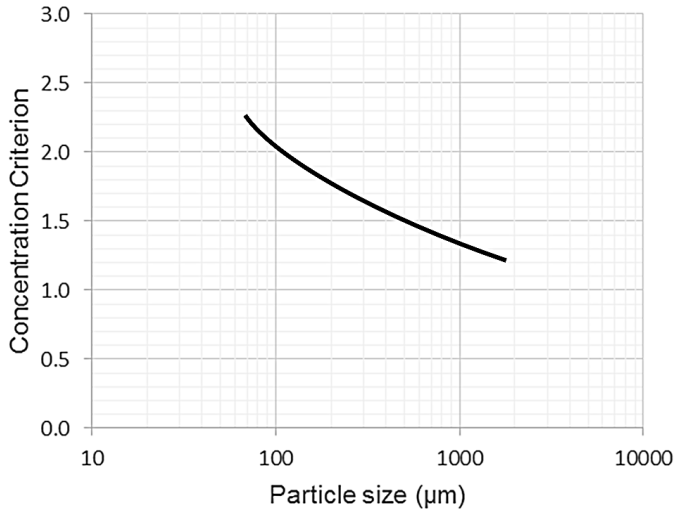

Figure 2-6. The graph shows the limit size curve of gravity separation from concentration criterion (CC) (Gupta and Yan, 2006).

Aside from the density, size, and shape of particles affect their movements in a fluid (Endoh, 2001; Gupta and Yan, 2006; Wills and Napier-Munn, 2006). For example, Pita and Castilho (2016) modified the CC equation and included terms for the settling velocities of non-spherical particles based on their experiments (Eq. 2-29).

$$CC_s = \frac{\rho_H - \rho_F}{\rho_L - \rho_F} \times \frac{\frac{v_{\infty_H}}{v^*_{\infty_H}}}{\frac{v_{\infty_L}}{v^*_{\infty_L}}} \quad (2\text{-}29)$$

where $v_{\infty H}$, $v_{\infty L}$ are the actual velocity of particles and $v_{\infty}{}^{*}{}_{H}$, $v_{\infty}{}^{*}{}_{L}$ are the settling velocity of sphere that have the same volume of heavy (*H*) and light (*L*) particles, respectively.

They also showed that CC_s was a better indicator of separation efficiency than CC in jig separation of non-spherical plastic particles and the separation efficiency was strongly influenced by the aspect ratio (Pita and Castilho, 2016).

In recycling, air table is often used because of its low-cost and ease of operation. The separation efficiency of air tables is also influenced by particle size and shape (Shimizu et al., 2002; Yoshida et al., 1998). From the separation of the PVC (heavy fraction) and other plastics (light fraction), the result shows that PVC that have disk-like were recovered in the light product since disk-like particles are easily blown up by air that is introduced from the bottom that reduced friction (Shimizu et al., 2002; Yoshida et al., 1998).

2.2.3.3 Centrifugal separation

Separation methods using centrifugal force are well-suited for fine particles. For example, Koppalkar (2013) determined the effect of particle shape in separation efficiency of Knelson concentrator by Eq. (2-30):

$$\eta(D_P) = \frac{\alpha\pi\emptyset {D_P}^2 \left(\rho_P - \rho_{pulp}\right)}{9\mu D_C} \quad (2\text{-}30)$$

where D_P is particle diameter, α is a constant, D_C is the diameter of the cyclone, ρ_{pulp} density of pulp, and ∅ is the shape factor (Corey shape factor that can be determined by Eq. 2-31).

$$\emptyset = \frac{S}{\sqrt{IL}} \quad (2\text{-}31)$$

2.2.3.4 Magnetic and electrical separation

Magnetic separation is a method to separate magnetic and non-magnetic particles while electrical separation uses the differences in electrical properties of materials. When both magnetic and electrical properties of materials are utilized for separation, it is usually referred to as eddy current separation (Wills and Napier-Munn, 2006). These separation methods are also affected by particle shape.

In magnetic separation, for example, the strength of magnetic field is not the only influential

factor, gravitational force and fluid dynamic drag force, which depends on the shape of particles, are also important (Stener, 2015).

For electrical separation, the particle shape can affect the charge in the corona field, which can be determined from flatness ratio and particle orientation (Lindley and Rowson, 1997; Zhang and Forssberg, 1997).

Eddy current separation is most often applied to concentrate non-ferrous metals from waste streams that contain mainly non-metallic particles (Maraspin et al., 2004). Forces and torques acting on a particle during eddy current separation are decided by the interaction with the magnetic field, friction with a conveyor belt and drag forces due to air (Maraspin et al., 2004). An alternating magnetic field produces eddy currents, which induce a magnetic field inside and around the conductive particles (i.e., metals). This secondary magnetic field reacts with the magnetic field of the rotor, resulting in the formation of a repulsive force, called Lorenz force, which deflects the conducting particles away from the material flow. While non-conductive particles, such as plastics, move under the combined effect of gravitational, centrifugal and frictional forces without being affected by the repulsive force (Yazici et al., 2010).

The most important factors determining the deflection behavior of a material are shape, size, orientation and deflection coefficient of a particle. The deflection coefficient is the ratio of electrical conductivity and density of a particle (Yazici et al., 2010).

$$\text{Deflection coefficient} = \frac{\sigma}{\rho_P} \tag{2-32}$$

where σ is electrical conductivity of particle ($\Omega^{-1}m^{-1}$)

The higher the deflection coefficient, the higher is the repulsive force (Lorentz force) exerted on the particle. Deflection coefficient is larger for non-ferrous metals that have low density such as aluminum, and smaller with higher density metals like copper. The repulsive force is increased with increasing size of conductive particles. Disk-like particles generate much higher deflections than sphere-like particles (Yazici et al., 2010; Zhang et al., 1998). This causes almost vertical take-off trajectories of disk-like particles compared with rod-like particles (Maraspin et al., 2004). However, the final trajectories of these particles after leaving the belt are influenced also by size, shape, and density.

2.2.3.5 Flotation

Flotation is a physical-chemical process that separates materials based on the differences in their surface wettabilities (i.e., hydrophilic and hydrophobic). Particles are mixed with water and air is

injected to generate air bubbles. The bubbles attach to the surface of hydrophobic particles and the particles float up and are recovered as froth products while hydrophilic particles go to the tailing. In addition to wettability, the shape, size, and density of particles are equally important parameters in flotation (Wills and Napier-Munn, 2006).

Pita and Castilho (2017) studied the role of size, shape, and density of particles on the separation of plastics by froth flotation. For coarse particles, floatability are strongly influenced by density, size, and shape (Pita and Castilho, 2017; Shen et al., 2001). The disk -like particles having a larger surface area than a sphere can have a larger amount of attached bubbles than a sphere-like particles. Because of this, when particle size and hydrophobicity are similar, floatability of disk-like particles is higher than that of sphere-like particles (Pita and Castilho, 2017).

Particle roughness and roundness also affect the floatability of the particle (Shen et al., 2001; Verrelli et al., 2014). The increase in surface roughness causes a longer attachment time on air bubble due to less slipping that improves the flotation recovery (Verrelli et al., 2014). An angular particle having a larger surface area can have a larger amount of attached bubbles than rounded particle, resulting in higher floatability (Shen et al., 2001). Roughness and roundness of particles depend on size reduction method (Rahimi et al., 2012). Rod mill products have higher roughness, lower roundness, and more irregular shape than that of ball mill (Rahimi et al., 2012). It was observed that dry ground products had higher roughness than wet ground products (Rahimi et al., 2012).

2.2.4 Particle shape separation

As mentioned above, physical separation is affected by particle shape. Applying this, shape separation methods based on sliding ability, rollability, and the passing rate through a screen have been developed (Beunder, 2000; Ohya, 1997). Shape separation has lower running cost than other separation technique because of its simple mechanism (Koyanaka et al., 1997).

2.2.4.1 Sliding ability and rollability

The most widely used methods to separate particles according to their shape, is to use their ability to roll and slide down a slope (Beunder, 2000; Ohya, 1997). It is usually applied to separate disk-like particles from other particles based on the differences of flatness ratio (Furuuchi and Gotoh, 1992).

Using rollability, an inclined chute method has been developed: disk-like particles have higher friction on the chute so that the descending velocity becomes lower, while sphere-like particles roll down by gravity and get higher velocity (Furuuchi and Gotoh, 1992). In a spiral shape separator, particles are fed into the top part of a stationary spiral, and sphere-like particles roll down by gravity and were collected outside the vessel because it can roll down faster than disk-like particles (Barton,

1979).

Inclined rotating disc method separates the different shape particles based on the trajectory difference between sphere-like particles and disk-like particles (Furuuchi and Gotoh, 1992; Ohya, 1997).

For the inclined rotating cylinder with blades method, particles are fed into the center of the cylinder. When the cylinder rotates, the disk-like particles are carried up to the top due to the mechanical action of the blade that shoveled them up, but the sphere-like particle moves to bottom side by the gravity (Furuuchi et al., 1990; Furuuchi and Gotoh, 1988) Inclined vibrating plate consists of a tilted plate that is inclined on the direction perpendicular to the movement direction (horizontal direction), sphere-like particle move down as a result of the inclination, while disk-like particles move upward due to vibration (Barton, 1979; Endoh, 2001; Koyanaka et al., 1997; Lee, 1997).

In a rotating cone method, particles are fed from near the peak of rotating cone, the sphere-like particles that have faster velocities move down to the edge of the cone, the disk-like particles climb up the cone slope to the top by the spiral scraper (Beunder et al., 2002).

Inclined conveyor belt method called as the RecGlass device is used for glass recovery (Carvalho et al., 2015). The glass particles have disk-shape while stones have sphere-like. Depending on the belt material, speed, slope and feed position, the disk-like particles move upwards and the sphere-like ones roll down. In another inclined conveyor belt method, a belt is inclined and tilted to one side edge. Particles are fed to the bottom part of the inclined belt, and the disk-like particles are carried up to the top by the belt motion, while the sphere-like particles roll down to the side edge of the belt due to the tilt of the belt (Beunder, 2000; Koyanaka et al., 1997).

Horizontal circular motion plate method uses circular plate fixed on the shaking table of a gyratory screen. Sphere-like particles move to the central collector while disk-like particle travels along the wall (Beunder, 2000; Kousaka et al., 1981).

2.2.4.2 Probability of passage

Screens can be used to separate sphere-like and rod-like particles. The probability of passage of sphere-like particles are higher than rod-like particles (Ohya, 1997). As explained previously, the probability of passage is dependent on the number of patterns or orientations of the particle and screen aperture. For rod-like particles (low elongation ratio), the residence time increases because rod-like particles take a long time to change their orientations and pass through the screen aperture (Beunder and Rem, 1999; Furuuchi and Gotoh, 1992). In recycling operations, the presence of wires complicates the separation process because these processes are often designed for sphere-like particles (Furuuchi et al., 1993). The wires can be recovered using the difference in residence times in a type of cascade

sieves because the probability of passage of wires is lower than sphere-like particles (Beunder and Rem, 1999). A rotating screen or trommel can also be applied to separate rod-like and sphere-like particles because the residence time of particles in the trommel relates to the particle shape. Hence particles can be separated according to the elongation ratio (Ohya, 1997; Ohya et al., 1999).

2.2.4.3 Other shape separation techniques

Other than the rollability and probability of passage, there are other techniques that can separate particles based on their shape. For example, the Leap-bound picker, consisting of a feeding chute, rotating the elastic drum, and splitter. This method recovers valuable materials with the dry separation based on differences in the frictional coefficient as a function of density and shape, deciding the repulsive ratio of leap bound (Park et al., 1994). The bouncing velocities of the particle depending on the type of collision (plastic or elastic), the velocity before the collision, and particle shape (Beunder, 2000). The sphere-like particle can get faster velocity and bounce farther than disk-like particles (Park et al., 1994).

A nail roll separator is used for separating bent wires from other particles: bent wires are trapped by the nail on the roll and are carried to a recovery box while other particles roll down to a separate recovery box (Park et al., 1994). Another idea uses the different adhesion force with different particle shapes: particles are fed from the hopper on a rotary drum and held to the small circular vacuum holes on the drum with a different adhesive force, decided by the shape of the particle (Furuuchi et al., 1990; Furuuchi and Gotoh, 1992). Spherical particles are held more tightly than non-spherical ones because of the narrower gap between the particle and the hole. Also, the surface roughness of particles as well as their elongation or flatness may affect the performance of the shape separator.

2.3 The application of gravity separation for coal cleaning and resources recycling: a review

Gravity separation, a process that separates particles based on density differences, is one of the oldest techniques in mineral processing that is still widely used especially in coal cleaning primarily because of the simplicity of its operation, low cost, and high efficiency (Wills and Napier-Munn, 2006). In recent years, increasing demand for mineral resources coupled with the higher generation of wastes have become critical problems of our modern society. One promising technique to address these concerns and lead to the development of a more sustainable society is the application of gravity concentration in the recycling of wastes. This section reviews the development of gravity separation and its application in coal cleaning and resources recycling.

2.3.1 Gravity separation in coal cleaning

Coal is one of the world's most important fossil fuels (Boylu et al., 2015). It plays a critical role in power generation plants and steel making. The International Energy Agency (IEA) projected that global coal demand would annually grow steadily by about 0.4% until 2040 (Zhou et al., 2016).

Direct combustion of coal releases SO_x that causes acid rain, so modern coal-fired power plants employ clean coal technologies such as pre-combustion (e.g., ultra-clean coal) and post-combustion (e.g., gas cleaning technology) are used (Yu et al., 2016).

Coal cleaning is a simple and effective method to separate combustible matter from gangue minerals (Zhang et al., 2014). Fig. 2-7 shows that about 80% of coal is treated by gravity separation such as jig, dense medium, cyclone, and spirals (Ito, 2008). Fig. 2-8 shows particle size dependence of coal cleaning methods. Conventional methods are used for coarse particle size (>0.5 mm) while more advanced techniques like flotation are the method of choice for fine particle (Ito, 2008).

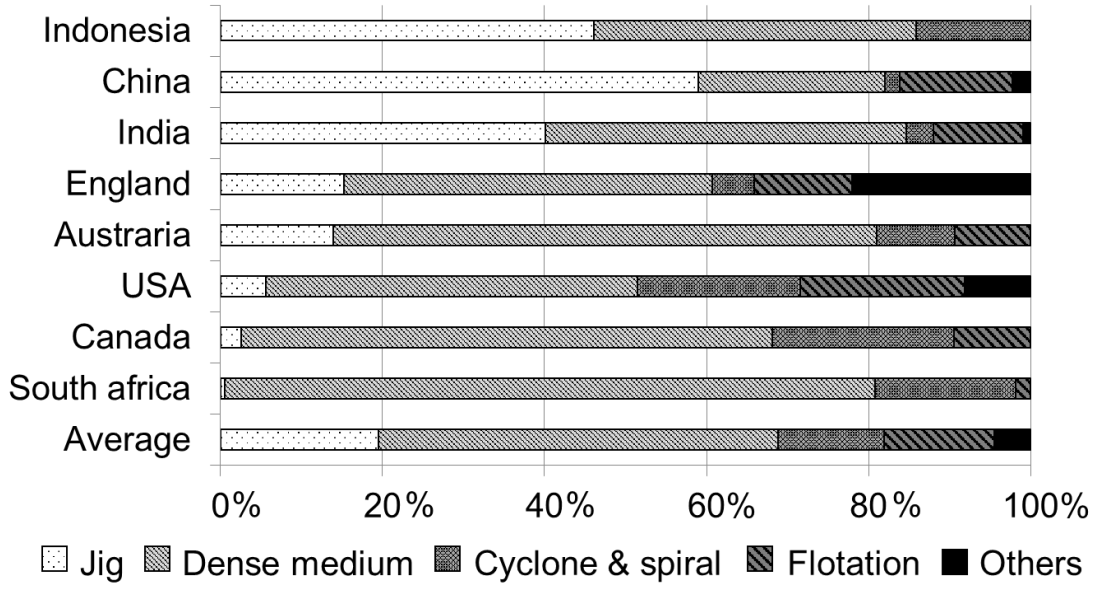

Figure 2-7. Usage of coal cleaning methods worldwide (Ito, 2008).

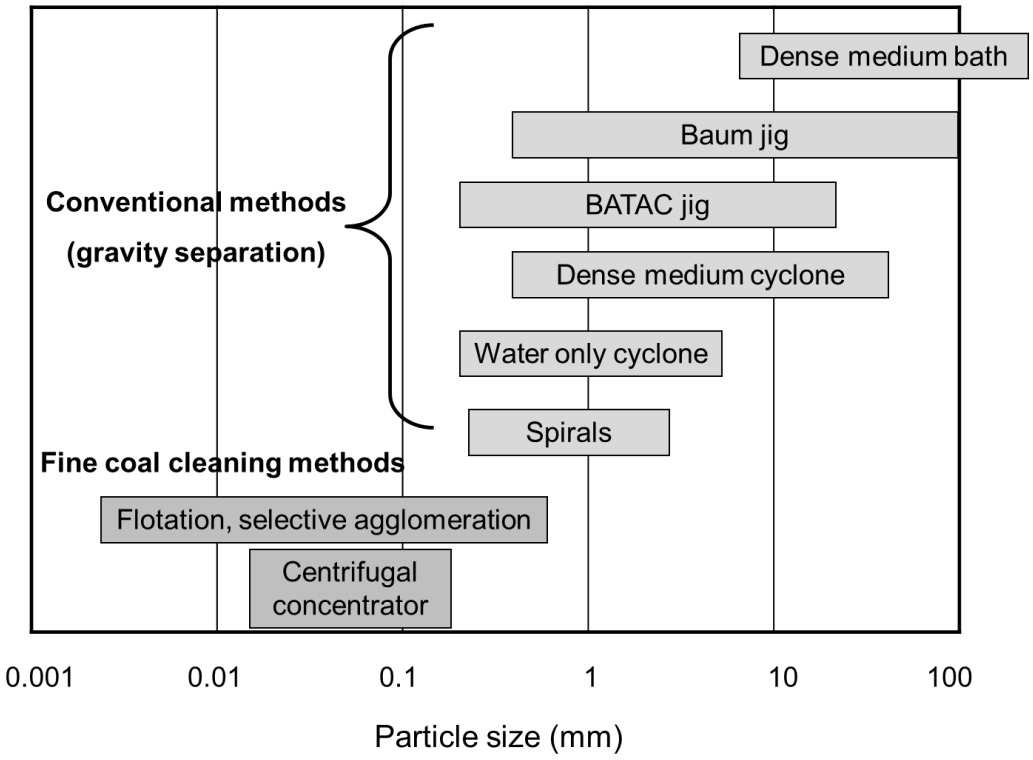

Figure 2-8. Particle size dependence of coal cleaning methods (Ito, 2008).

2.3.1.1 Conventional methods

I) Jig

Jigging is one of the oldest methods of gravity concentration that is still widely used for coal cleaning. In the jig, the separation of minerals of different specific gravity is accomplished in a bed that is rendered fluid by a pulsating current of water so as to induce stratification. The aim is to "fluidize" the bed of material being treated controlling dilation so that the heavier, smaller particles penetrate the interstices of the bed while the larger high specific gravity particles fall under a condition similar to hindered settling (Wills and Napier-Munn, 2006).

There are two types of air pulsated jig that is commonly used in the coal industry: Baum and TACUB. The Baum jig has been used for almost 100 years and is still the dominant device used by coal cleaning plants. In this type of jig, air pressure is injected into an air chamber adjacent to the separation chamber, which caused water to pulsate inducing stratification (Wills and Napier-Munn, 2006).

The TACUB (Takakuwa air chamber under bed) jig, commercially marketed as the BATAC® jig, was developed by Professor Emeritus K. Takakuwa of Hokkaido University (Ito et al., 2010; Tsunekawa et al., 2005). Similar to the Baum jig, the Batac jig is pneumatically operated but without the side air chamber. Instead, it is designed with a series of multiple air chambers, usually two cells

under the separation chamber extending to its full width, a configuration that gives a more uniform air distribution (Fig. 2-9). It uses electronically controlled air valves, which provide sharper cut-off of air input and exhaust (Barton, 1979).

There are many recent studies about the improvement of jigging performance for coal cleaning by mathematical modeling and simulation of particle motion (Ahmed, 2011; Cierpisz et al., 2016). Because stratification is a relatively complex process many interrelated parameters have to be considered (Kawatra and Carlson, 2013). For example, some parameters are inherently controllable (manipulated variables) that can be optimized in a given pulsation cycle (e.g., strokes, bed thickness, water level) (Ahmed, 2011; Cierpisz et al., 2016; Kawatra and Carlson, 2013). Ahmed (2011) reported that the number of strokes and bed thickness were the most important among these controllable parameters. However, some uncontrollable factors (disturbance variables) also play crucial roles in jig separation like feed grade, specific gravity of each component, size distribution, and particle shape (Ahmed, 2011; Cierpisz et al., 2016; Kawatra and Carlson, 2013).

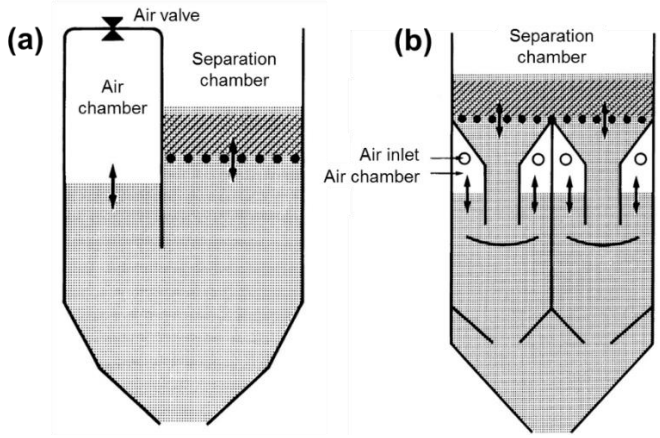

Figure 2-9. Schematic diagrams of (a) Baum jig and (b) TACUB or Batac jig (Wills and Napier-Munn, 2006).

II) Dense medium separators

Dense medium separation (DMS), also known as heavy medium separation (HMS), heavy liquid separation (HLS), separates two materials with different densities using a fluid medium with a density intermediate between the two materials. This causes the lighter particles (e.g., coal) to float while the heavier materials (e.g., shale or high-ash coal) to sink (Wills and Napier-Munn, 2006). The medium usually used is a suspension of fine magnetite in water which could be recirculated after washing, magnetic separation and demagnetization (Kademli and Gulsoy, 2013; Kuang et al., 2014).

DMS is classified into two general categories: static and dynamic. Static-type DMS separates

particles by gravity only while the medium is static. This process is suitable for particles greater than 12.5 mm. Two types of vessels are used: bath and drum. The bath is a large open tank with the circulation of finely pulverized magnetite suspension while the drum is a rotating longitudinal cylindrical vessel where waste rocks sink that are collected by lifters to be discharged into launder (Meyer and Craig, 2015).

Two types of cyclone are used in coal cleaning: dense medium cyclone (DMC) and water only cyclone (WOC). DMC is costlier than WOC but can achieve much sharper separations than WOC, making it suitable for cleaning coal containing gangue minerals with similar density as coal (Lu et al., 2016). Fine particles (0.5-8.0 mm) separation can be achieved in dynamic separators because centrifugal force is more effective than gravitational force (Dou et al., 2015b; Wills and Napier-Munn, 2006)). Table 2-2 summarizes some recent studies about coal cleaning using DMS.

Table 2-2. Recent studies of DMS in coal cleaning.

Studies	**Description**	**Ref.**
Vessel	Large diameter DMC	Korte&Engelbrecht, 2014; Meyers et al., 2014
Medium	Effects of size distribution of medium	Firth et al., 2012
	Effects of medium composite	Firth et al., 2012
		O'Brien et al., 2014
Modeling	Real-time prediction model	Guanghui et al., 2012
	Computational fluid dynamic and discrete element method (CFD-DEM) model	Chen et al., 2012
		Kuang et al., 2014
	Volume of fluid (VOF) multiphase model	Kuang et al., 2014
	Two-fluid model (TEM) or mixture model	Kuang et al., 2014
	Dynamic and steady-state model	Meyer and Craig, 2014
	Soft sensor model	Dou et al., 2015a, b
Monitoring instruments	Electrical impedance spectrometer (EIS)	Firth et al., 2014
	Intelligent medium density control	Wang et al., 2015b

III) Water-only cyclone

The water-only cyclone (WOC) is used to separate particles in the size range of 0.5-6 mm. Similar to DMC and hydrocyclone, centrifugal force accelerates the settling rate of particles thereby separating particles based on size, shape, and specific gravity (Hacifazlioglu, 2012a). Particles with faster settling particles move to the wall of the cyclone, where velocity is the lowest, and then migrate to the apex opening. Due to drag force, the slower-settling particles move towards the zone of low pressure along the axis and are carried upward as overflow through the vortex-finder (Wills and Napier-Munn, 2006).

Because of its simplicity, small space requirements, lack of moving parts, low operating costs, low maintenance requirements without dense medium, the WOC is still used in coal beneficiation (Lu et al., 2016).

Recently, many modifications to WOC for coal cleaning have been studied. Some examples include modified WOC (MWOC) or horizontal cyclone (Hacifazlioglu, 2012a, b), air-injector WOC (Liu et al., 2013), and cyclone column separator (CCS) (Dong et al., 2013).

IV) Spirals

Spiral concentrators are flowing film type separators that stratifies the particles by gravity (Barry et al., 2015). Humphrey's coal spirals are commonly used to process coal in the size range of approximately 0.15 mm to 1 mm (Barry et al., 2015; Wills and Napier-Munn, 2006). It consists of a corkscrew-shaped device that separates coal from waste rock by selective segregation that occurs when particles move in the flowing film along the helical trough (Mohanty et al, 2014; Wills and Napier-Munn, 2006). Spirals are often employed in combination with other water-based separators (e.g., WOC) to improve performance (Hacifazlioglu, 2012b).

V) Others

There are also several recently developed gravity separators that are applied in coal cleaning. For example, Reflux classifier consisting of a fluidized bed with a system of parallel inclined channels mounted above (Campbell et al., 2015; Galvin et al., 2014; Iveson et al., 2015), Teetered bed separators (TBS), and Floatex density separator (FDS) that are developed to process nominal size range of 0.1-1 mm (Hacifazlioglu, 2012b; Kumar et al., 2013).

2.3.1.2 Dry gravity separation

Nowadays, coal cleaning is mostly carried out by wet processes due to their high separation efficiency (Boylu et al., 2015; Ghosh et al., 2014; Kademli and Gulsoy, 2013; Sahu et al., 2013; Yang et al., 2013a). However, wet processes consequently need a large quantity of water and are difficult to employed in dry areas where water supplies are limited. Cold regions also pose handling problem because temperature could drop below the water freezing point (Fu et al., 2016; Ghosh et al., 2014; Kademli and Gulsoy, 2013; Yang et al., 2013b; Yu et al., 2016; Zhang et al., 2014; Zhou et al., 2016). To address these issues, several dry gravity separators including air jigs, fluidized bed, and air table have been developed.

I) Air jig

Air jig or pneumatic jig was developed using the same principles as wet jig. Stump air flow jig and Allair jig are two of the most commonly used air jigs in coal cleaning (Boylu et al., 2015).

II) Fluidized bed separator

Similar to DMS, air dense medium fluidized beds (ADMFB) separators use air and dense solid (e.g., magnetite powder) to create the fluidized medium that has a density intermediate between the materials to be separated. It is suitable for 6-50 mm-sized coal (Fu et al., 2016; Kademli and Gulsoy, 2013; Sahu et al., 2013; Zhang et al., 2014). For 1-6 mm size fraction, vibrated fluidized bed (VFB) separator uses air injection from the bottom to segregate the particles based on density, size, and shape (Ghosh et al., 2014; Yang et al., 2013a). This process is similar to jig separation whereby the separation mechanism can be referred to as bubble-driven jigging mechanism. Like traditional jig separation, the separation efficiency is dependent on the bubble-driven jigging cycles, air velocity, vibration intensity, bed height and fluidizing time (Yang et al., 2013b).

III) Air table

Air tables employ the stratification of materials by a combination of fluidizing air flow and other principles (Fig. 2-10). Air flows through the screen from the bottom of the deck to lighter coal particles to the lower end of the deck. The heavier gangue minerals remain on the surface of the screen and are moved sideways towards the higher end due to desk vibration (Chalavadi et al., 2016; Ghosh et al., 2014). Similar to wet shaking table technique in mineral processing, separation efficiency of air tables is influenced by the vibration amplitude (A), frequency (f), angle (θ) and air flow (Yu et al., 2016). Air inside the bed creates dust particles, which are sucked into an overhead hood and then recovered by a dust collector cyclone with a cloth filter (Kademli and Gulsoy, 2013). Currently, a mobile pilot-scale air table commercially known as FGX separator and compound separator with high efficiency are widely used in coal processing (Kademli and Gulsoy, 2013; Yu et al., 2016).

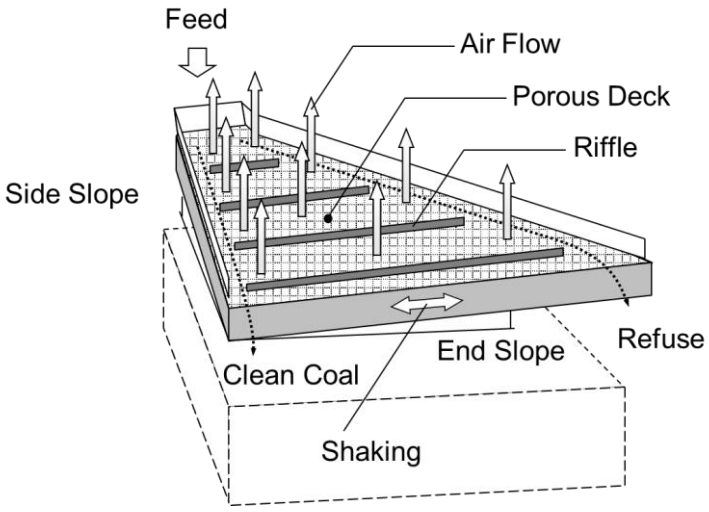

Figure 2-10. A schematic diagram of an air table.

2.3.1.3 Fine coal cleaning methods

Advanced coal cleaning techniques were introduced to treat fine coal (-1 mm) (Lu et al., 2016). Froth flotation, a surface-based separation processes, has been used extensively in advanced coal cleaning by applying the principles of surface chemistry to purify coal from gangue minerals (Galvin et al., 2014; Uslu et al., 2012).

Gravity-based separation techniques have also been applied to recover the fine coal. These equipment are developed for the removal of fine pyrite (FeS_2) that has specific gravity of 5.0. Separation under a normal gravitational field of 1G is difficult for under 0.1 mm size particles due to their low settling velocities. The settling velocity of very fine particles can be increased by applying an artificially enhanced gravitational field using centrifugal force. Several enhanced gravity separators (EGS) are primarily developed for desulfurization and has recently evolved to achieve efficient separation of fine gold particles on a commercial scale (Boylu, 2013; Hacifazlioglu, 2012b; Mohanty and Honaker, 1999; Singh and Das, 2013). EGS can be categorized into three groups: jig type, fluidized bed type, and flowing film type.

I) Jig type: Kelsey jig and Altair jig

A schematic diagram of a Kelsey centrifugal jig (KCJ) is shown in Fig. 2-11. It works on the principles of a conventional jig employing a centrifugal force field. The unit is capable of generating centrifugal fields up to 100G, consists of a series of hutches which are rotated on a fixed central feed pipe. Feed slurry enters through the pipe and flows outward across the bed of ragging. Lighter coal flows through the surface of the ragging bed supported by a cylindrical screen that is mounted across the top of each hutch and overflows the top of the separator, while high-density minerals pass downward through the ragging and screen which are discharged through actuated valves (Singh and Das, 2013). The Altair centrifugal jig is simpler in design with a lower number of moving parts than a Kelsey jig. The Altair jig also achieve an enhanced gravity field of nearly 100G (Mohanty and Honaker, 1999).

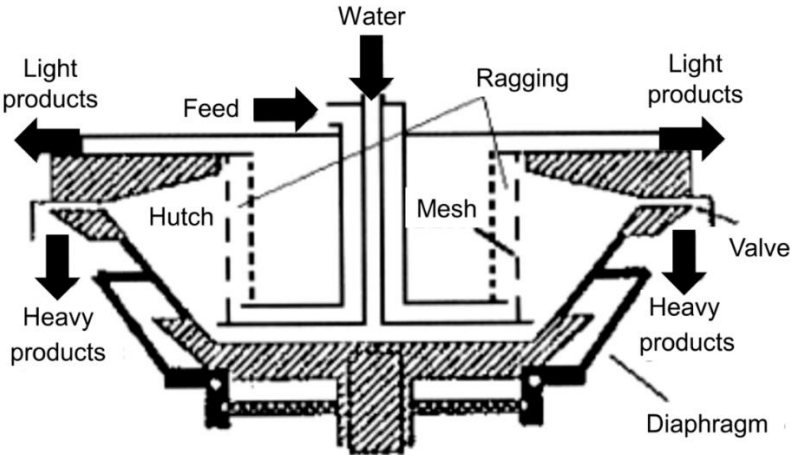

Figure 2-11. A schematic diagram of a Kelsey jig.

II) Fluidized bed type: Knelson concentrator

The Knelson concentrator, a compact centrifugal separator is a hindered settling device, related to a hydrosizer, with an active fluidized bed to capture the heavy minerals with centrifugal force equivalent 200G (Singh and Das, 2013; Uslu et al., 2012). It consists of a rotating truncated cone (bowl) which is stair-stepped by several ring-type partitions (Fig. 2-12). Feed slurry is injected through a central feed pipe and is allowed to flow countercurrent between each partition until it overflows the top of the rotating bowl. Rinse water forced through perforations in the rotating bowl creates a fluidized bed of particles between each partition. Particles that have higher density than fluidized bed are trapped in the retention zone between the partitions, while lighter particles are flushed out over the partitions. One of its disadvantages is the large amount of water (up to 2-3 times the feed flow) required to fluidize the particle bed (Uslu et al., 2012).

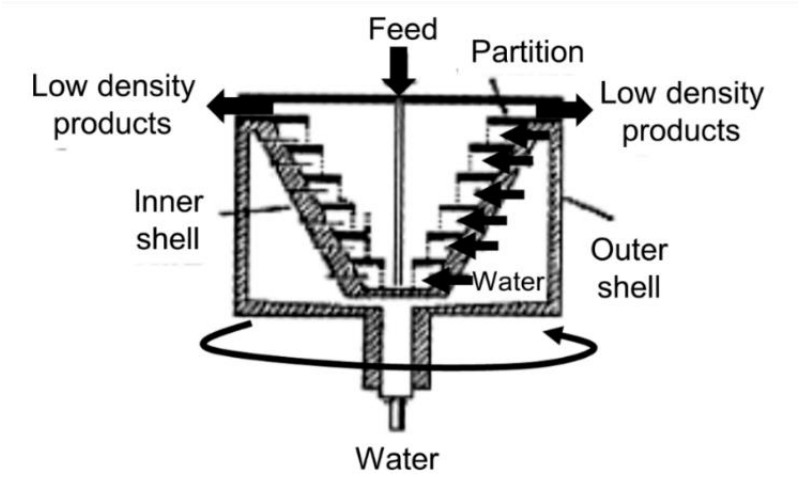

Figure 2-12. A schematic diagram of a Knelson concentrator.

III) Flowing film type: Falcon concentrator

A Falcon concentrator is a spinning fluidized bed EGS, which is basically a combination of a sluice and a continuous centrifuge having the highest centrifugal force of up to 300G. It enables the treatment of particles even down to 10 μm. Similar to Knelson concentrator, it consists of a fast-spinning smooth-surface truncated bowl (Fig. 2-13). Feed slurry is fed from the bottom of the cone and forms a thin flowing film of particles at its wall that become stratified based on differences in density. Light particles like coal can move to the top layer and discharge over the top of the cone, while heavy particles sliding along the inner surface of the cone are discharged through the cone wall (Kroll-Rabotin et al., 2013; Singh and Das, 2013).

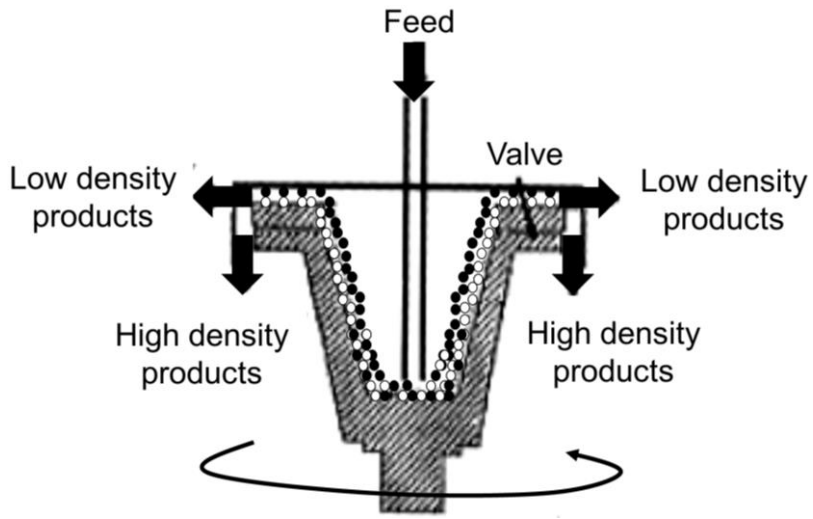

Figure 2-13. A schematic diagram of a Falcon concentrator

The probable error (E_p) is a guide to the separation efficiency. Fig. 2-14 shows the particle size dependence of E_p of each coal cleaning method. Generally, perfect separation of coarse particles is easier to achieve while for fine particles, EGS are needed to obtain similar E_p (Ito, 2008).

However, the industrial use of EGS around the world has not yet been put into practice in the coal-washing industry. The primary reason for this is that their capacities are low, and the operating-maintenance costs are quite high (Hacifazlioglu, 2012b).

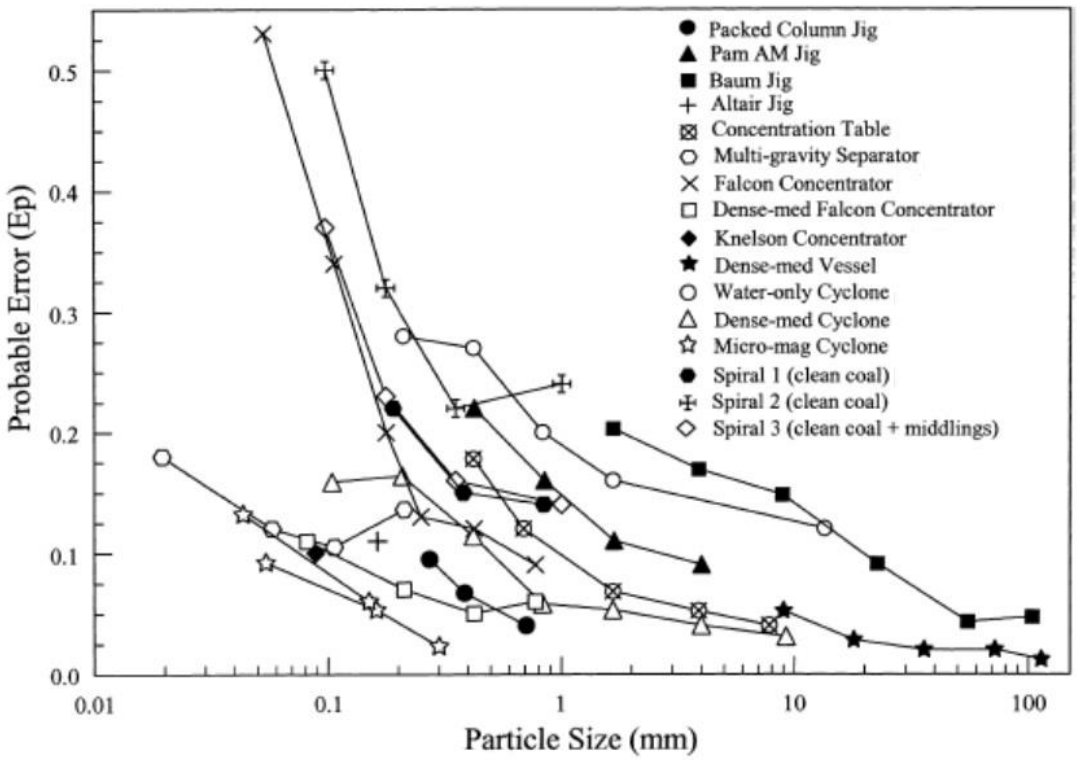

Figure 2-14. Particle size dependence of probable error (E_p) of each coal cleaning method (Ito, 2008).

2.3.2 Gravity separation in resources recycling

Many separation methods applied for resources recycling are modified versions of those originally designed for mineral processing. Among these methods, density-based techniques are increasingly getting popular due to the simplicity of their operation, low cost, and high efficiency (Wills and Napier-Munn, 2006).

2.3.2.1 Advanced jig separation for recycling

The TACUB or Batac jig used in mineral processing and coal cleaning was modified for recycling processes by Professor Emeritus M. Tsunekawa of Hokkaido University and reported that the modified TACUB jig called RETAC jig (R&E, Co., Ltd.) is well-suited for the separation of metal-plastic and plastic-plastic mixtures because of the precise control of the wave form during operation (Ito et al., 2010; Tsunekawa et al., 2005). In recent years, jig separation has become an integral part of many recycling plants for plastic-plastic separation. It has been applied to separate various plastics for material recycling (e.g., polystyrene (PS), acrylonitrile butadiene styrene (ABS), and polyethylene terephthalate (PET)) from copy machines (Tsunekawa et al., 2005) as well as plastics, metals, and printed circuit boards (PCBs) from mobile phones). In addition, this technique also has been applied to remove polyvinyl chloride (PVC), that containing Cl^- which have adverse effects on boilers, from

other kinds of plastic prior thermal recycling (Kikuchi et al., 2008; Kuwayama et al., 2011). The outline of a desktop type batch-wise RETAC jig is shown in Fig. 2-15(a).

Reverse jig (Fig. 2-15(b)) is a modified RETAC jig that could separate particles having lighter densities than water by adding a screen on top of the separation chamber. Similar to the conventional RETAC jig, reverse jig separates particles by stratification based on their densities. In the separation chamber, particles move up and down below the top screen and stratification occurs because of differences of levitation velocities. It was successfully applied to separate polypropylene (PP) and high-density polyethylene (HDPE) from waste containers (Ito et al., 2010).

Recently, the principle of gravity separation and flotation have been combined as density/surface-based technique. Hybrid jig (Fig. 2-15(c)) is another modified version of the RETAC jig that can separate particles having similar densities but different surface wettability. An aeration tube is installed under the screen (particle bed) to generate air bubbles inside the separation chamber. When bubbles attach to particles, their "apparent" density becomes lower in comparison to particles without any attached bubbles. Because of density differences induced by bubble attachment, these particles can be recovered on the top layer due to jigging stratification. Many parameters related to hybrid jig (e.g., surface tension, surface modification (wetting agents), bubble size) had been investigated using model plastics (e.g., PET, PVC, polypropylene with glass fiber (PPGF), and high impact polystyrene (HIPS)). It was successfully applied to separate plastics, metals, and PCBs from mobile phones.

Reverse hybrid jig (Fig. 2-15(d)) is combination of reverse and hybrid jig that is designed to separate particles having lighter densities than water, which having similar densities but different wettability (e.g., polyethylene (PE), and cross-linked polyethylene (XLPE)).

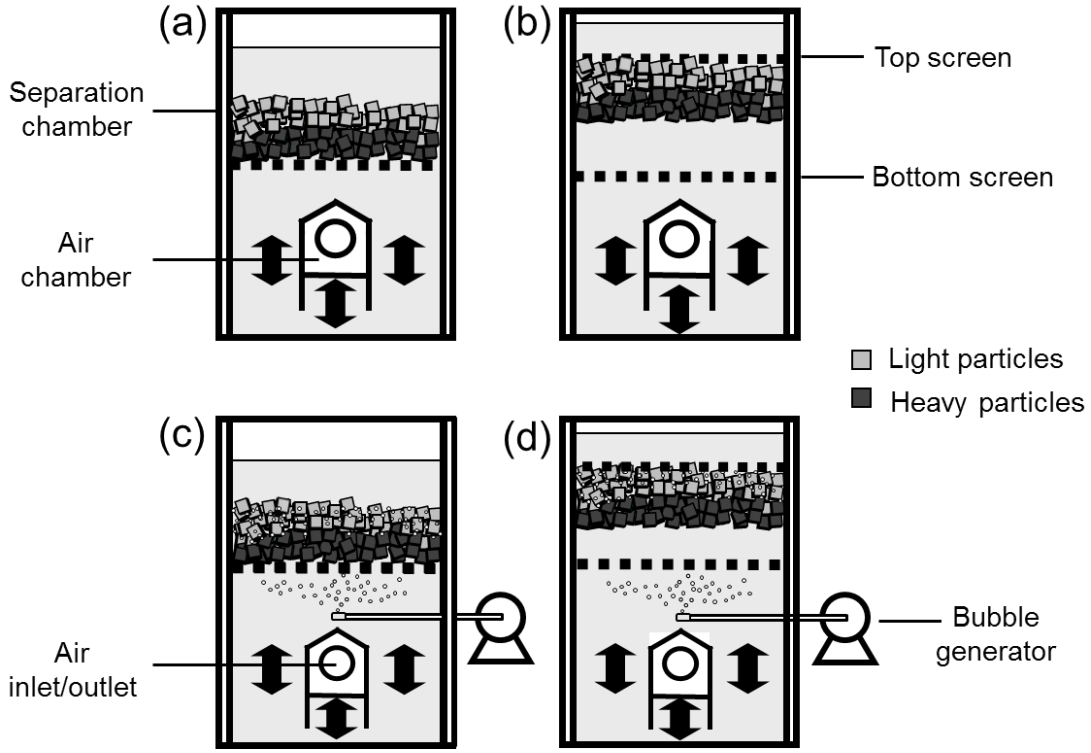

Figure 2-15. A schematic diagram of (a) RETAC jig, (b) reverse jig, (c) hybrid jig, and (d) reverse hybrid jig.

2.3.2.2 Air cyclone

The cyclone can be applied as a dry separation device in recycling. For example, commercial scale cyclone has been applied to separate PET bottle flakes from PVC label. Due to centrifugal force, the denser PET flakes move faster to the walls and fall down to the bottom as underflow product, whereas the lighter PVC film is recovered in the overflow.

2.3.2.3 Air table

Dry flowing film-type gravity separators such as air table are used to recycle copper/aluminum from electrical wires by separating the plastic insulation like PVC from metallic wires.

References

Ahmed, M.M., 2011. Optimization of a jigging process using statistical technique. Int. J. Coal Prep. Util. 31, 112–123. https://doi.org/10.1080/19392699.2010.549383

Arasan, S., Akbulut, S., Hasiloglu, A.S., 2011. Effect of particle size and shape on the grain-size distribution using image analysis. Int. J. Civil Struct. Eng. 1, 968–985.

Barton, A.F.M., 1979. Resource recovery and recycling. John Wiley & Sons Australia, Limited.

Barry, B., Klima, M.S., Cannon, F.S., 2015. Effect of hydroacoustic cavitation treatment on the spiral processing of bituminous coal. Int. J. Coal Prep. Util. 35, 76–87. https://doi.org/10.1080/19392699.2014.973107

Beunder, E.M., 2000. Influence of shape on particle behaviour in recycling techniques. Thesis (PhD), Delft University of Technology, Netherlands.

Beunder, E.M., Rem, P.C., 1999. Screening kinetics of cylindrical particles. Int. J. Miner. Process. 57, 73–81. https://doi.org/10.1016/S0301-7516(99)00007-1

Beunder, E.M., van Olst, K.A., Rem, P.C., 2002. Shape separation on a rotating cone. International Journal of Mineral Processing 67, 145–160. https://doi.org/10.1016/S0301-7516(02)00036-4

Bouwman, A.M., Bosma, J.C., Vonk, P., Wesselingh, J.A., Frijlink, H.W., 2004. Which shape factor(s) best describe granules? Powder Technol. 146, 66–72. https://doi.org/10.1016/j.powtec.2004.04.044

Boylu, F., 2013. Modeling of free and hindered settling conditions for fine coal beneficiation through a Falcon concentrator. Int. J. Coal Prep. Util. 33, 277–289. https://doi.org/10.1080/19392699.2013.818986

Boylu, F., Çinku, K., Çetinel, T., Karakaş, F., Güven, O., KaraağaçlIoğlu, I.E., Çelik, M.S., 2015. Effect of coal moisture on the treatment of a lignitic coal through a semi-pilot-scale pneumatic stratification jig. Int. J. Coal Prep. Util. 35, 143–154. https://doi.org/10.1080/19392699.2015.1005743

Brozek, M., Surowiak, A., 2007. Effect of particle shape on jig separation efficiency. Physicochemical Problems of Mineral Processing. Vol. 41, 397-413.

Campbell, Q.P., le Roux, M., Smith, I.G.T., 2015. Water-only laboratory coal fractionation using the reflux classifier. Miner. Eng. 83, 59–63. https://doi.org/10.1016/j.mineng.2015.08.015

Carvalho, M.T., Dias, N., Brogueira, P., 2015. Separation by particle shape — The RecGlass device. International Journal of Mineral Processing 140, 1–7. https://doi.org/10.1016/j.minpro.2015.04.016

Chalavadi, G., Singh, R.K., Sharma, M., Singh, R., Das, A., 2016. Development of a generalized strategy for dry beneficiation of fine coal over a vibrating inclined deck. Int. J. Coal Prep. Util. 36, 10–27. https://doi.org/10.1080/19392699.2015.1048804

Chen, J., Chu, K.W., Zou, R.P., Yu, A.B., Vince, A., 2012. Prediction of the performance of dense medium cyclones in coal preparation. Miner. Eng. 31, 59–70. https://doi.org/10.1016/j.mineng.2011.11.010

Chikerema, P., Moys, M., 2012. Effects of Particle Size, Shape, and Density on the Performance of an Air Fluidized Bed in Dry Coal Beneficiation. Int. J. Coal Prep. Util. 32, 80–94. https://doi.org/10.1080/19392699.2011.640297

Cierpisz, S., Kryca, M., Sobierajski, W., 2016. Control of coal separation in a jig using a radiometric meter. Miner. Eng. 95, 59–65. https://doi.org/10.1016/j.mineng.2016.06.014

Concha, F., 2014. Solid-Liquid Separation in the Mining Industry, Fluid Mechanics and Its Applications. Springer International Publishing.

Dong, L., Fan, M., Yang, H., 2013. Separation performance of a cyclone column separator with complicated positive and negative cones. Int. J. Miner. Process. 122, 43–46. https://doi.org/10.1016/j.minpro.2013.04.009

Dou, D., Yang, J., Liu, J., Zhang, H., 2015a. A novel distribution rate predicting method of dense medium cyclone in the Taixi coal preparation plant. Int. J. Miner. Process. 142, 51–55. https://doi.org/10.1016/j.minpro.2015.04.015

Dou, D., Yang, J., Liu, J., Zhang, Z., Zhang, H., 2015b. Soft-sensor modeling for separation performance of dense-medium cyclone by field data. Int. J. Coal Prep. Util. 35, 155–164. https://doi.org/10.1080/19392699.2015.1005744

Endoh, S., Koga, J., Yamaguchi, K., 1984. The sieving rate of cylinder particles. KONA. 2, 7–15. https://doi.org/10.14356/kona.1984005

Endoh et al., “Study of shape separation of particles using fluid fields -Dynamic properties of irregular shaped particles in wet cyclones-”, Journal of the society of powder technology (Japan), Vol.29, No. 11, pp. 838–844, 1992.

Endoh, S., 2001. Separation and sorting of solid waste particles. J. Soc. Powder Technol., Japan, 2001, Vol. 38, pp. 347-354.

Firth, B., Holtham, P., O’Brien, M., Hu, S., Dixon, R., Burger, A., Sheridan, G., 2014. Investigation of recently developed monitoring instruments for DMC circuits at new Acland. Int. J. Coal Prep. Util. 34, 112–120. https://doi.org/10.1080/19392699.2014.869922

Firth, B., O’Brien, M., McNally, C., 2012. Medium quality and DMC performance – Composition of plant mediums. Int. J. Coal Prep. Util. 32, 11–24. https://doi.org/10.1080/19392699.2011.610765

Furuuchi, M., Gotoh, K., 1988. Continuous shape separation of binary mixture of granular particles. Powder Technology 54, 31–37. https://doi.org/10.1016/0032-5910(88)80046-9

Furuuchi, M., Gotoh, K., 1992. Shape separation of particles. Powder Technology 73, 1–9. https://doi.org/10.1016/0032-5910(92)87001-Q

Furuuchi, M., Ohno, E., Gotoh, K., 1990. Shape characteristics of granular materials precisely classified by a shape separator. Advanced Powder Technology 1, 89–100. https://doi.org/10.1163/156855290X00108

Furuuchi, M., Yamada, C., Gotoh, K., 1993. Shape separation of particulates by a rotating horizontal sieve drum. Powder Technology 75, 113–118. https://doi.org/10.1016/0032-5910(93)80071-H

Fu, Z., Zhao, Y., Yang, X., Luo, Z., Zhao, J., 2016. Fine coal beneficiation via air-dense medium fluidized beds with improved magnetite powders. Int. J. Coal Prep. Util. 36, 55–68. https://doi.org/10.1080/19392699.2014.967849

Gabitto, J., Tsouris, C., 2008. Drag coefficient and settling velocity for particles of cylindrical shape. Powder Technology 183, 314–322. https://doi.org/10.1016/j.powtec.2007.07.031

Galvin, K.P., Harvey, N.G., Dickinson, J.E., 2014. Fluidized bed desliming in fine particle flotation – Part III flotation of difficult to clean coal. Miner. Eng. 66–68, 94–101. https://doi.org/10.1016/j.mineng.2014.02.008

Ghosh, T., Honaker, R.Q., Patil, D., Parekh, B.K., 2014. Upgrading Low-Rank Coal Using a Dry, Density-Based Separator Technology. Int. J. Coal Prep. Util. 34, 198–209. https://doi.org/10.1080/19392699.2014.869934

Graham, D.J., Midgley, N.G., 2000. Graphical representation of particle shape using triangular diagrams: an Excel spreadsheet method. Earth Surface Processes and Landforms 25, 1473–1477. https://doi.org/10.1002/1096-9837(200012)25:13<1473::AID-ESP158>3.0.CO;2-C

Guanghui, W., Yali, K., Zhangguo, W., Ying, W., Li, J., 2012. A real-time prediction model for production index in process of dense-medium separation. Int. J. Coal Prep. Util. 32, 298–309. https://doi.org/10.1080/19392699.2012.717565

Gupta, A., Yan, D.S., 2006. Mineral Processing Design and Operation – An Introduction, Perth, Australia.

Hacifazlioglu, H., 2012a. Optimization of some parameters in a modified water-only cyclone for metallurgical coal production from high-ash fine coking coals. Int. J. Coal Prep. Util. 32, 290–297. https://doi.org/10.1080/19392699.2012.717564

Hacifazlioglu, H., 2012b. Application of the modified water-only cyclone for cleaning fine coals in a Turkish washery, and comparison of its performance results with those of spiral and flotation. Fuel Proc. Tech. 102, 11–17. https://doi.org/10.1016/j.fuproc.2012.04.011

Hölzer, A., Sommerfeld, M., 2008. New simple correlation formula for the drag coefficient of non-spherical particles. Powder Technol. 184, 361–365. https://doi.org/10.1016/j.powtec.2007.08.021

Hori, K., Tsunekawa, M., Hiroyoshi, N., Ito, M., 2009a. Optimum water pulsation of jig separation for crushed plastic particles. Int. J. Miner. Process. 92, 103–108. https://doi.org/10.1016/j.minpro.2009.01.001

Hori, K., Tsunekawa, M., Ueda, M., Hiroyoshi, N., Ito, M., Okada, H., 2009b. Development of a new gravity separator for plastics —a hybrid-jig—. Mater. Trans. 50, 2844–2847. https://doi.org/10.2320/matertrans.M-M2009825

Ito, M., 2008. Recent developments in advanced coal cleaning. J. MMIJ 124, 865–870. https://doi.org/10.2473/journalofmmij.124.865

Ito, M., Tsunekawa, M., Ishida, E., Kawai, K., Takahashi, T., Abe, N., Hiroyoshi, N., 2010. Reverse jig separation of shredded floating plastics — separation of polypropylene and high density polyethylene. Int. J. Miner. Process. 97, 96–99. https://doi.org/10.1016/j.minpro.2010.08.007

Iveson, S.M., Hunter, D.M., Galvin, K.P., 2015. A water-based method for measuring density-based partition curves of separators used in coal and mineral processing. Miner. Eng. 79, 196–211. https://doi.org/10.1016/j.mineng.2015.06.008

Kademli, M., Gulsoy, O.Y., 2013. Investigation of using table type air separators for coal cleaning. Int. J. Coal Prep. Util. 33, 1–11. https://doi.org/10.1080/19392699.2012.717566

Kashiwaya, K., Noumachi, T., Hiroyoshi, N., Ito, M., Tsunekawa, M., 2012. Effect of particle shape on hydrocyclone classification. Powder Technology 226, 147–156. https://doi.org/10.1016/j.powtec.2012.04.036

Kawatra, S.K., Carlson, J.T., 2013. Beneficiation of Phosphate Ore. Society for Mining, Metallurgy, and Exploration, Englewood, Colorado.

Kikuchi, R., Kukacka, J., Raschman, R., 2008. Grouping of mixed waste plastics according to chlorine content. Sep. Purif. Technol. 61, 75–81. https://doi.org/10.1016/j.seppur.2007.10.001

Koppalkar, S., et al., 2013. Evolution of gold gravity recovery in grinding circuits – a critical review. CIM Journal. 167-174.

Korte, G.J., Engelbrecht, J., 2014. Dense medium cyclones. Int. J. Coal Prep. Util. 34, 49–58. https://doi.org/10.1080/19392699.2013.845009

Kousaka, Y., Okuyama, K., Payatakes, A.C., 1981. Physical meaning and evaluation of dynamic shape factor of aggregate particles. Journal of Colloid and Interface Science 84, 91–99. https://doi.org/10.1016/0021-9797(81)90262-9

Koyanaka, S., Endoh, S., Iwata, H., 1995. The recycling of printed wiring board scraps using a shape sorting technique. J. Soc. Powder Technol., Japan 32, 385–391. https://doi.org/10.4164/sptj.32.385

Koyanaka, S., Ohya, H., Endoh, S., Iwata, H., Ditl, P., 1997. Recovering copper from electric cable wastes using a particle shape separation technique. Advanced Powder Technology 8, 103–111. https://doi.org/10.1016/S0921-8831(08)60469-0

Krumbein, W.C., 1940. Flood gravel of San Gabriel Canyon, California. GSA Bulletin 51, 639–676. https://doi.org/10.1130/GSAB-51-639

Kroll-Rabotin, J.-S., Bourgeois, F., Climent, É., 2013. Physical analysis and modeling of the Falcon concentrator for beneficiation of ultrafine particles. Int. J. Miner. Process. 121, 39–50. https://doi.org/10.1016/j.minpro.2013.02.009

Kuang, S., Qi, Z., Yu, A.B., Vince, A., Barnett, G.D., Barnett, P.J., 2014. CFD modeling and analysis of the multiphase flow and performance of dense medium cyclones. Miner. Eng. 62, 43–54. https://doi.org/10.1016/j.mineng.2013.10.012

Kumar, C.R., Bhoja, S.K., Tripathy, S.K., Mohanan, S., Venugopalan, T., Suresh, N., 2013. Classification performance evaluation of floatex density separator for coal fines. Fuel 108, 303–310. https://doi.org/10.1016/j.fuel.2013.02.033

Kuwayama, Y., Ito, M., Hiroyoshi, N., Tsunekawa, M., 2011. Jig separation of crushed automobile shredded residue and its evaluation by float and sink analysis. J. Mater. Cycles. Waste Manag. 13, 240–246. https://doi.org/10.1007/s10163-011-0008-y

Lau, R., Chuah, H.K.L., 2013. Dynamic shape factor for particles of various shapes in the intermediate settling regime. Advanced Powder Technology 24, 306–310. https://doi.org/10.1016/j.apt.2012.08.001

Lee, J., et.al, 1997. Recovery of copper, tin and lead from the spent printed circuit boards (PCBs) by the shape separation method. Journal of the mining and materials processing institute of Japan. 113, 357-362.

Lees, G., 1964. The measurement of particle shape and its influence in engineering materials. Journal of British Granite and Whinstone Federation 4, 1–22.

Lewis, D.W., McConchie, D., 1994. Analytical Sedimentology. Springer US.

Lindley, K.S., Rowson, N.A., 1997. Feed preparation factors affecting the efficiency of electrostatic separation. Physical Separation in Science and Engineering. 8, 161-173. https://doi.org/10.1155/1997/70156

Liu, A., Gao, J., Fan, M., 2013. Performance of an air-injected water-only cyclone for the separation of fine coal. Int. J. Coal Prep. Util. 33, 218–224. https://doi.org/10.1080/19392699.2013.790817

Loth, E., 2008. Drag of non-spherical solid particles of regular and irregular shape. Powder Technol. 182, 342–353. https://doi.org/10.1016/j.powtec.2007.06.001

Lu, S., Lu, X., Yuan, Z., Zhang, C., Liu, J., Liu, P., Zhang, Y., 2016. The beneficiation of fine coal by a combination of three-product cyclone and fine screen. Int. J. Coal Prep. Util. 36, 207–217. https://doi.org/10.1080/19392699.2015.1100876

Maraspin, F., Bevilacqua, P., Rem, P., 2004. Modelling the throw of metals and nonmetals in eddy current separations. Int. J. Miner. Process. 73, 1–11. https://doi.org/10.1016/S0301-7516(03)00081-4

Masuda, H., Higashitani, K., Yoshida, H., 2006. Powder Technology Handbook, third ed. Taylor & Francis Group.

Meyer, E.J., Craig, I.K., 2015. Dynamic model for a dense medium drum separator in coal beneficiation. Miner. Eng. 77, 78–85. https://doi.org/10.1016/j.mineng.2015.03.002

Meyer, E.J., Craig, I.K., 2014. Coal dense medium separation dynamic and steady-state modelling for process control. Miner. Eng. 65, 98–108. https://doi.org/10.1016/j.mineng.2014.05.018

Meyers, A., Sherritt, G., Jones, A., O'Keeffe, M., 2014. Large-diameter dense medium cyclone performance in low-density/high near-gravity environment. Int. J. Coal Prep. Util. 34, 133–144. https://doi.org/10.1080/19392699.2014.869925

Mgangira, M.B., Komba, J., 2014. Correlations between aggregate particle shape parameters and size based on images captured using a 3-D laser scanning device. PEAT 15, 27–36. https://doi.org/10.2478/ijpeat-2013-0010

Mohanty, M., Zhang, B., Wang, H., Mahajan, A., Akbari, H., Bashir, Z., Ramamoorthy, S., Hirschi, J., 2014. Development and demonstration of an automation and control system for coal spirals. Int. J. Coal Prep. Util. 34, 157–171. https://doi.org/10.1080/19392699.2014.869930

Mohanty, M.K., Honaker, R.Q., 1999. Evaluation of the Altair centrifugal jig for fine coal separation. Int. J. Coal Prep. Util. 20, 85–106. https://doi.org/10.1080/07349349908945594

Mora, C.F., Kwan, A.K.H., 2000. Sphericity, shape factor, and convexity measurement of coarse aggregate for concrete using digital image processing. Cement and Concrete Research 30, 351–358. https://doi.org/10.1016/S0008-8846(99)00259-8

Muchová, L., Mooij, M., van Kooy, L., Berkhout, P., 2005. A cascade wire separator. Int. J. Miner. Process. 78, 40–48. https://doi.org/10.1016/j.minpro.2005.07.005

O'Brien, M., Firth, B., McNally, C., 2014. Effect of medium composition on dense medium cyclone operation. Int. J. Coal Prep. Util. 34, 121–132. https://doi.org/10.1080/19392699.2014.869924

Ohya, H., 1997. Study on Shape Separation of Particulate Materials. Thesis (PhD), National Institute for Resources and Environment, MITI, Japan.

Ohya, H., Iwata, H., Koyanaka, S., Endoh, S., 1999. Particle shape separation using horizontally circular motion plate. Resources Processing, Japan. 46, 13–18. https://doi.org/10.4144/rpsj1986.46.13

Park, C.H., Bae, K.H., Son, B.C., 1994. On the dry sorting machine, leap-bound picker; sorting mechanism and application (Part I). Resources Processing 41, 165–174. https://doi.org/10.4144/rpsj1986.41.165

Pita, F., Castilho, A., 2016. Influence of shape and size of the particles on jigging separation of plastics mixture. Waste. Manage. 48, 89-94. https://doi.org/10.1016/j.wasman.2015.10.034.

Pita, F., Castilho, A., 2017. Separation of plastics by froth flotation. The role of size, shape and density of the particles. Waste Manag. 60, 91–99. https://doi.org/10.1016/j.wasman.2016.07.041

Rahimi, M., Aslani, M.R., Rezai, B., 2012. Influence of surface roughness on flotation kinetics of quartz. J. Cent. South Univ. Technol. 19, 1206–1211. https://doi.org/10.1007/s11771-012-1130-2.

Sahu, A.K., Tripathy, A., Biswal, S.K., 2013. Study on particle dynamics in different cross sectional shapes of air dense medium fluidized bed separator. Fuel 111, 472–477. https://doi.org/10.1016/j.fuel.2013.04.011

Shen, H., Forssberg, E., Pugh, R.J., 2001. Selective flotation separation of plastics by particle control. Resources, Conservation and Recycling 33, 37–50. https://doi.org/10.1016/S0921-3449(01)00056-8

Shimizu, H., Miyazawa, T., Yamakaki, S., 2002. Dry separation technology of waste plastics. NKK Technical report, Japan. 176, 40-44.

Singh, R.K., Das, A., 2013. Analysis of separation response of Kelsey centrifugal jig in processing fine coal. Fuel Proc. Tech. 115, 71–78. https://doi.org/10.1016/j.fuproc.2013.04.005

Sneed, E.D., Folk, R.L., 1958. Pebbles in the Lower Colorado River, Texas a Study in Particle Morphogenesis. The Journal of Geology 66, 114–150.

Stener, J., 2015. Wet Low-Intensity Magnetic Separation: Measurement Methods and Modelling. Thesis (PhD), Lulea University of Technology, Sweden.

Stückrath, T., Völker, G., Meng, J., 2006. Classification of Shape and Underwater Motion Properties of Rock. Third Chinese-German Joint Symposium on Coastal and Ocean Engineering , National Cheng Kung University, Tainan ,November 8-16.

Tsunekawa, M., Naoi, B., Ogawa, S., Hori, K., Hiroyoshi, N., Ito, M., Hirajima, T., 2005. Jig separation of plastics from scrapped copy machines. Int. J. Miner. Process. 76, 67–74. https://doi.org/10.1016/j.minpro.2004.12.001

Tsunekawa, M., Kobayashi, R., Hori, K., Okada, H., Abe, N., Hiroyoshi, N., Ito, M., 2012. Newly developed discharge device for jig separation of plastics to recover higher grade bottom layer product. Int. J. Miner. Process. 114–117, 27–29. https://doi.org/10.1016/j.minpro.2012.09.003

Turton, R., Levenspiel, O., 1986. A short note on the drag correlation for spheres. Powder Technology 47, 83–86. https://doi.org/10.1016/0032-5910(86)80012-2

Uslu, T., Sahinoglu, E., Yavuz, M., 2012. Desulphurization and deashing of oxidized fine coal by Knelson concentrator. Fuel Proc. Tech. 101, 94–100. https://doi.org/10.1016/j.fuproc.2012.04.002

Verrelli, D.I., Bruckard, W.J., Koh, P.T.L., Schwarz, M.P., Follink, B., 2014. Particle shape effects in flotation. Part 1: Microscale experimental observations. Miner. Eng. 58, 80–89. https://doi.org/10.1016/j.mineng.2014.01.004

Wadell, H., 1932. Volume, Shape, and Roundness of Rock Particles. The Journal of Geology 40, 443–451.

Wang, Z., Kuang, Y., Deng, J., Wang, G., Ji, L., 2015b. Research on the intelligent control of the dense medium separation process in coal preparation plant. Int. J. Miner. Process. 142, 46–50. https://doi.org/10.1016/j.minpro.2015.05.001

Wentworth, C.K., 1919. A Laboratory and Field Study of Cobble Abrasion. The Journal of Geology 27, 507–521.

Wills, B.A., Napier-Munn, T.J., 2006. Mineral Processing Technology, seventh ed. Pergamon press, Oxford.

Yamamoto, K., Shiraiwa, M., Honda, Y., Sugimoto, M., 2009. Continuous separation of differently shaped particles in a horizontal flowing wet settler. J. Soc. Powder Technol., Japan 46, 688–697. https://doi.org/10.4164/sptj.46.688

Yamane, K., Ishihara, S., Soda, R., Kano, J., Saito, F., 2012. DEM simulation of sieving process about rod-like particles. J. Soc. Powder Technol., Japan 49, 818–826. https://doi.org/10.4164/sptj.49.818

Yang, X., Zhao, Y., Luo, Z., Song, S., Chen, Z., 2013a. Fine coal dry beneficiation using autogenous medium in a vibrated fluidized bed. Int. J. Miner. Process. 125, 86–91. https://doi.org/10.1016/j.minpro.2013.10.003

Yang, X., Zhao, Y., Luo, Z., Song, S., Duan, C., Dong, L., 2013b. Fine coal dry cleaning using a vibrated gas-fluidized bed. Fuel Proc. Tech. 106, 338–343. https://doi.org/10.1016/j.fuproc.2012.08.019

Yang, W.C., 2013. Handbook of Fluidization and Fluid-Particle Systems. Marcel Dekker, Inc., New York.

Yazici, E., R, Y., Deveci, H., Alp, I., 2010. Eddy Current Separation of Metals from E-wastes. The XIIth International Mineral Processing Symposium, Cappadocia-Nevsehir, Turkey, October 6-8.

Yoshida, T. et al., 1998. An advanced air-sorting method to separate shredded aluminum and copper waste. Waste management research, Japan. 9, 95–103.

Yu, X., Luo, Z., Li, H., Yang, X., Zhou, E., Jiang, H., Wu, J., Song, S., Cai, L., 2016. Effect of vibration on the separation efficiency of high-sulfur coal in a compound dry separator. Int. J. Miner. Process. 157, 195–204. https://doi.org/10.1016/j.minpro.2016.10.008

Zingg, T., 1935. Bietrahe zur Schotteranalyse. 15, 1935 Schweiz. Miner. Petrog. 15, 139-140.

Zhang, B., Zhao, Y., Luo, Z., Song, S., Li, G., Sheng, C., 2014. Utilizing an Air-Dense Medium Fluidized Bed Dry Separating System for Preparing a Low-Ash Coal. Int. J. Coal Prep. Util. 34, 285–295. https://doi.org/10.1080/19392699.2014.880695

Zhang, S., Forssberg, E., 1997. Mechanical separation-oriented characterization of electronic scrap. Resources, Conservation and Recycling 21, 247–269. https://doi.org/10.1016/S0921-3449(97)00039-6

Zhang, S., Forssberg, E., Arvidson, B., Moss, W., 1998. Aluminum recovery from electronic scrap by High-Force® eddy-current separators. Resources, Conservation and Recycling 23, 225–241. https://doi.org/10.1016/S0921-3449(98)00022-6

Zhou, E., Zhao, Y., Duan, C., Yang, X., Yu, X., Li, G., Liufeng, Y., Fan, X., Zhang, Y., 2016. Fluidization characteristics and fine coal dry beneficiation using a pronation-grille baffle dense phase medium fluidized bed. Fuel 185, 555–564. https://doi.org/10.1016/j.fuel.2016.08.029

CHAPTER 3 – THE EFFECTS OF PARTICLE GEOMETRY ON JIG SEPARATION EFFICIENCY OF CRUSHED PLASTICS

3.1 Introduction

In jigs, separation is facilitated by the differences in particle motion and velocity. For example, Brozek and Surowiak (2007) reported that the velocity of particles during jig separation is affected by not only the particle's density but also its geometrical properties like size and shape. This means that understanding the effects of particle size and shape is important in designing jig separation processes appropriate for the separation of various materials in plastic-dominated wastes. There are many studies about the effects of particle size on jig separation. For example, Woollacott and Silwamba (2016) reported that when the spherical glass beads (same density and shape) of different diameters (size) is mixed, size segregation mechanisms changed during jig separation depending on the differences in particle diameters. In contrast, only a few studies have been done on the effects of particle shape on jig separation efficiency especially in resources recycling. For crushed plastics, Pita and Castilho (2016) reported that particle shape became more important during jig separation at coarser particle size distribution. One limitation of the previous work of Pita and Castilho (2016) was the use of a very narrow size distribution range of crushed plastics that do not represent real plastics in wastes. Moreover, these authors did not evaluate in detail how crushing influenced changes in size and shape and why the shape of particles strongly affected the separation efficiency of jig separation.

These two issues will be addressed in this chapter because they are critical in the design of appropriate jig separation techniques for resources recycling. Specifically, the objectives of this study are as follows: (1) elucidate the effects of crushing on the geometrical properties of crushed plastics, (2) investigate the probability of passage of crushed particles during screening, (3) determine the effects of particle shape on the settling velocity, and (4) evaluate the jig separation efficiency of crushed single-type and mixed-type plastics with a wide variety of size and shape.

3.2 Materials and methods

3.2.1 Sample preparation and characterization

2-mm and 3-mm thick acrylonitrile butadiene styrene (ABS, specific gravity (SG) = 1.03) and polystyrene (PS, SG = 1.06) boards were crushed by a cutting mill (Orient mill, VH16, Seishin Enterprise Co., Ltd, Japan) to obtain samples shown in Table 3-1. For sample characterization, +2.0–8.0 mm samples (A-1, A-2, P-1 and P-2) were sieved to +2.0–2.8, +2.8–4.0, +4.0–5.6 and +5.6–8.0

mm and the short (*S*), intermediate (*I*) and long (*L*) axes (Fig. 3-1) of one hundred particles from each size fraction were measured using a Vernier caliper.

Table 3-1. A brief description of samples used in this study.

Samples	Type of plastic (abbreviation)	Board thickness [mm]	SG	Size fraction [mm]
A-1	Acrylonitrile butadiene styrene (ABS)	2	1.03	+2.0–8.0
A-2		3		
P-1	Polystyrene (PS)	2	1.06	
P-2		3		

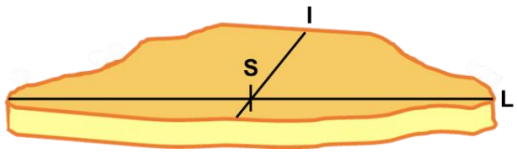

Figure 3-1. A schematic diagram showing the short (*S*), intermediate (*I*) and long (*L*) axes of crushed plastic particles.

3.2.2 Jig separation experiments

A desktop-type batch-wise RETAC jig with a separation chamber 145-mm long, 155-mm wide and 320-mm high was used in the experiments (Fig. 3-2). The jig separation experiments were carried out under the following conditions: displacement of 20 mm, frequency of water pulsation equal to 30 cycles/minute, addition of 15 ppm of Di-2-ethylhexyl sodium sulfosuccinate (AOT, $C_{20}H_{37}NaO_7S$, Wako Pure Chemical Industries, Ltd., Japan) as a wetting agent, and separation time of 3 minutes. After each experiment, the products were divided into six layers from the top (Fig. 3-2) and collected using a vacuum sampling system.

3.2.2.1 Jig separation of single-type plastic samples

200 g of each type of plastic sample (A-1, A-2, P-1 and P-2) (Table 3-1) was fed into the jig separation chamber and jig separation was carried out individually under the conditions outlined in the previous sub-section. After the experiments, sieving was carried out on each layer to determine the size distribution of the products.

3.2.2.2 Jig separation of mixed-type plastic samples

For these experiments, four mixtures of ABS and PS were used as follows: (i) A-1 (100 g) and P-1 (100 g), (ii) A-1 (100 g) and P-2 (100 g), (iii) A-2 (100 g) and P-1 (100 g), and (iv) A-2 (100 g) and P-2 (100 g). After jig separation, ABS and PS in each layer were separated by hand to determine the purity of jig products.

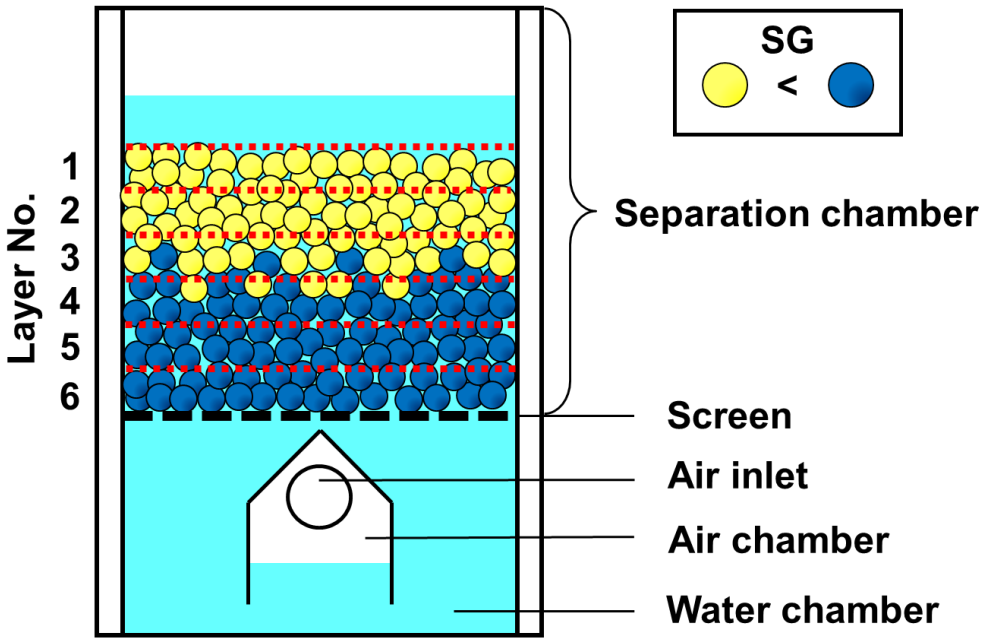

Figure 3-2. A schematic illustration of a desktop-type batch-wise RETAC jig and how the products were partitioned into 6 layers.

3.2.3 Settling velocity measurements in static water

Settling velocities of crushed plastic particles were measured in the jig separation chamber (60-mm long, 60-mm wide and 150-mm high) filled with water under static conditions. Twenty random particles from each size fraction (+2.0–2.8, +2.8–4.0, +4.0–5.6 and +5.6–8.0 mm) were dropped one by one with different initial orientations from the water surface (Fig. 3-3). The average settling velocities of the particles were obtained by image analysis (WinRoof, Mitani Corporation, Japan) from high-definition video recordings of the experiments.

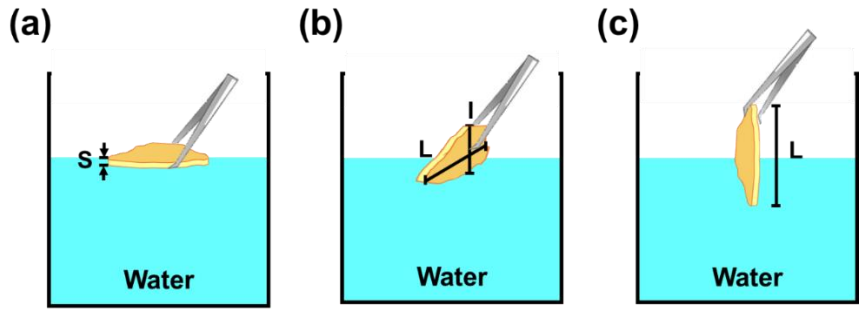

Figure 3-3. Initial orientations of crushed plastic particles for the settling velocity measurements.

3.3 Results and discussion

3.3.1 Sample characterization

Three descriptors were used in this study to describe the shape of particles: (1) operational sphericity, (2) flatness ratio and (3) elongation ratio. Sphericity is a three-dimensional shape descriptor generally viewed with reference to a sphere. Wadell (1932) defined operational sphericity (ψ) as the ratio of particle surface area to the area of a sphere that has the same volume as the particle and is given by the following equation:

$$Operational\ sphericity\ (\psi) = \left(\frac{SI}{L^2}\right)^{\frac{1}{3}} \tag{3-1}$$

where *S*, *I* and *L* are the short, intermediate and long axis dimensions of the particle, respectively (Fig. 3-1). Based on this equation, a sphere has a sphericity equal to 1 while particles having other shapes have sphericities < 1 (Mora and Kwan, 2000).

Although sphericity could differentiate spheres from non-spherical particles, this descriptor cannot distinguish non-spherical shapes like rod-like and disk-like particles. To describe particle shapes in more detail, Zingg (1935) developed a more versatile shape classification scheme that uses flatness ratio ($\emptyset_{Flat}$) (Eq. 3-2) and elongation ratio($\emptyset_{Elong}$) (Eq. 3-3) based on particle dimensions along the three principal axes, which are defined as follows:

$$\emptyset_{Flat} = \frac{S}{I} \tag{3-2}$$

$$\emptyset_{Elong} = \frac{I}{L} \tag{3-3}$$

A sphere has $\emptyset_{Flat}$ and $\emptyset_{Elong}$ of one ($S = I = L$) while particles having other shapes show $\emptyset_{Flat}$ and $\emptyset_{Elong}$ of less than one (low $\emptyset_{Flat}$ = disk-like and low $\emptyset_{Elong}$ = rod-like).

Based on the values of $\emptyset_{Flat}$ and $\emptyset_{Elong}$, particle shape could be classified into four types: sphere-like, disk-like, rod-like and blade-like (Arasan et al., 2011). Fig. 3-4 shows the Zingg diagram superimposed with curves of operational sphericity.

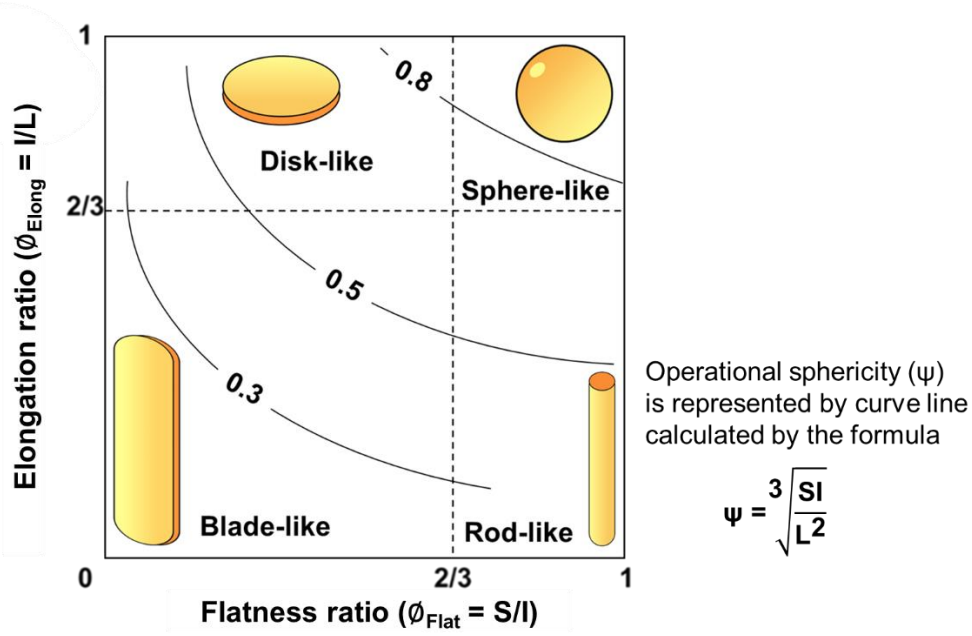

Figure 3-4. The Zingg diagram superimposed with operational sphericity (Zingg, 1935).

Fig. 3-5 shows the Zingg diagrams of crushed plastics and the average values of ψ, $Ø_{Flat}$, and $Ø_{Elong}$ are summarized in Table 3-2. These results showed that after crushing, more sphere-like particles were generated from P-2 while disk-like particles were more abundant in A-1. Fig. 3-6 shows the average $Ø_{Flat}$ and $Ø_{Elong}$ in each size fraction of the crushed plastic samples. The $Ø_{Flat}$ of samples decreased with increasing particle size but values of $Ø_{Elong}$ were very similar regardless of particle size. This difference could be attributed to the unique way that plastic boards of uniform thickness (e.g., housings and casings of waste electrical and electronic equipment (WEEE)) are crushed (Fig. 3-7); that is, size reduction mainly occurs in the intermediate (breadth, *I*) and long (length, *L*) axis directions rather than in the short (thickness, *S*) axis direction. In other words, the $Ø_{Flat}$ (*S*/*I*) tends to increase as particles become smaller due to the preferential crushing that occurs along the intermediate axis while the short axis (i.e., thickness) remains constant. In comparison, $Ø_{Elong}$ (*I*/*L*) is not related to the thickness or short axis, so large particles retained the board's disk-like shape while finer ones are more sphere-like (Fig. 3-7).

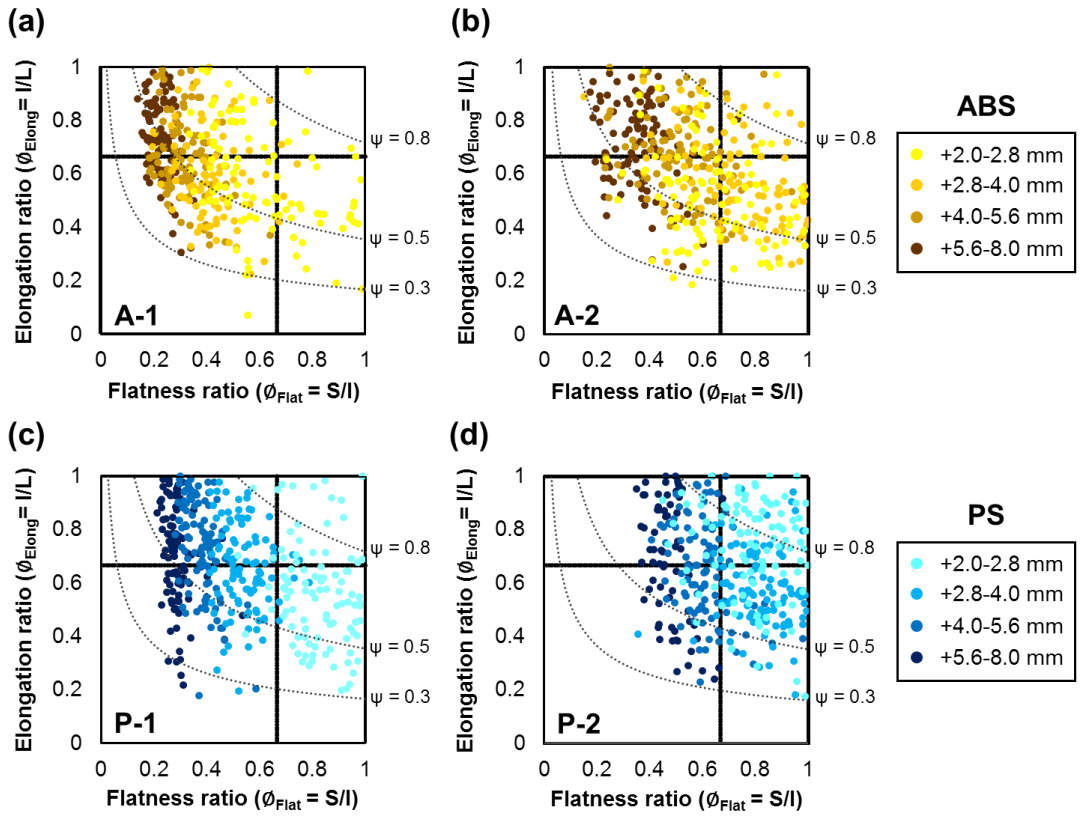

Figure 3-5. Zingg diagrams showing the particle shape distribution and operational sphericity of samples (a) A-1, (b) A-2, (c) P-1, and (d) P-2.

Table 3-2. Average values of operational sphericity (ψ), flatness ratio ($Ø_{Flat}$), and elongation ratio ($Ø_{Elong}$) calculated by Eq. (3-1), (3-2) and (3-3), respectively.

Samples	**Operational sphericity (ψ)**	**Flatness ratio ($Ø_{Flat}$)**	**Elongation ratio ($Ø_{Elong}$)**
A-1	0.52 ± 0.03	0.39 ± 0.14	0.64 ± 0.06
A-2	0.58 ± 0.03	0.56 ± 0.14	0.63 ± 0.08
P-1	0.59 ± 0.02	0.51 ± 0.20	0.66 ± 0.06
P-2	0.66 ± 0.06	0.67 ± 0.14	0.66 ± 0.05

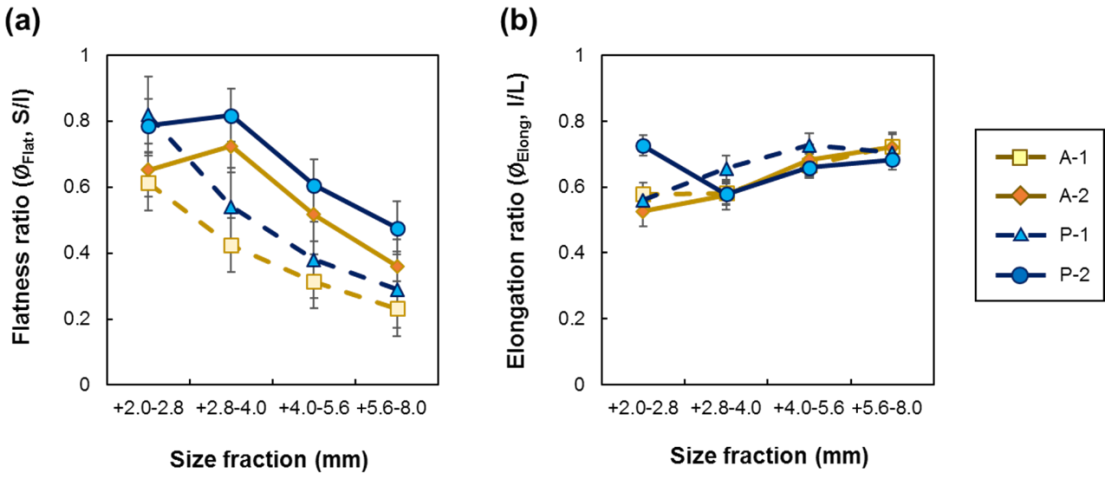

Figure 3-6. Changes in the average values of (a) flatness ratio ($Ø_{Flat}$) and (b) elongation ratio($Ø_{Elong}$) of plastic samples as a function of particle size distribution.

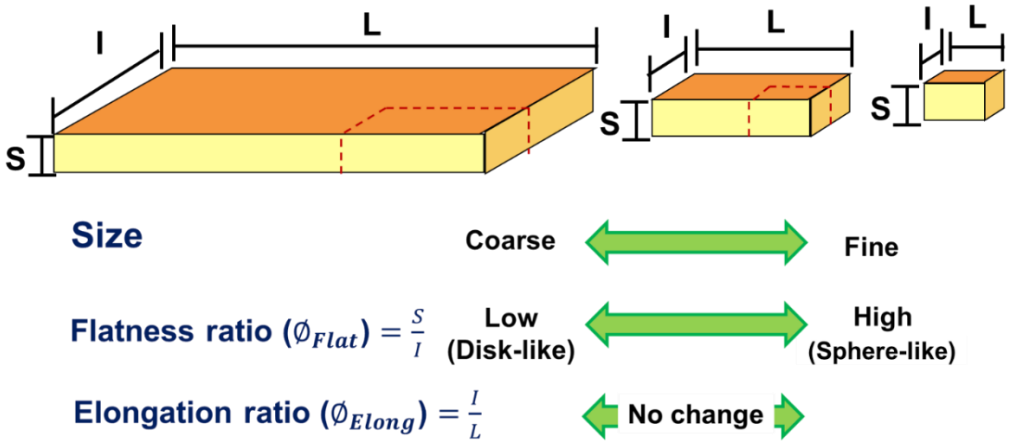

Figure 3-7. A schematic diagram of particle shape changes during crushing.

3.3.2 Settling velocity measurements in static water

In physical separation especially gravity-based techniques, various materials are separated in a fluid media like water or air (Brozek and Surowiak, 2007; Concha, 2013). In this fluid medium, a particle's movement defined by its settling velocity is not only influenced by the particle's composition (i.e., SG) and size but also by its shape (Barton, 1979; Gabitto and Tsouris, 2008). This means that in gravity separation techniques like jigs, separation efficiency, which is dependent on the differences of settling velocities of particles, is strongly influenced by their SG, size and shape.

In a RETAC jig, water pulsation is comprised of 4 steps: (1) rising, (2) initial holding, (3) downwelling, and (4) final holding (Fig. 3-8). In step (1), water rises to lift particles and dilate the

particle bed (i.e., fluidization). Once the rising movement of the fluid stops in step (2), particles start to settle down in water under static condition. Particles that do not reach the bottom continue to settle down in steps (3) and (4) before starting the next cycle. Based on previous studies of the authors, step (2) is the most important step among these 4 steps in a RETAC jig (Hori et al, 2009; Ito et al, 2010).

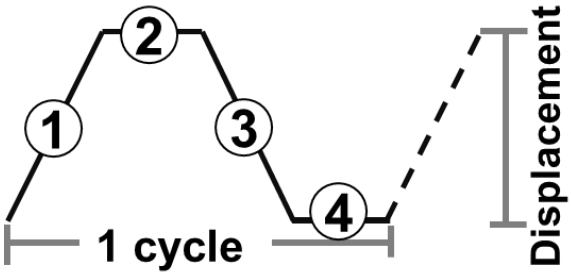

Figure 3-8. The four steps in the wave-form pattern of a RETAC jig.

In this section, the effects of particle size and shape on the settling velocity of crushed plastics in static water with different initial orientations (Fig. 3-3) were investigated. The results showed that the settling velocity was independent of the particle's initial orientation (Fig. 3-9) because as the particles settle down, they rapidly reoriented towards a sort of "stable" orientation as they reached terminal velocity (This "stable" orientation is very similar to that shown in Fig. 3-3a) (Dharmarajah, 1982; Masuda et al, 2006; Yang, 2013).

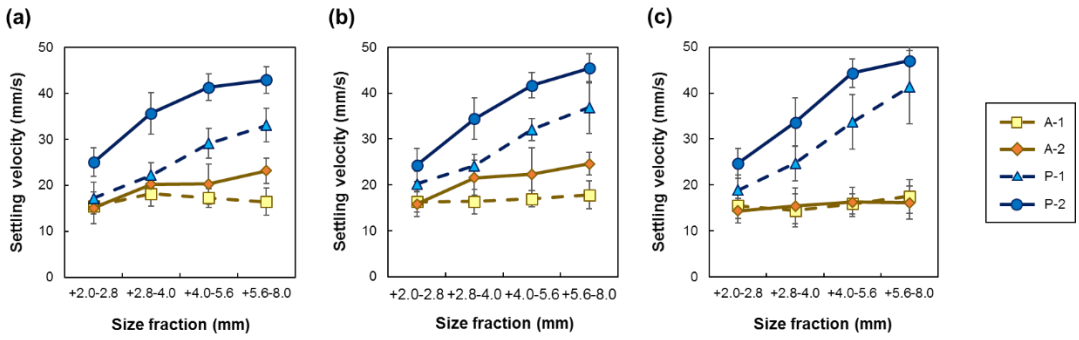

Figure 3-9. Average settling velocities of samples at different size fractions with initial orientation: (a) Fig. 3-3a, (b) Fig. 3-3b and (c) Fig. 3-3c.

Fig. 3-10 illustrates the average settling velocities of randomly selected particles from A-1, A-2, P-1 and P-2 of various size fractions (+2.0–2.8, +2.8–4.0, +4.0–5.6, and +5.6–8.0 mm) and the results showed three important points. In terms of the size fraction, settling velocity of sphere-like PS (P-2) increased with increasing particle size while that of disk-like ABS (A-1) was independent of the particle size. In term of the initial thickness of plastic boards, particles from thicker plastic boards (e.g., 3-mm thick A-2) had higher settling velocities compared with the thinner plastic boards (e.g., 2-mm thick A-1) because particles in the former were relatively larger, heavier and had more sphere-like shapes. The effects of SG on the settling velocity was more straightforward; that is, particles of PS (SG = 1.06) had relatively faster settling velocities than those of ABS (SG = 1.03) because they are heavier.

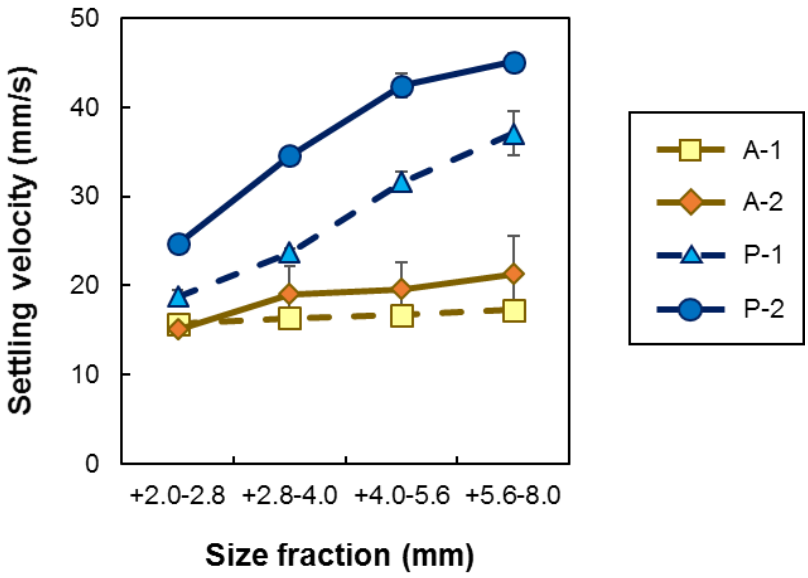

Figure 3-10. Average settling velocities of random particles from different size fractions.

A particle settling down in water is strongly influenced by three forces, gravity (F_G; Eq. 3-4), buoyancy (F_B; Eq. 3-5) and drag force (F_D; Eq. 3-6), and its settling velocity is determined by the balance between these three forces (Eq. 3-7).

$$F_G = mg \tag{3-4}$$

$$F_B = \frac{m}{\rho_P}\rho_F g \tag{3-5}$$

$$F_D = C_D A \frac{\rho_F v^2}{2} \tag{3-6}$$

$$m\frac{dv}{dt} = mg - \frac{m}{\rho_P}\rho_P - C_D A\left(\frac{\rho_P v^2}{2}\right) \tag{3-7}$$

where m = mass of the particle (kg); $m = \rho_P V$ (V = volume of particle (m^3))

v = velocity of particle (m/s)

t = time (s)

g = gravitational acceleration (m/s^2)

ρ_P = density of particle (kg/m^3)

ρ_F = density of fluid (kg/m^3)

C_D = drag coefficient

and A = projection area of particle (m^2)

When a particle reaches terminal velocity (v_∞), acceleration (dv/dt) becomes zero and Eq. (3-7) can be simplified to Eq. (3-8).

$$0 = (\rho_P - \rho_F)gV - C_D A\left(\frac{\rho_F {v_\infty}^2}{2}\right) \tag{3-8}$$

If the particle is a sphere, the projection area (A) is given by Eq. (3-9).

$$A = \frac{\pi D^2}{4} \tag{3-9}$$

The drag coefficient (C_D) in Eq. (3-8), could also be expressed as a function of the Reynolds number (Re_p) assuming a laminar flow regime during particle settling ($Re_p < 2$) (Eqs. 3-10&11).

$$Re_p = \frac{vD\rho_F}{\mu} \tag{3-10}$$

$$C_D = 24/Re_p \tag{3-11}$$

where μ is the viscosity of fluid (Pa·s)

By substituting Eqs. (3-9,10&11) to Eq. (3-8), the terminal velocity of a sphere could be calculated and is given as;

$$v_\infty = \frac{(\rho_P - \rho_F)g}{3\pi\mu}\frac{V}{D} \tag{3-12}$$

Using Eq. (3-12), the settling velocity results in Fig. 3-10 can be discussed from two different perspectives: (1) when the particle volume (V) is the same using fluid mechanics, and (2) when the particle sizes (D) are equal using the concepts of mineral processing.

Fig. 3-11 illustrates the balance of forces acting on a particle having the same volume but different shapes. In fluid mechanics, the movement of a particle in fluid is commonly discussed in terms of its volume (Yang, 2013). When two particles of equal volume (V) but of different shapes settle down in a fluid, the settling velocity of the more disk-like particle is generally slower than the sphere-like particle (Eq. 3-12). This is because the drag force acting on the more disk-like particle is larger than that of the more sphere-like particle due to the larger projection area (A) and larger projection area diameter (D_a) of the former (Masuda et al, 2006; Yang, 2013).

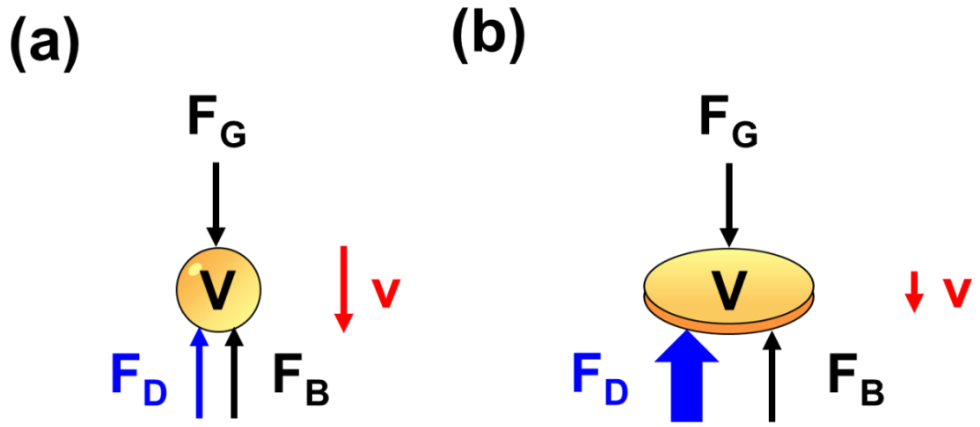

Figure 3-11. Schematic diagrams of the balances of forces acting on particles with the same volume (V) but different shapes: (a) sphere-like, and (b) disk-like.

In mineral processing and resources recycling especially when gravity separation is used, sizing is commonly applied prior to separation since particle size is an important parameter for separation. For coarse particles, sizing is usually carried out using screens while for fine particles, size classification using a fluid (e.g., spiral classifier, hydrocyclone) is used (Wills and Napier-Munn, 2006). In the case of jig separation, industrial screens are usually applied for coarse particles (>0.5 mm), so the probability of passage, which is evaluated using particle diameter, is essential. The particle size of an ideal particle like a sphere is easily defined by its geometrical diameter (D) while for non-spherical particles, their sizes could be defined by several statistical diameters (e.g., Feret's and

Martin's diameters), which are usually measured using two or three-dimensional image analysis (Masuda et al, 2006). Another way to define the size of a non-spherical particle is to use equivalent volume diameter (D_V), which is defined as the diameter of a sphere that have the same volume as the non-spherical particle (Yang, 2013).

During screening, a sphere can pass through the screen if it has a diameter (D) smaller than the screen aperture (Beunder, 2000; Beunder and Rem, 1999; Wills and Napier-Munn, 2006) while for a disk ($\emptyset_{Flat}<1$ and $\emptyset_{Elong}=1$), its probability of passage is dependent on the equivalent projection area diameter (D_a) as shown in Fig. 3-12. A disk can pass through the screen if it has D_a smaller than the screen aperture. Screening of crushed plastics showed that only particles with I (breadth, intermediate axis direction) shorter than the screen aperture could pass. This means that the same size fraction (e.g., 5.6-8.0 mm) after screening contains particles with the same I but different V because their thicknesses (S) are not the same.

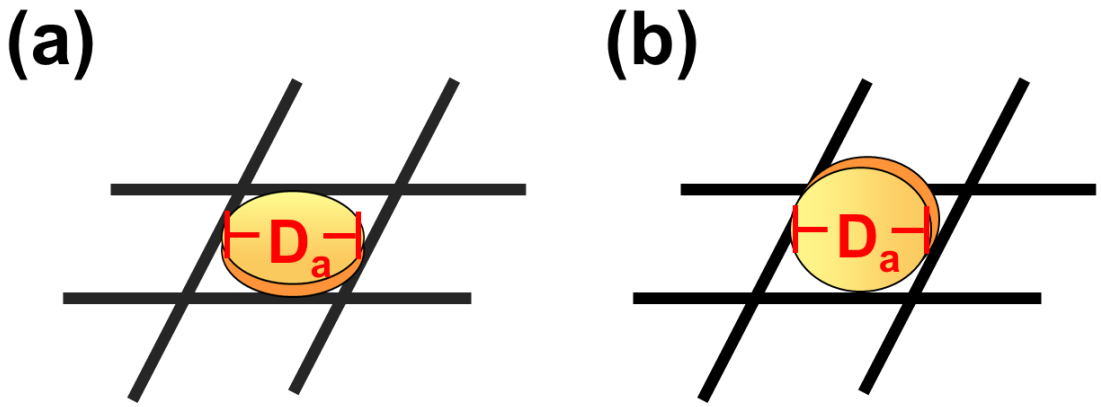

Figure 3-12. A schematic diagram of the probability of passage of disk-like particles at different orientations relative to the screen's aperture.

Fig. 3-13 illustrates the balance of forces acting on particles with the same D_a but different shapes. Note that in Eq. (3-12), V is a function of the both gravity and buoyancy forces, when a sphere and a disk are compared in term of their settling velocities, the former will have a higher settling velocity than the latter because V of a sphere is larger than a disk. This phenomenon can be explained by the observed results in Fig. 3-10. In addition, the settling velocity of crushed plastics is affected by the initial thickness of plastic boards prior to crushing. For examples, A-2 (ψ_{avg} = 0.58) and P-2 (ψ_{avg} = 0.65), both 3-mm thick, had higher settling velocity than A-1 (ψ_{avg} = 0.52) and P-1 (ψ_{avg} = 0.58), which came from thinner boards (Fig. 3-10).

The results of settling velocity in terms of the size fraction (Fig. 3-10) could be explained by the change of particles shape during crushing. As explained above, size reduction of board-shaped materials like housing and casings of home appliances and electronic devices mainly occurred on the intermediate (breadth, *I*) and long (length, *L*) axis directions but scarcely on the short (thickness, *S*) axis direction resulting in more disk-like particles in the coarser fractions while finer fractions have more sphere-like components. In other words, the relationship between volume (*V*) and projection area diameter (D_a) is different depending on the shape of particles.

For a sphere where $V = \pi D^3/6$; $V_{sphere} \propto D^3$, Eq. (3-12) can be expressed as Eq. (3-13).

$$v_{\infty-sphere} = \frac{(\rho_P - \rho_F)g}{18\mu} D^2 \tag{3-13}$$

From Eq. (3-13), the settling velocity increase with increasing particle size (*D*) that was in line with the settling velocity results P-2 that having sphere-like shape in all size fractions indicated that settling velocity of sphere-like particles have higher dependent on particle size (Fig. 3-10). While for A-1 that contained coarse fraction having more disk-like shape (A-1, +5.6-8.0 mm, $\psi_{avg} = 0.49$) while fine fraction having more sphere-like shape (A-1, +2.0-2.8 mm, $\psi_{avg} = 0.57$), was independent of the particle size.

For a disk with $V = \pi D_a^2 S/4$ and $V_{disk} \propto D^2$ (D_a=*I*=*L* and *S*<<D_a), Eq. (12) could be written as Eq. (3-14).

$$v_{\infty-disk} = \frac{(\rho_P - \rho_F)gS}{12\mu} D \tag{3-14}$$

Since the relationship of volume (*V*) and projection area diameter (D_a) changes depending on the shape of particles ($V \propto D^3$ and $V \propto D^2$), it follows that the relationship of settling velocity (v_∞) and projection area diameter (D_a) also depends on the shape of particles ($v_{\infty\text{-}sphere} \propto D^2$ and $v_{\infty\text{-}disk} \propto D$). These equations, for example, could satisfactorily explain the settling velocity results observed in sample A-1. When the particle size (D_a) increased from fine particle, sphere-like shape settling velocity did not increase due to the particle shape changed to be disk-like (relationship of settling velocity (v_∞) and projection area diameter (D_a) become smaller). These was also in line with the discussion in terms of fluid mechanics; that is, increasing of particle size (D_a) could increase gravity force (F_G) due to the increasing *V* while increasing the particle size (D_a) could also increase drag force (F_D) due to the change of particles shape, indicating that the effects of size and shape were negated (Fig. 3-10).

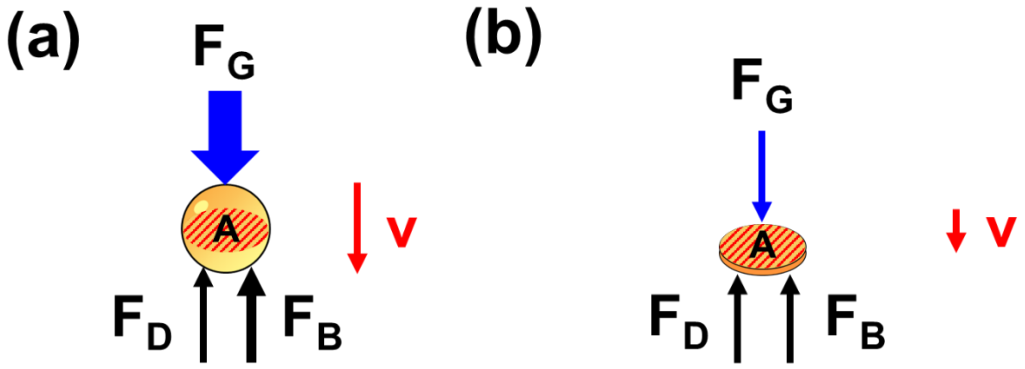

Figure 3-13. Schematic diagrams of the balances of forces acting on particles with the same projection area (A) and equivalent projection area diameter (D_a) but different shapes: (a) sphere-like, and (b) disk-like.

3.3.3 Jig separation

3.3.3.1 Jig separation of single-type plastic samples

The results above indicate that particle geometry (i.e., particle size and shape) is crucial during jig separation because of its strong influence on the settling velocity of particles, so to investigate how the shape of particles affect jig separation without the influence of SG, experiments were carried out using single-type crushed A-1, A-2, P-1 and P-2 with particle size distribution of +2–8 mm. After jig separation, the products were divided into six layers from the top (Fig. 3-2) and products from each layer was screened to determine their size distribution.

Fig. 3-14 shows the particle size distribution in each layer after jig separation of single-type crushed ABS and PS (+2–8 mm). The jig separation results for P-2 showed that coarse particles were recovered in the bottom layer while fine particles were mostly recovered in the top layer (Fig. 3-14(d)) because this crushed plastic sample is dominated by sphere-like particles regardless of the size fraction. When majority of particles are sphere-like, their settling velocity in a fluid increases with increasing particle diameter (D), which means that size segregation during jig separation largely occurs due to differences in settling velocities of fine and coarse particles as explained earlier (Fig. 3-15(a)) (Woollacott and Silwamba, 2016).

In contrast, coarse, disk-like particles were recovered in the top layer while the fine, sphere-like particles were predominantly found in the bottom layers in the case of A-1 ($\emptyset_{Flat}$ of this sample drastically decreased with increasing particle size) (Fig. 3-13(a)). Although the settling velocity results of A-1 showed similar values at all size fractions (Fig. 3-10). This interesting phenomenon could be attributed to the effects of consolidation trickling. As explained earlier, water pulsation in a RETAC jig has four steps and in step (2), particles start to settle down in water under static condition. During

this period, coarse and fine particles of A-1 are all settling down with similar settling velocities (Fig. 3-15(b)). However, if the settling period (steps 2 and 3) are long enough, consolidation trickling may occur (Fig. 3-15(b)). Consolidation trickling is a phenomenon whereby smaller particles move downwards under the influence of gravity through interstices generated the interlocking of larger particles (Wills and Napier-Munn, 2006). The effects of consolidation tricking are further magnified in step (3) of the water pulsation cycle because of water suction (Fig. 3-15(b)). In contrast, A-2 and P-1 that have settling velocities and $\emptyset_{Flat}$ values between A-1 and P-2 showed similar size in all layers because consolidation tricking was minimized the larger differences in settling velocities of coarse and fine particles (Fig. 3-10).

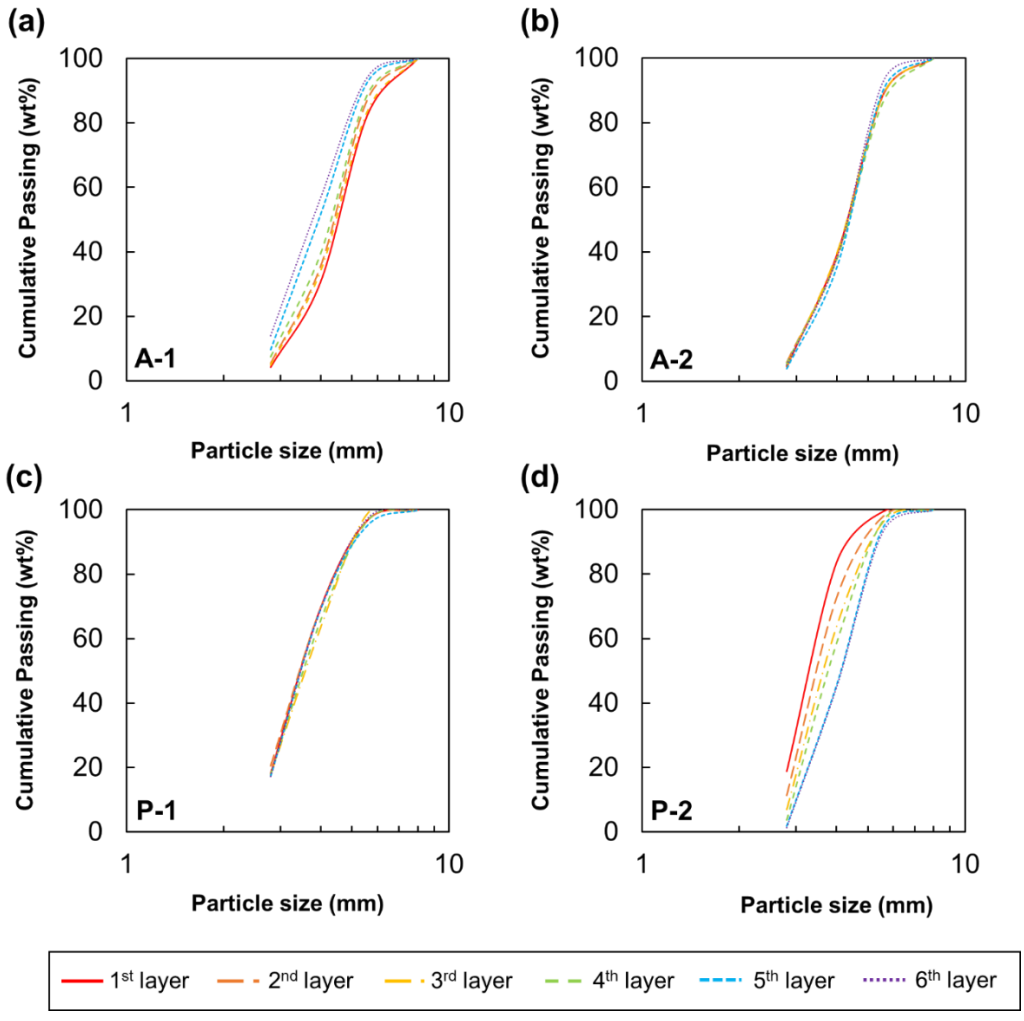

Figure. 3-14. Size distribution of each layer after jig separation of (a) A-1, (b) A-2, (c) P-1, and (d) P-2.

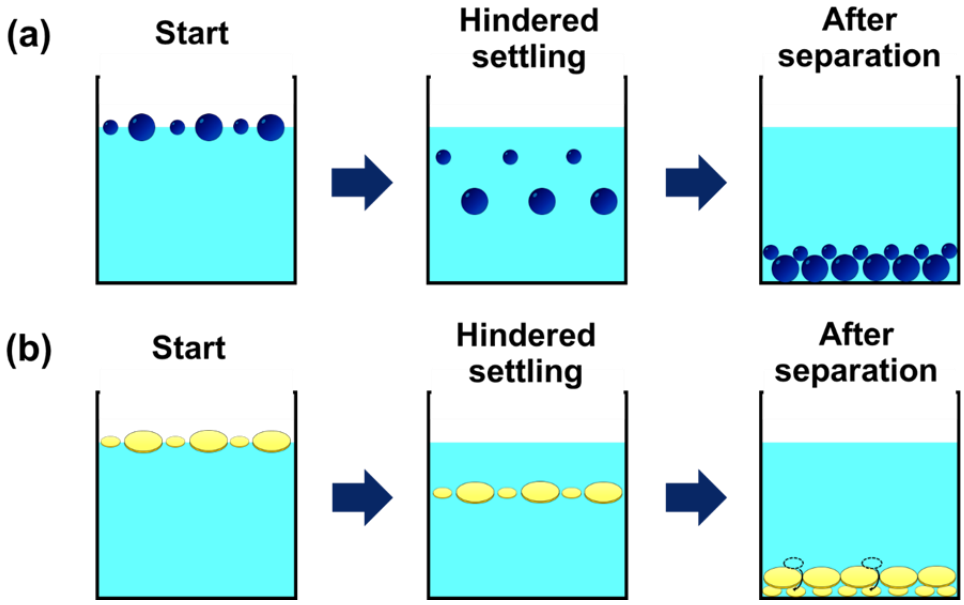

Figure. 3-15. Schematic diagrams of size segregation during jig separation of (a) sphere-like particles (i.e., P-2), and (b) disk-like particles (i.e., A-1).

3.3.3.2 Jig separation of mixed-type plastic samples

To investigate the effects of shape on jig separation, mixtures of lighter ABS (A-1 or A-2) and heavier PS (P-1 or P-2) were used for these experiments. After the experiments, products were divided into six layers from the top (Fig. 3-2) and plastics in each layer were separated by hand to determine their purity.

Fig. 3-16 shows the distribution of ABS and PS in the different layers after jig separation. Under all conditions, light, ABS particles were recovered in top layers while heavy, PS particles were recovered in bottom layers, which means that SG is the most important parameter in jig separation when $0.2 < \emptyset_{Flat} < 0.9$. Better separation was also observed when the plastic mixture is composed of light, disk-like particles (A-1) and heavy, sphere-like particles (P-2) (Fig. 3-16b). Unfortunately, separation of the plastic mixture of light, sphere-like particles (A-2) and heavy, disk-like particles (P-1) was difficult because of their very similar settling velocities (Fig. 3-16c).

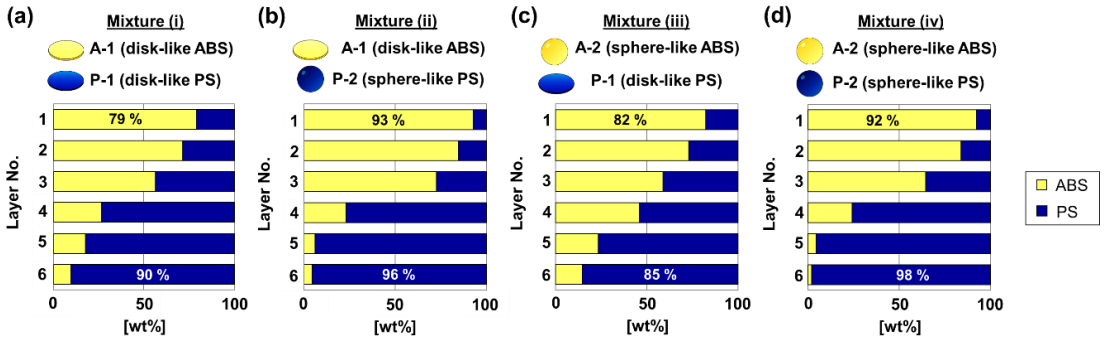

Figure 3-16. Distribution of ABS and PS in each layer after jig separation of (a) mixture (i) (A-1 and P-1), (b) mixture (ii) (A-1 and P-2), (c) mixture (iii) (A-2 and P-1) and (d) mixture (iv) (A-2 and P-2).

Fig. 3-17 illustrates the partial separation efficiency curves of jig separation. The horizontal axis represents the distance from the bottom screen (H: height of the center position of each layer) and the vertical axis is equal to the purity of ABS in each layer. The sharpness index (SI) was calculated from the partial separation efficiency curves shown in Fig. 3-17 by following equation:

$$SI = \frac{Height_{84.13} - Height_{50}}{Height_{50}} \tag{3-15}$$

where $Height_{50}$ and $Height_{84.13}$ are the height when the purity is 50 and 84.13%, respectively. The SI value is low when the separation efficiency is high. SI of mixture (ii) was the lowest (SI = 0.38) while that of mixture (iii) was the highest (SI = 0.74).

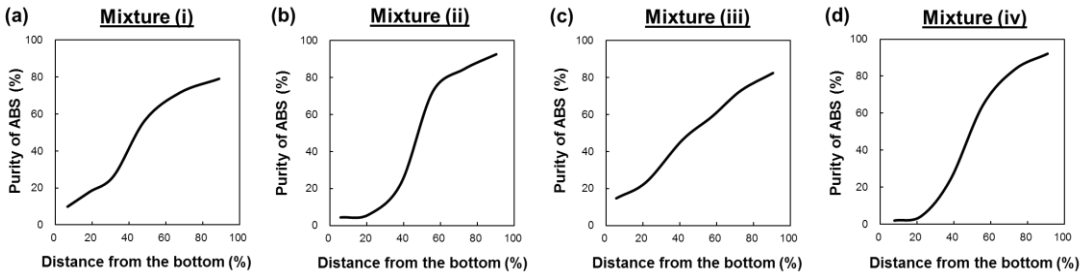

Figure 3-17. Partial separation efficiency curves after jig separation of (a) mixture (i) (A-1 and P-1), (b) mixture (ii) (A-1 and P-2), (c) mixture (iii) (A-2 and P-1) and (d) mixture (iv) (A-2 and P-2).

Fig. 3-18 shows the relationship between the ratio of settling velocity of heavy and light particles (v_{heavy}/v_{light}, average v of all size fractions in Fig. 3-10) and SI. The results showed that better jig separation was obtained when the differences of settling velocities were large (i.e., high v_{heavy}/v_{light}),

which means that separation efficiency during jig separation of crushed plastics is dependent on not only SG but also the shape of particles.

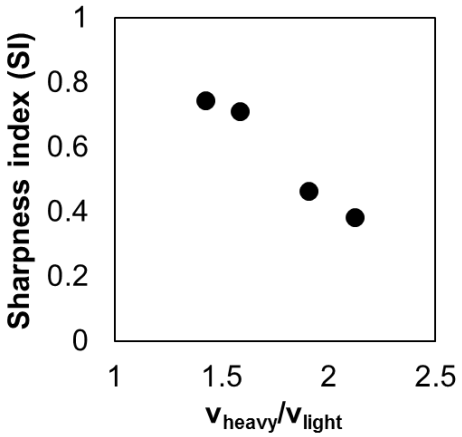

Figure 3-17. Relationship between sharpness index (SI) and v_{heavy}/v_{light}.

3.4 Conclusions

This chapter investigated the effects of particle geometry (i.e., size and shape) on jig separation of crushed plastics and the findings of this study are summarized as follows:

- When board-like plastic materials are crushed (e.g., housings and casings of waste electrical and electronic equipment (WEEE)), the flatness ratio ($\emptyset_{Flat}$) of particles tends to decrease with increasing size while the elongation ratio ($\emptyset_{Elong}$) remains relatively constant regardless of the particle size.
- Settling velocity of particles are affected by SG, size and shape.
- In term of SG, PS had faster settling velocities than ABS because it is heavier (i.e., higher SG).
- In terms of the size fraction, settling velocity of sphere-like PS (P-2) increased with increasing particle size while that of disk-like ABS (A-1) was independent of the particle size.
- In terms of the initial plastic board thickness, particles from thicker plastic boards (e.g., A-2, 3-mm thick) had higher settling velocities than those from thicker plastic boards (e.g., A-1, 2-mm thick).
- In the jig separation of single-type crushed plastic having sphere-like particles in all size fractions, coarse particles were recovered in the bottom layer while fine particles were mostly recovered in the top layer. In contrast, the behavior of crushed plastics with coarse, disk-like particles and fine,

sphere-like particles were different; that is, coarse particles were recovered in the top layer while fine particles were recovered in the bottom layer. Because the coarse and fine particles have similar settling velocities in static water, this phenomenon was attributed to consolidation trickling during jig separation.

- In the jig separation of mixed-type crushed plastics, light particles were recovered in top layers and heavy particles were recovered in bottom layers in all conditions indicating that SG is the most important parameter when $0.2 < \emptyset_{Flat} < 0.9$. Jig separation is improved when the mixture is composed of light, disk like particles and heavy, sphere-like particles. In contrast, it is more difficult to separate mixed plastics with light, sphere-like particles and heavy, disk-like particles.
- The jig separation efficiency is strongly influenced by the SG and shape of particles because separation is dependent on the differences in settling velocities of particles.

References

Arasan, S., Akbulut S., Hasiloglu A.S., 2011. Effect of particle size and shape on the grain-size distribution using Image analysis. Int. J. Civil Struct. Eng. 1, 968–985, https://doi.org/10.6088/ijcser.00202010083.

Barton, A.F.M., 1979. Resources Recovery and Recycling, John Wiley & Sons, New York.

Beunder, E.M., 2000. Influence of shape on particle behaviour in recycling techniques. https://www.env.go.jp/en/recycle/smcs/attach/hcswm.pdf (accessed 25 December 2017)

Beunder, E.M., Rem, P.C., 1999. Screening kinetics of cylindrical particles. Int. J. Miner. Process. 57, 73-81. https://doi.org/10.1016/S0301-7516(99)00007-1.

Brozek, M., Surowiak, A., 2007. Effect of particle shape on jig separation efficiency. Physicochem. Probl. Miner. Process. 41, 397-413.

Concha, F., 2013. Solid-Liquid Separation in the Mining Industry, Springer International Publishing, Switzerland.

Dharmarajah, A.H., 1982. Effect of particle shape on prediction of velocity voidage relationship in fluidized solid-liquid systems. https://lib.dr.iastate.edu/rtd/7535/ (accessed 23 February 2019)

Gabitto, J., Tsouris, C., 2008. Drag coefficient and settling velocity for particles of cylindrical shape", Powder Technol. 183, 314-322. https://doi.org/10.1016/j.powtec.2007.07.031.

Hori, K., Tsunekawa, Hiroyoshi, N., Ito, M., 2009. Optimum water pulsation of jig separation for crushed plastic particles. Int. J. Miner. Process. 92, 103-108. https://doi.org/10.1016/j.minpro.2009.01.001.

Ito, M., Tsunekawa, M., Ishida, E., Kawai, K., Takahashi, T., Abe, N., Hiroyoshi, N., 2010. Reverse jig separation of shredded floating plastic - separation of polypropylene and high density polyethylene. Int. J. Miner. Process. 97, 96-99. https://doi.org/10.1016/j.minpro.2010.08.007.

Masuda, H., Higashitani, K., Yoshida, H., 2006. Powder Technology Handbook, third ed. Taylor &Francis Group, Florida.

Mora, C.F., Kwan, A.K.H., 2000. Sphericity, shape factor, and convexity measurement of coarse aggregate for concrete using digital image processing. Cement Concrete Res. 30, 351-358. https://doi.org/10.1016/S0008-8846(99)00259-8.

Wadell, H., 1932. Volume, shape, and roundness of rock particles. J. Geol. 40, 443-451.

Wills, B.A., Napier-Munn, T.J., 2006. Mineral Processing Technology, seventh ed. Pergamon press, Oxford.

Woollacott, L.C., Silwamba, M., 2016. An experimental study of size segregation in a batch jig. Miner. Eng. 94, 41-50. https://doi.org/10.1016/j.mineng.2016.04.003.

Yang, W.C., 2013. Handbook of Fluidization and Fluid-Particle Systems, Marcel Dekker, Inc., New York.

Zingg, T, 1935. Bietrahe zur Schotteranalyse. 15, 1935 Schweiz. Miner. Petrog. 15, 139-140.

CHAPTER 4 – IMPROVEMENT OF JIG EFFICIENCY BY MODIFIED WATER PULSATION, AND NOVEL METHODS TO ESTIMATE THE SEPARATION EFFICIENCY AND SETTLING VELOCITY OF CRUSHED PLASTICS USING GEOMETRICAL PARAMETERS

4.1 Introduction

In the previous chapter 3, the effects of particle geometry (i.e., size and shape) on jig separation of crushed plastics were investigated and the results showed that the flatness ratio ($\emptyset_{Flat}$) is an important geometrical shape descriptor that affected the settling velocity of particles as well as jig separation efficiency. However, in the crushed plastic samples, the both of flatness ratio ($\emptyset_{Flat}$) and elongation ratio ($\emptyset_{Elong}$) were varied. To investigate only the effects of flatness ratio ($\emptyset_{Flat}$) on the jig separation in more details, the model plastics samples of square prism (cuboids with $\emptyset_{Elong} = 1$) having similar volumes (V) but different $\emptyset_{Flat}$ were used in this chapter.

Particle motion analysis of model plastic samples in static water was carried out and jig separation with various combination of shape of model plastic samples mixtures were carried out. To estimate the jig separation efficiency (SI), development of empirical equation to calculate settling velocity (v_∞) using flatness ratio ($\emptyset_{Flat}$) and projection area (A) was proposed and using v_∞, shape settling factor (SSF), a dynamic shape factor, was obtained. However, in this method, measurement of terminal velocity of each sample by experiment is needed. Thus, flatness ratio difference ($\Delta\emptyset_{Flat}$) using static shape factor was proposed to estimate SI by simple method using image analysis. In addition, to reduce the effects of particle shape on jig separation efficiency, particle motion during water pulsation were analyzed, and waveform modification was proposed.

4.2 Materials and methods

4.2.1 Sample preparation and characterization

4.2.1.1 Preparation and characterization of crushed plastic samples

Acrylonitrile butadiene styrene (ABS, specific gravity (SG) = 1.03) and polystyrene (PS, SG = 1.06) boards with 2-mm and 3-mm thickness were crushed by a cutting mill (Orient mill, VH16, Seishin Enterprise Co., Ltd, Japan) to obtain 4 crushed plastic samples: crushed 2-mm thick ABS board (A-1_C), crushed 3-mm thick ABS board (A-2_C), crushed 2-mm thick PS board (P-1_C), and crushed 3-mm thick PS board (P-2_C). For sample characterization, +2.0-8.0 mm samples (i.e., A-1_C, A-2_C, P-1_C, P-

2_C) were sieved to +2.0-2.8, +2.8-4.0, +4.0-5.6, and +5.6-8.0 mm size fraction and the short, intermediate, and long axes (*S*, *I*, and *L*, respectively, (Fig. 4-1(a)) of hundred particles from each size fraction were measured using a Vernier caliper, the projection area (i.e., area viewed in the direction perpendicular to the plane of the greatest stability of the particle, *A* (Masuda et al., 2006; Yang, 2013) of twenty particles from each size fraction was measured by image analysis (WinRoof-2018, Mitani Corporation, Japan), and equivalent volume diameter (i.e., diameter of a sphere that has the same volume as particle, D^*), flatness ratio ($\emptyset_{Flat}$), and elongation ratio($\emptyset_{Elong}$) were calculated by Eqs. (2-7), (3-2), and (3-3), respectively. A sphere has $\emptyset_{Flat}$ and $\emptyset_{Elong}$ of one (S=I=L), while particles that have other shapes have $\emptyset_{Flat}$ and $\emptyset_{Elong}$ of less than one (low $\emptyset_{Flat}$ = disk-like and low $\emptyset_{Elong}$ = rod-like).

4.2.1.2 Preparation and characterization of model plastic samples

ABS boards with 2- to 5-mm thickness and PS boards with 2- and 3-mm thickness were cut using a rotary cutter into square prism (cuboids with $\emptyset_{Elong}$ = 1). All samples have similar volumes (V) and D^* (Eq. 2-7) but different $\emptyset_{Flat}$ (Eq. 3-2), as shown in Table 4-1 and (Fig. 4-1(b)).

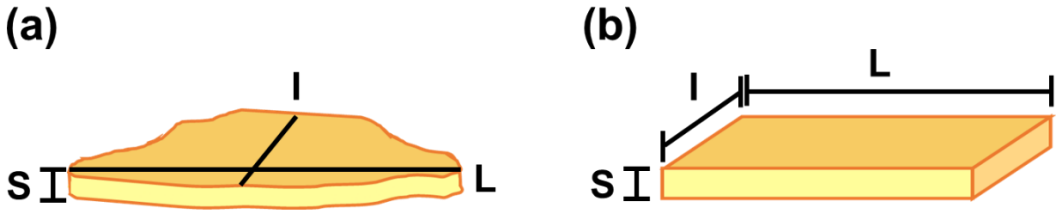

Figure 4-1. A schematic diagram showing the short (S), intermediate (I) and long (L) axes of plastic particles; (a) crushed plastic sample and (b) model plastic sample.

Table 4-1. Physical properties of model plastic samples.

Samples	Plastics	SG	*S* (mm)	*I* (mm)	*L* (mm)	$V = S \cdot I \cdot L$ (mm^3)	$D^* = (6\,S{\cdot}I{\cdot}L\,\pi)^{1/3}$ (mm)	$\emptyset_{Flat}$ = *S/I*	$A = I \cdot L$ (mm^2)
A-1M	ABS	1.03	2.00	8.00	8.00	128.00	6.25	0.25	64.00
A-2M	ABS	1.03	3.00	6.50	6.50	126.75	6.23	0.46	42.25
A-3M	ABS	1.03	4.00	5.50	5.50	121.00	6.14	0.73	30.25
A-4M	ABS	1.03	5.00	5.00	5.00	125.00	6.20	1.00	25.00
P-1M	PS	1.06	2.00	8.00	8.00	128.00	6.25	0.25	64.00
P-2M	PS	1.06	3.00	6.50	6.50	126.75	6.23	0.46	42.25

4.2.2 Jig separation experiments

Small separation chamber (60-mm long, 60-mm wide and 150-mm high, water volume of 1 L) connected to RETAC jig air chamber was used (Fig. 4-2). Jig separation was carried out using eight plastic mixtures of ABS (30 g) and PS (30 g): (i_M) A-1_M and P-1_M, (ii_M) A-1_M and P-2_M, (iii_M) A-2_M and P-1_M, (iv_M) A-2_M and P-2_M, (v_M) A-3_M and P-1_M, (vi_M) A-3_M and P-2_M, (vii_M) A-4_M and P-1_M, and ($viii_M$) A-4_M and P-2_M. Each mixture was fed into the jig separation chamber and separation was carried out under the following conditions: displacement of 20 mm, frequency of water pulsation 30 cycles/minute, water volume of 18 L, addition of 15 ppm of Di-2-ethylhexyl sodium sulfosuccinate (AOT, $C_{20}H_{37}NaO_7S$, Wako Pure Chemical Industries, Ltd., Japan) as a wetting agent, and separation time of 3 minutes (same conditions as jig separation of crushed plastic samples (Chapter 3) with similar particle bed thickness (40 mm)). After each experiment, the products were divided into 3 layers from the top (Fig. 4-2) and the purity of jig products were determined by hand-picking.

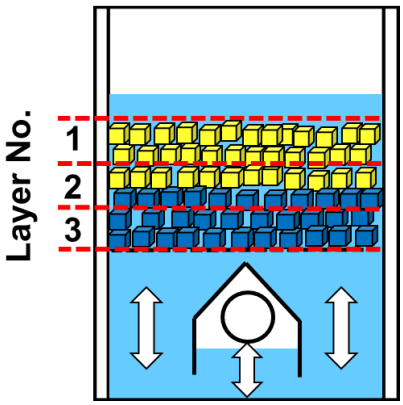

Figure 4-2. A schematic illustration of a desktop-type batch-wise RETAC jig and how the products were partitioned into 3 layers.

4.2.3 Motion analysis of particles

4.2.3.1 Analysis in static water

The settling behavior of one particle in static water was analyzed in the water chamber (15 ppm AOT). For crushed plastic samples, twenty particles from each size fraction (+2.0–2.8, +2.8–4.0, +4.0–5.6 and +5.6–8.0 mm) of A-1_C, A-2_C, P-1_C, and P-2_C were dropped one by one from the water surface at two different orientations (Fig. 4-3(a)). For model plastic samples, twenty particles of A-1_M, A-2_M, A-3_M, A-4_M (Table 4-1) were dropped one by one from the water surface at three different orientations (Fig. 4-3(b)). The distance from the water surface with time was analyzed by image analysis (WinRoof, Mitani Corporation, Japan).

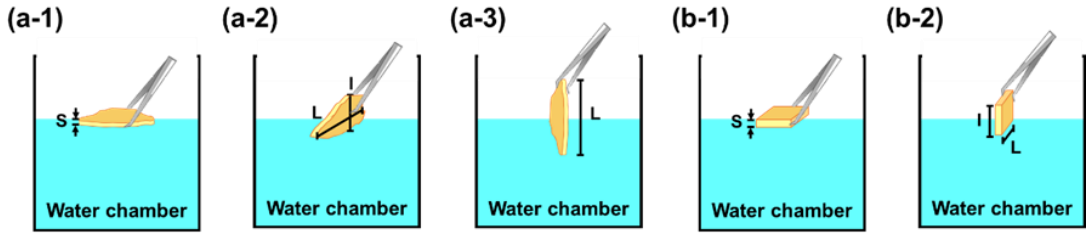

Figure 4-3. Initial orientations of plastic particles for the settling velocity measurements in static water; (a) crushed plastic samples and (b) model plastic samples.

4.2.3.2 Analysis during water pulsation

The particle motion during water pulsation was analyzed in the jig separation chamber (60-mm long, 60-mm wide and 150-mm high). Each type of plastic sample (A-1_M, A-2_M, A-3_M, A-4_M, P-1_M, and P-2_M) (Table 4-1) having similar particle bed thickness (40 mm) with jig separation experiment was fed into the jig separation chamber (15 ppm AOT) and water pulsation (displacement of 20 mm and frequency of water pulsation equal to 30 cycles/minute) was introduced for 10 min. In this experiment, 10 wt% of colored particles was added and the particle motion of colored particles was analyzed by image analysis (WinRoof, Mitani Corporation, Japan) and 2D motion analysis software (DIPP-Motion V, Ditect Co., Ltd., Japan).

4.3 Results and discussion

4.3.1 Estimation of settling velocity using flatness ratio and projection area

In this section, estimation of settling velocity using flatness ratio and projection area was proposed. Generally, SG of heavy materials, light materials, and fluid medium are used to calculate concentration criterion (CC, as described later, in Eq. 4-12) that is the important factor to predict the separation efficiency (e.g., sharpness index (SI)). However, CC calculated by SG is not applicable for crushed plastics generated from board-like shape (e.g., housing and casings) because the jig separation efficiency is affected by not only the SG but also of the shape of particles as discussed previously. In a laminar or Stokes' law regime, CC can be expressed by the ratio of terminal velocity (v_∞) of heavy and light particles as described later (Eq. 4-13). In this section, estimation of terminal velocity using geometrical parameter (i.e., $\emptyset_{Flat}$, A) is proposed to predict the separation efficiency.

As described in introduction, based on previous studies of the authors, step 2 (particles settle down in static condition) is the most important step among these 4 steps in a RETAC jig (Hori et al, 2009; Ito et al, 2010) so, the effects of shape (i.e, $\emptyset_{Flat}$) on the terminal velocity of model plastics

sample in static water with different initial orientations (Fig. 4-3) were investigated. The effects of initial particle orientation on the terminal velocity were negligible (Fig. 4-4). Visual inspection of particle orientations towards the final stages of the experiment showed that most particles re-oriented such that the short (*S*, thickness) axis was perpendicular to the water surface (i.e., projection area was parallel to the water surface (Fig. 4-3(b-1)). (Dharmarajah, 1982; Masuda et al, 2006; Yang, 2013).

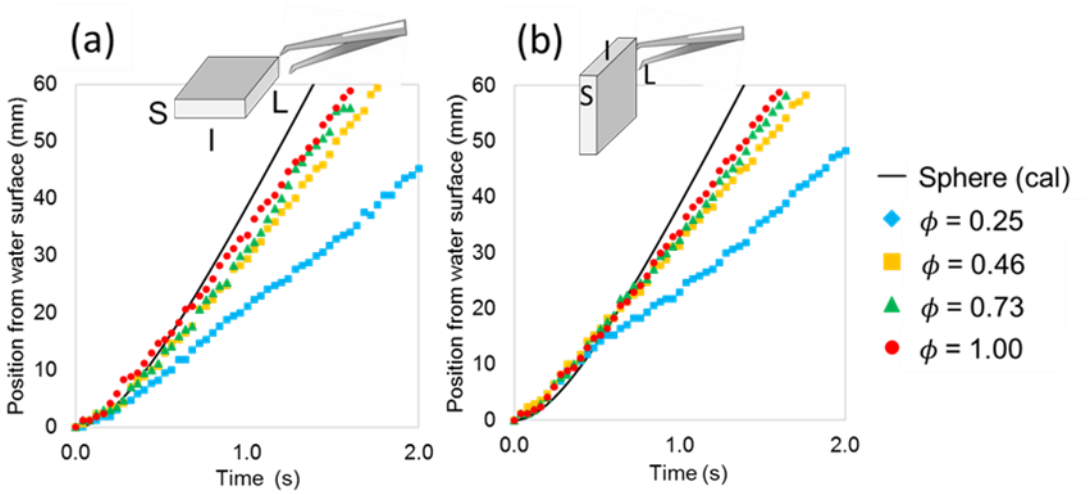

Figure 4-4. Settling distance of model plastic particles having equivalent volume from water surface by time at different initial orientations; (a) projection area (*A*) was parallel to the water surface (Fig. 4-3(b-1)) and (b) projection area (*A*) was perpendicular to the water surface (Fig. 4-3(b-2)).

Fig. 4-5 showed the measured settling distance from the water surface by time of model plastic samples (ABS) with different $\emptyset_{Flat}$ (Table 3-1) and that of a perfect sphere ($\emptyset_{Flat}$ =1.00) of the same volume, which was calculated from Eq. (4-1) as a function of time.

A particle settling down in water is strongly influenced by three forces, namely gravity, buoyancy, and drag force, and its settling velocity (v) is determined by the balance between these three forces (Eq. 4-1).

$$m\frac{dv}{dt} = g(\rho_P - \rho_F)V - C_D A\left(\frac{\rho_F v^2}{2}\right) \quad (4\text{-}1)$$

where m = mass of the particle (kg)

v = velocity of particle (m/s)

t = time (s)

g = gravitational acceleration (m/s^2)

ρ_P = density of particle (kg/m^3)

ρ_F = density of fluid (kg/m^3)

V = volume of particle (m^3)

C_D = drag coefficient

Generally, the particle starts to settle down with acceleration (dv/dt) in initial state and after that acceleration become zero indicating a particle reaches terminal velocity (v_∞) (Eq. 4-2).

$$0 = (\rho_P - \rho_F)gV - C_D A\left(\frac{\rho_F {v_\infty}^2}{2}\right) \tag{4-2a}$$

$$(\rho_P - \rho_F)gV = C_D A\left(\frac{\rho_F {v_\infty}^2}{2}\right) \tag{4-2b}$$

The terminal velocity of a perfect sphere (i.e., slope of line in Fig. 4-5) was the fastest while for those with intermediate shapes, particles with higher $\emptyset_{Flat}$ (sphere-like particles) have higher terminal velocities than those with low $\emptyset_{Flat}$ (disk-like particles) because of higher drag force (Hölzer and Sommerfeld, 2008). These results imply that the settling and terminal velocities of disk- and sphere-like particles were different, and that both parameters were directly related to the $\emptyset_{Flat}$ that was in line with the results of crushed plastic samples. As described above, terminal velocity of heavy and light particles is needed to predict the jig separation efficiency however, measurement of terminal velocity by experiment is take time. Terminal velocity of a sphere has been studied by various researches while only a few studies have been done on the terminal velocity of non-spherical particle especially for crushed plastics generated from board-like shape (e.g., housing and casings). In this section, a novel method to estimate terminal velocity of crushed plastics using terminal velocity of a sphere with same volume (equivalent volume sphere) and geometrical parameters ($\emptyset_{Flat}$ and A) is proposed.

Two particles having different shape ($\emptyset_{Flat}$) but similar SG and volume shows same values of gravity and buoyancy force so, Eq. 4-2 could be expressed in the term of an irregular particle and a sphere as:

$$C_D A\left(\frac{\rho_F {v_\infty}^2}{2}\right) = C_D^* A^*\left(\frac{\rho_F {v_\infty^*}^2}{2}\right) \tag{4-3a}$$

$$\frac{v_\infty}{v_\infty^*} = \sqrt{\left(\frac{A^*}{A}\right)\left(\frac{C_D^*}{C_D}\right)} \tag{4-3b}$$

$$v_\infty = v_\infty^* \sqrt{\left(\frac{A^*}{A}\right)\left(\frac{C_D^*}{C_D}\right)} \tag{4-3c}$$

where v_∞ = terminal velocity of particle

$v_\infty{}^*$ = terminal velocity of equivalent volume sphere

$C_D{}^*$ = drag coefficient of equivalent volume sphere

A^* = projection area of equivalent volume sphere

From Eq. (4-3b), $v_\infty / v_\infty{}^*$ could be calculated from the projection area ratio of a sphere (A^*) and a non-sphere (A) and their drag coefficient ratios ($C_D{}^*$ and C_D). In Eq. 4-1, the terminal velocity of a perfect sphere ($v_\infty{}^*$) where $V^* = 2\pi D^{*3}/3$ and $A^* = \pi D^{*2}/4$ can be calculated as:

$$v_\infty^* = \sqrt{\frac{4}{3}\frac{(\rho_P - \rho_F)}{\rho_F}\frac{gD^*}{C_D^*}} \tag{4-4}$$

The value of drag coefficient of a perfect sphere ($C_D{}^*$) depends on the fluid flow regime, which could be expressed by $C_D{}^* = f(Re_P{}^*)$ where $Re_P{}^*$ is the particle Reynolds number of a sphere.

$$Re_p{}^* = \frac{v^* D^* \rho_F}{\mu} \tag{4-5}$$

where μ is viscosity of fluid (Pa·s)

In a laminar or Stokes' law regime ($Re_p{}^* < 2$); $C_D{}^* = 24/Re_P{}^*$, hence:

$$v_\infty^* = \frac{(\rho_P - \rho_F)}{18}\frac{gD^{*2}}{\mu} \tag{4-6}$$

In an intermediate or transitional regime ($2 < Re_p{}^* < 500$); $C_D{}^* = 10/(Re_P{}^*)^{1/2}$, then the terminal velocity of a perfect sphere is given by

$$v_\infty^* = \sqrt[3]{\frac{4(\rho_P - \rho_F)^2}{225}\frac{g^2}{\mu\rho_F}}\, D^* \tag{4-7}$$

Meanwhile, in a turbulent or Newton's law regime ($Re_P{}^* > 500$), $C_D{}^* = 0.44$, the terminal velocity of a perfect sphere is given by

$$v_{\infty}^{*} = \sqrt{\frac{3(\rho_P - \rho_F)}{\rho_F} g D^{*}} \tag{4-8}$$

By calculating the Re_P (Eq. 4-5) based on the conditions of the experiments, the flow regime was found to be in the intermediate or transitional region (Eq. 4-7).

C_D/C_D^* can be calculated using the terminal velocity (slope of Fig. 4-5, v_{∞}^* and v_{∞}), projection area of model plastic samples ($A = I \cdot L$ in Table 4-1), and projection area of a perfect sphere ($A^* = \pi D^{*2}/4$). From these parameters, Eq. 4-9 was obtained and using this Eq. 4-9, C_D/C_D^* can be calculated from the values of $\emptyset_{Flat}$ (Fig. 4-6)

$$\frac{C_D}{C_D^*} \cong 2.93\ \emptyset_{Flat}^{\ 0.29} \tag{4-9}$$

Fig. 4-7 shows the terminal velocities obtained from settling velocity measurements and calculated terminal velocity from Eq. (4-3c), which was obtained using an intermediate regime (Eq. 4-7) and (Eq. 4-9) and projection areas (A) measured by image analysis and projection area of model plastic samples ($A = I \cdot L$ in Table 4-1). The results show that the experimental results with calculated values using projection area of model plastic samples (Fig. 4-7) and projection areas (A) measured by image analysis (Fig. 4-8) agreed well with only for +2.0-2.8 mm size fraction. This disagree at coarser size fraction may cause by the values of v_{∞}^* from the calculation and measurement was not same. To confirm this hypothesis, the settling velocity of spherical particle with same volume and SG of model plastic samples was measured. The results showed that the values of v_{∞}^* from the calculation was higher than that of measured value. However, the trend of v_{∞} could be observed. These results may be caused by the unique way plastic boards of uniform thickness (e.g., housings and casings of waste electrical and electronic equipment (WEEE)) are crushed that is, size reduction mainly occurs in the intermediate (breadth, I) and long (length, L) axis directions rather than in the short (thickness, S) axis direction indicating that flat surface (I-L plane) is remained. This flat surface is the most stable orientation for both during image analysis and during settling down (final orientation), indicating that the terminal velocity could be defined using $\emptyset_{Flat}$ (Eq. 4-9) and measured projection area by image analysis.

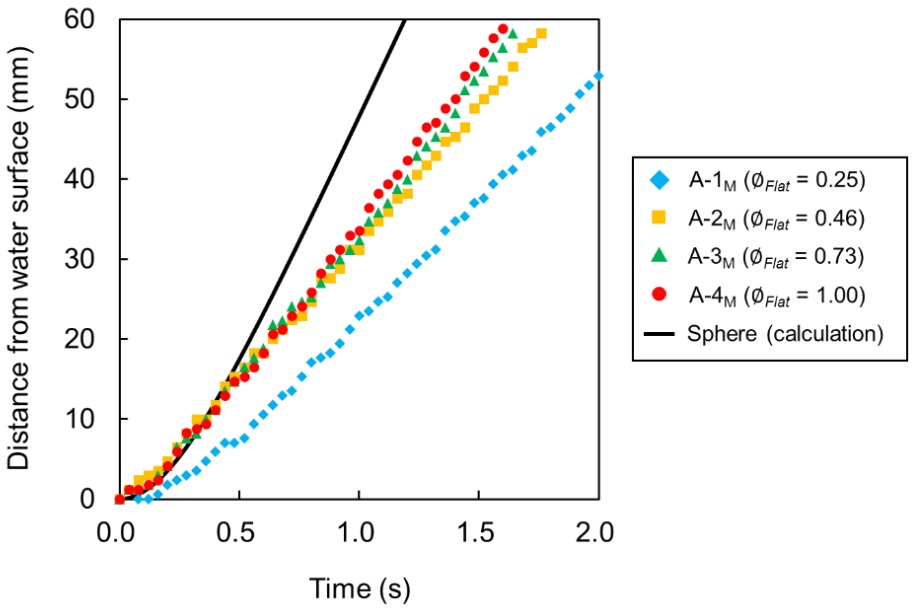

Figure 4-5. Settling distance of cut particles having equivalent volume from water surface by time.

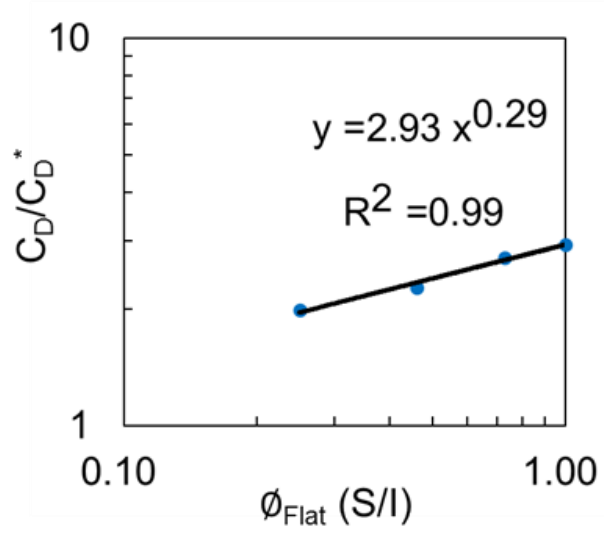

Figure 4-6. Relationship between flatness ratio ($\emptyset_{Flat}$) and C_D/C_D^*.

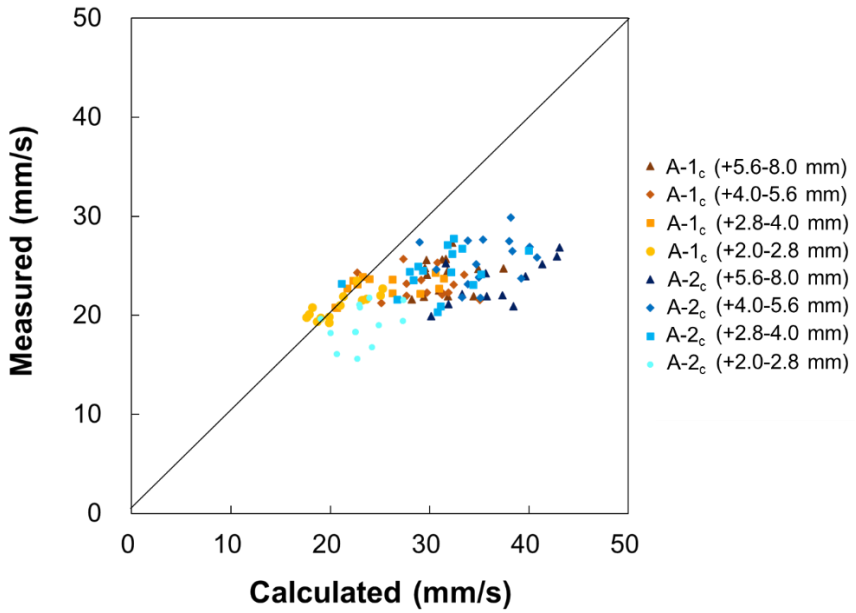

Figure 4-7. Terminal velocity of crushed plastic samples (A-1$_C$ and A-2$_C$) obtained from calculation (using projection area ratio (A/A^*) of model plastic samples) and settling velocity measurement.

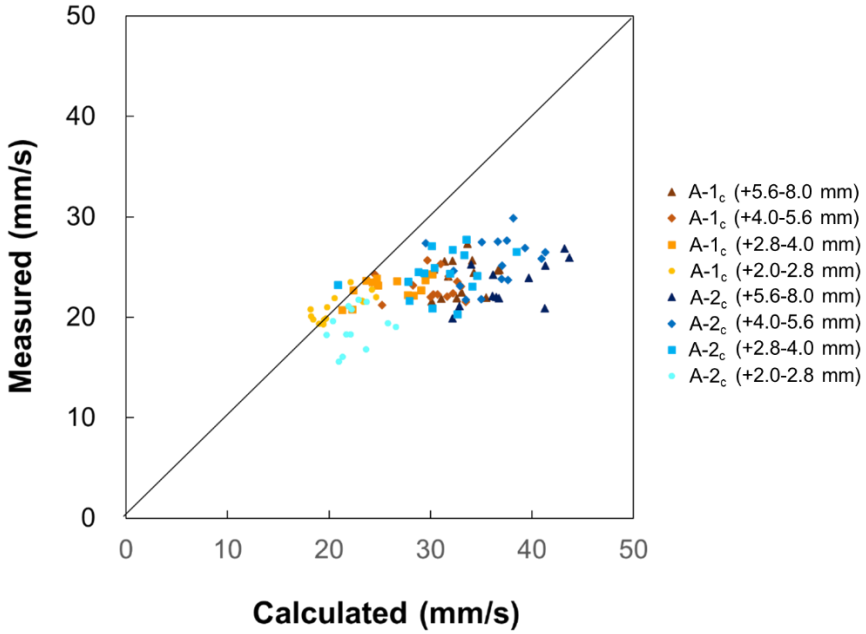

Figure 4-8. Terminal velocity of crushed plastic samples (A-1$_C$ and A-2$_C$) obtained from calculation (using projection area ratio (A/A^*) of crushed plastic samples) and settling velocity measurement.

4.3.2 Estimation of jig separation efficiency using flatness ratio difference and modified concentration criteria

In previous section, effects of particle shape on the crushing, settling velocity and jig separation efficiency were discussed and from those results it was found that flatness ratio is the most important shape parameter. In this section, estimation of purity of jig products and sharpness index (SI) using shape factors were proposed.

Jig separation was carried out using eight plastic mixtures of model plastic samples (square prism) with same particle volume but different thickness (*S*), breadth (*I*), and length (*L*). After jig separation, products were divided into 3 layers from top (Fig. 4-2) and the purity of jig products were determined by hand-picking.

Fig. 4-9 shows the relationship between the distance from the bottom of each layer (height of the center position of the top, middle, and bottom layers) (Fig. 4-2) (horizontal axis) and purity of light plastic (ABS) in each layer product after jig separation (vertical axis). The sharpness index (SI) can be calculated from Fig. 4-9 by following equation:

$$SI = \frac{Height_{84.13} - Height_{50}}{Height_{50}} \tag{4-10}$$

where $Height_{50}$ and $Height_{84.13}$ are the height when the purity is 50 and 84.13%, respectively. In general, lower values of SI are obtained when the separation efficiency is high. The results showed that better separation was achieved for the (ii_M)-mixture (Fig. 4-9(b)) while the separation of ABS and PS in the (iii_M)-mixture was the worst (Fig. 4-9(g)) indicating that SI is affected by the combination of cuboid having different dimension. where $\emptyset_{Flat\ H}$ and $\emptyset_{Flat\ L}$ are flatness ratio of heavy and light particles, respectively.

To estimate the separation efficiency, flatness ratio difference ($\Delta\emptyset_{Flat}$), new parameter from $\emptyset_{Flat}$, was introduced in this study (Eq. 4-11).

$$\Delta\emptyset_{Flat} = \emptyset_{Flat_H} - \emptyset_{Flat_L} \tag{4-11}$$

Fig. 4-10(a) shows the relationship of $\Delta\emptyset_{Flat}$ (horizontal axis), calculated from Eq. (4-11) using $\emptyset_{Flat}$ in Table 4-1, and (a-1) purity of light plastic (ABS) in top layer products, (a-2) purity of heavy plastic (PS) in bottom layer products, and (a-3) SI of jig separation (vertical axis). The results showed that purity of ABS in top layer product and purity of PS in bottom layer product increased with increasing of $\Delta\emptyset_{Flat}$ while SI was decreased. These results suggest that $\Delta\emptyset_{Flat}$ obtained from $\emptyset_{Flat}$ (static shape factor) can be used to estimate jig separation efficiency when density or SG of heavy and light

materials (ρ_H and ρ_L, respectively) are constant.

In mineral processing, the concentration criterion (CC) is commonly used to determine whether gravity separation is applicable for the recovery of target materials in a particular sample. The concentration criterion (CC) can be defined as (Gupta and Yan, 2006; Wills and Napier-Munn, 2006).

$$CC = \frac{\rho_H - \rho_F}{\rho_L - \rho_F} \tag{4-12}$$

Using Stokes' law regime (Eq. 4-6), CC can be expressed by the ratio of terminal velocity (v_∞) of heavy and light particles as:

$$CC = \frac{SG_H - SG_F}{SG_L - SG_F} = \frac{v^*_{\infty H}}{v^*_{\infty L}} \tag{4-13}$$

The higher the value of CC, the easier it is to separate materials in the sample (Gupta and Yan, 2006; Wills and Napier-Munn, 2006). This equation, however, is not applicable because the separation efficiency is affected by not only the SG but also of the shape of particles as discussed previously. To modify the CC and include the effects of particle shape, a dynamic shape factor called shape settling factor (SSF) was introduced (Eq. 4-15) (Gupta and Yan, 2006).

$$SSF = \frac{v_\infty}{v^*_\infty} \tag{4-14}$$

The SSF is defined as the ratio of the terminal velocity in static water of a non-spherical particle (v_∞) and the terminal velocity in static water of a spherical particle having same D^* ($v_\infty{}^*$). Using SSF (Eq. 4-15), the modified concentration criterion (CC_s) was obtained as follows (Pita and Castiho, 2016):

$$CC_s = = \frac{\rho_H - \rho_F}{\rho_L - \rho_F} \times \frac{SSF_H}{SSF_L} = \frac{\rho_H - \rho_F}{\rho_L - \rho_F} \times \frac{\frac{v_{\infty H}}{v^*_{\infty H}}}{\frac{v_{\infty L}}{v^*_{\infty L}}} = \frac{v_{\infty H}}{v_{\infty L}} \tag{4-15}$$

Meanwhile, in a turbulent or Newton's law regime ($Re_p{}^* > 500$), $C_D{}^* = 0.44$, the terminal velocity of a perfect sphere is given by:

where $v_{\infty H}$ is the terminal velocity in static water of a heavy, non-spherical particle (*H*),

$v_{\infty l}$ is the terminal velocity in static water of a light, non-spherical particle (*L*),

$v_\infty{}^*{}_H$ is the terminal velocity in static water of heavy, spherical particle having the same D^* as *H*,

$v_{\infty}{}^{*}{}_{L}$ is the terminal velocity in static water of light, spherical particle having same D^{*} as L,

SSF_H is the shape settling factor of the heavy particle (H), and

SSG_L is shape settling factor of the light particle (L).

Fig. 4-10(b) shows the relationship of CC_s (horizontal axis), calculated from Eq. (4-15), and (b-1) purity of light plastic (ABS) in top layer products, (b-2) purity of heavy plastic (PS) in bottom layer products, and (b-3) SI of jig separation (vertical axis). The results showed that purity of ABS in top layer products and purity of PS in bottom layer products increased while SI decreased with increasing of CC_s.

Both of $\Delta\emptyset_{Flat}$ and CC_s could be applied to estimate jig separation efficiency in recycling plants, however, due to $\Delta\emptyset_{Flat}$ do not contain SG information indicating that $\Delta\emptyset_{Flat}$ can used to estimate jig separation efficiency only when SG_H and SG_L are constant. While CC_s contain SG information thus CC_s can be widely used.

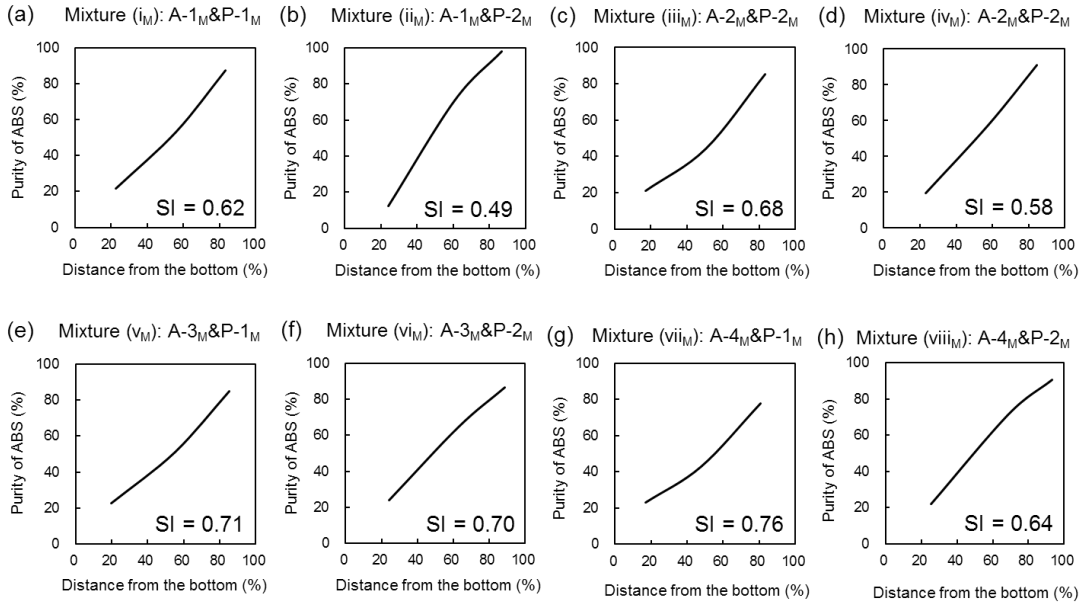

Figure 4-9. The relationship between distance from the bottom and purity of ABS after jig separation using normal waveform of (a) mixture (i_M), (b) mixture (ii_M), (c) mixture (iii_M), (d) mixture (iv_M), (e) mixture (v_M), (f) mixture (vi_M), (g) mixture (vii_M), and (h) mixture ($viii_M$) with the values of sharpness index (SI).

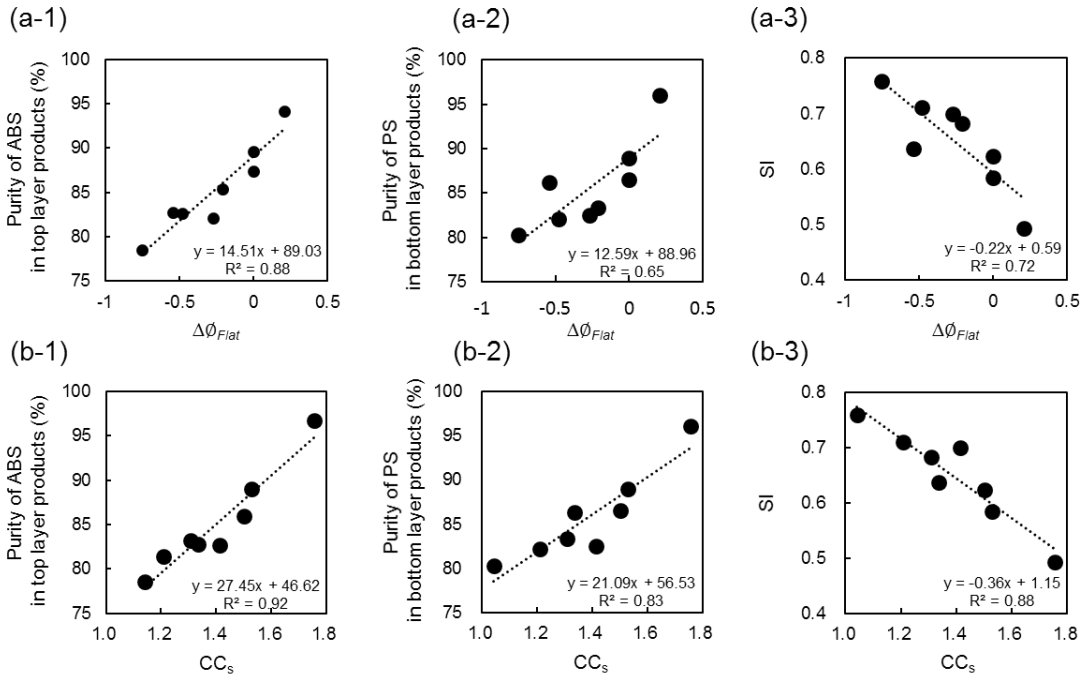

Figure 4-10. (a) The relationship of $\Delta\emptyset_{Flat}$ with (a-1) purity of light plastic (ABS) in top layer product, (a-2) purity of heavy plastic (PS) in bottom layer products, and (a-3) sharpness index and (b) the relationship of CC_s with (b-1) purity of light plastic (ABS) in top layer products, (b-2) purity of heavy plastic (PS) in bottom layer products, and (b-3) sharpness index (SI).

4.3.3 Effects of flatness ratio on the particle motion during water pulsation and improvement of jig separation efficiency by modified water pulsation

In previous session, effects of flatness ratio on the settling behavior of a particle in static water were elucidated. However, during jig separation not only one particle presences in the system with static condition but many particles are presented with water pulsation. In a RETAC jig, water pulsation is comprised of 4 steps: (1) rising, (2) initial holding, (3) downwelling, and (4) final holding (Fig. 3-8). In step (1), water rises to lift particles and dilate the particle bed (i.e., fluidization). Once the rising movement of the fluid stops in step (2), particles start to settle down in water under static condition. Particles that did not reach the bottom continue to settle down in steps (3) and (4) before starting the next cycle (Hori et al, 2009; Ito et al, 2010). In this section, particle motion during these four steps of water pulsation was investigated using single type of model plastic samples (i_M or ii_M or iii_M or iv_M) that have similar D^* but different $\emptyset_{Flat}$.

Fig. 4-11 shows particle position change with time from initial position. The results showed that in step (1) (water rising step), disk-like particles rose faster than sphere-like particles (Fig. 4-11a). Particle rising velocity (v_{rising}) can be calculated by Eq. (4-17) and the water rising velocity (u) is same but settling velocity of the disk-like particles ($v_{disk\text{-}like}$) is lower than that of sphere-like particles

($v_{\text{disk-like}}$) as described in previous section

$$v_{rising} = u - v \tag{4-17}$$

However, in step (2) and (3), particle velocities (slope) of disk-like particles and sphere-like particles was almost the same (Figs. 4-11(b)&(c)). These results can be explained by the hinder settling behavior. In step (1), the particle layer was expanded due to water rising this caused the increase of porosity (ε) of the particle layer. As discussed earlier, disk-like particles rose up higher than that of sphere-like indicating the average porosity of particle layer was higher than sphere-like. Hinder settling velocity can be calculated by the terminal velocity of a particle in static water (v_∞) and porosity (ε) of particle layer (Eq. 4-18)

$$v_\varepsilon = v_\infty(1 - C_V) = v_\infty \varepsilon^M \tag{4-18}$$

When C_v is volume concentration and M is constant that can be calculated from Re_P (Eq. 4-5) by Eq. (4-19) (ε and C_v value is between 0 to 1).

$$M = \frac{4.7(1 + 0.15{Re_p}^{0.687})}{1 + 0.253{Re_p}^{0.687}} \tag{4-19}$$

Eq. (4-18) shows that hinder settling velocity of high porosity condition (disk-like particles) is higher than that of lower porosity condition (sphere-like particles). However, due to the effects of flatness ratio on the settling velocity of a particle in static water (v_∞), sphere-like particle has higher settling velocity than that of disk-like particle. Due to these reasons, the effects of particle shape on the settling velocity and porosity became negated and hinder settling velocity (v_ε) of disk-like and sphere-like particles showed similar values.

Using these results, modification of waveform to reduce the effects of particle shape on jig separation was proposed. Since the effects of particle shape mostly found in step (1) so, time of step (1) was reduced into half (0.5 s to 0.25 s) as shown in Fig. 4-12. By the reducing of time on step (1) into half, the water rising velocity (u) is increase twice indicating that difference of v_{rising} become smaller (Eq. 4-17) and effects of particle shape can be reduced. Because the mixture (ii_M) and (vii_M) showed the highest and lowest separation efficiency in jig separation experiments of model plastic sample in Figs. 4-9(b)&(g) (normal waveform), these samples were used for jig separation with proposed waveform. Fig. 4-13 shows the partial separation curve with modified waveform. The results showed that the separation efficiency of mixture (ii_M) (Fig. 4-13(a)) decreased from the results with normal waveform (Fig. 4-9(b)). In contrast, the separation efficiency of mixture (vii_M) (Figs. 4-9(g) & 4-13(b)) increased. As the results, separation efficiency (SI), purity of ABS in top layer products and purity of PS in bottom layer products of both mixtures showed similar values with modified waveform.

These results show that both of particle shape and waveform affects the jig separation efficiency so, selection of suitable waveform is important, and this suitable waveform have to decided depending on the combination of particle shape in the plastic mixtures. For examples, normal waveform can be applied for the mixture of light materials having disk-like shape and heavy materials having sphere-like shape while modified waveform can achieve good separation for the mixture of light materials having sphere-like shape and heavy materials having disk-like shape. To recognize the particle shape of feed materials, image analysis method can be used as described above. In practical uses, online image analysis with automatic control of waveform is recommended prior to jig separation in recycling plants that feed compositions vary from time to time. For recycling plants that feed composition is stable, suitable crushing methods should be selected by using image analysis to obtained good jig separation.

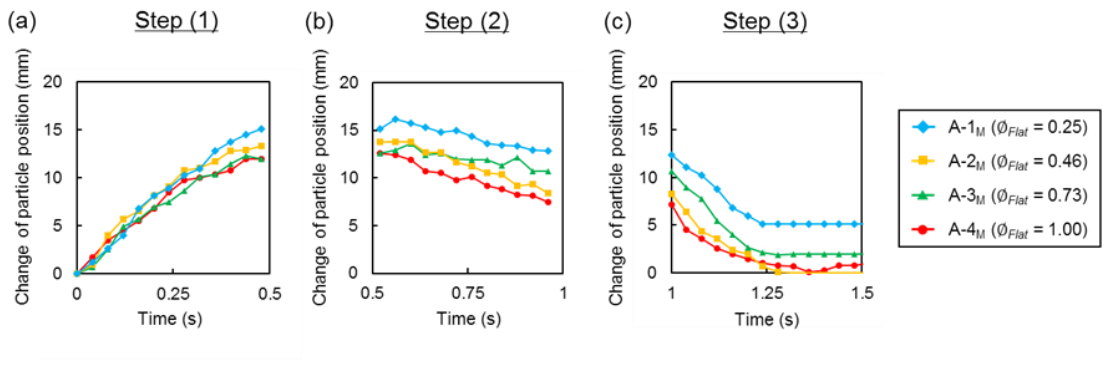

Figure 4-11. Particle position change with time from initial position of (a) step 1, (b) step 2, (c) step 3**.** Note: step (4), the particles have already reached the bottom surface so, no motion was occurred.

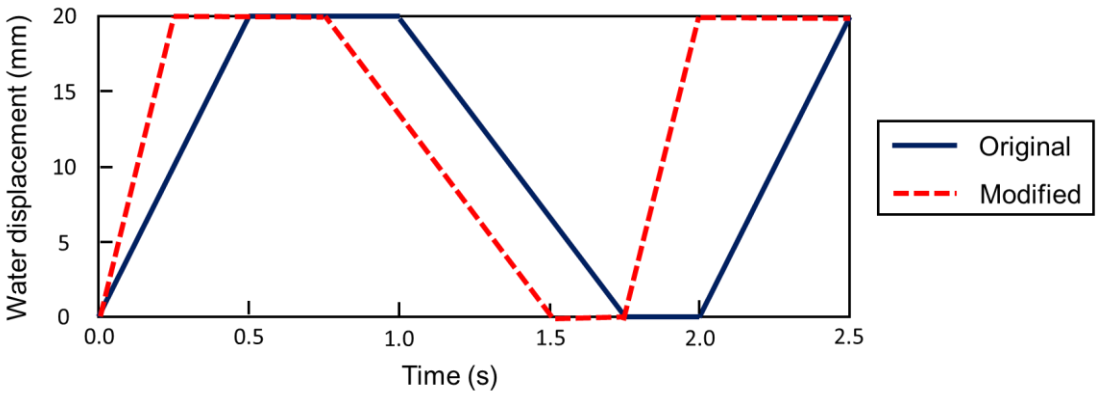

Figure 4-12. Waveform of RETAC jig separation.

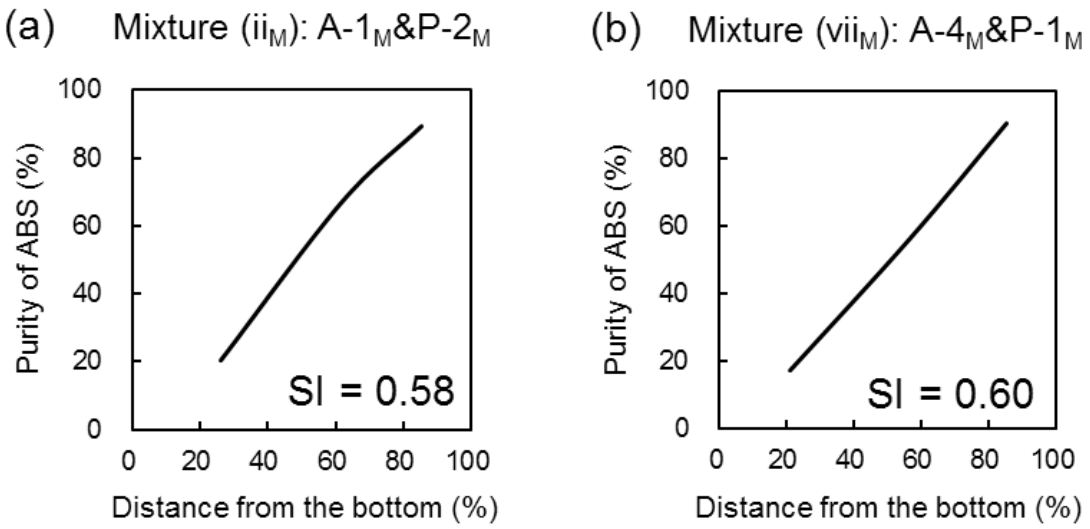

Figure 4-13. The relationship between distance from the bottom and purity of ABS after jig separation using modified waveform of (a) mixture (ii) and (b) mixture (vii).

4.4 Conclusions

In this chapter, empirical equation to calculate settling velocity of non-spherical particles using flatness ratio and projection area was developed, and a modified concentration criterion (CC_s) was proposed to estimate jig separation efficiency of non-spherical particles. The experimental results showed that sharpness index decreased with increasing CC_s calculated from the velocity of non-spherical particles. These results indicate that CC_s can be used to estimate jig separation efficiency of non-spherical particles. Based on the CC_s proposed here it was hypothesized that separation efficiency of the mixture of light, sphere-like particles and heavy, disk-like particles will be improved when the water rising velocity increase. This hypothesis was confirmed by the jig separation of the mixed plastic samples.

References

Dharmarajah, A.H., 1982. Effect of particle shape on prediction of velocity voidage relationship in fluidized solid-liquid systems. https://lib.dr.iastate.edu/rtd/7535/ (accessed 23 February 2019)

Gupta, A., Yan, D.S., 2006. Mineral Processing Design and Operation – An Introduction, Perth, Australia.

Hölzer, A., Sommerfeld, M., 2008. New simple correlation formula for the drag coefficient of non-spherical particles. Powder Technol. 184, 361–365. https://doi.org/10.1016/j.powtec.2007.08.021

Hori, K., Tsunekawa, M., Hiroyoshi, N., Ito, M., 2009. Optimum water pulsation of jig separation for crushed plastic particles. Int. J. Miner. Process. 92, 103–108. https://doi.org/10.1016/j.minpro.2009.01.001

Ito, M., Tsunekawa, M., Ishida, E., Kawai, K., Takahashi, T., Abe, N., Hiroyoshi, N., 2010. Reverse jig separation of shredded floating plastics — separation of polypropylene and high density polyethylene. Int. J. Miner. Process. 97, 96–99. https://doi.org/10.1016/j.minpro.2010.08.007

Masuda, H., Higashitani, K., Yoshida, H., 2006. Powder Technology Handbook, third ed. Taylor & Francis Group.

Pita, F., Castilho, A., 2016. Influence of shape and size of the particles on jigging separation of plastics mixture. Waste. Manage. 48, 89-94. https://doi.org/10.1016/j.wasman.2015.10.034.

Wills, B.A., Napier-Munn, T.J., 2006. Mineral Processing Technology, seventh ed. Pergamon press, Oxford.

Yang, W.C., 2013. Handbook of Fluidization and Fluid-Particle Systems. Marcel Dekker, Inc., New York.

CHAPTER 5 – IMPROVEMENT OF JIG EFFICIENCY BY SHAPE SEPARATION, AND A NOVEL METHOD TO ESTIMATE SEPARATION EFFICIENCY OF METAL WIRES IN CRUSHED ELECTRONIC WASTES USING BENDING BEHAVIOR AND ENTANGLEMENT FACTOR

5.1 Introduction

As described in the general introduction (chapter 1) about recycling laws, because the process flow for the recycling of large home appliances was already established, recycling plants simply applied this process to small home appliances. Although large pieces of metals could be recovered by magnetic and eddy current separation techniques, those with finer sizes could not be recovered and end up in the final plastic residues. This means that additional treatment is needed for the final plastic residues because they still contain substantial amounts of valuable metals especially copper (Cu).

In this chapter, the RETAC jig was applied to separate plastics and metals from several plastic-dominated residues of recycling plants that process discarded small home appliances. Preliminary experiments to treat real plastics-dominated residues using the RETAC jig showed very low separation efficiency because of Cu wire entanglement during jig separation that likely limited the upward motion of plastic particles in the separation chamber. To elucidate the factors and mechanisms involved in this entanglement phenomenon, jig separation of model samples was conducted under various conditions. To improve jig separation efficiency when plastics and wires are both present in samples, two methods of shape separation for Cu wire removal prior to jigging were evaluated. Moreover, the bending behavior of Cu wires and its role in the entanglement phenomenon was elucidated. Finally, a new parameter, the entanglement factor, is introduced to estimate jig separation efficiency of plastic-dominated residues from WEEE recycling plants.

5.2 Materials and methods

5.2.1 Samples

The plastic-dominated residues used in this study were obtained from a recycling facility in Japan. Fig. 5-1 shows the treatment flowchart for end-of-life small home appliances utilized in this company. Discarded small home appliances are first crushed and are then treated by low-intensity magnetic separation to separate magnetic (steel) and non-magnetic materials. The non-magnetic fraction is sieved using an 8-mm aperture screen to separate the fine fraction containing plastics, glass, wood,

paper, and various metals like Cu, aluminum (Al), and iron (Fe). Materials retained on the screen are treated by an eddy current separator to recover Al and the resulting product is hand sorted to recover stainless steel. The remaining materials are classified by a rotating screen (16-mm aperture size) into medium and coarse fractions, which are mostly composed of plastics, glasses, wood, paper, and various metals.

Samples from the coarse, medium, and fine fractions of the final residue were used in this chapter. Before jig separation, floating materials were removed by sink-float separation in water and the sink products were sieved through a 1-mm aperture screen. Materials retained on the screen were fed to the RETAC jig. This size fraction was selected because the lower operational limit of a BATAC jig is around 0.5 mm and the separation of particles with sizes less than this value is difficult (Gupta and Yan, 2006).

For the characterization of samples, size distribution was analyzed by sieving while the SG distribution was measure by sink-float analysis using water and zinc chloride ($ZnCl_2$, Wako Pure Chemical Industries, Ltd., Japan) (SG of 1.0, 1.2, 1.4, and 1.8). The different components of the products were separated by hand picking into three fractions: Cu wires, other metals (e.g., Al and Fe), and other materials (e.g., plastics, glasses, wood and paper). Metal contents grouped as "other metal fraction" were analyzed by an X-ray fluorescence (XRF) spectrometer (Rigaku EDXL300, Rigaku Corporation, Japan). An ashing furnace (Ishizuka Denki Seisakusho, Japan) was used to determine the combustible components in the "other material fraction", which is composed primarily of plastics. The ashing method involves slow heating to 815°C for 90 min, which was followed by burning of the samples at this temperature for 2 h. For metal analysis of "other material fraction", the samples were ground at low temperature with liquid nitrogen and dissolved in a microwave-assisted digester (Ethos, Milestone Inc., USA) using aqua regia, a 1:3 mixture of concentrated nitric acid (HNO_3) and hydrochloric acid (HCl) (Wako Pure Chemical Industries, Ltd., Japan). The leachates were then analyzed by inductively coupled plasma atomic emission spectroscopy (ICP-AES, ICPE-9820, Shimadzu Corporation, Japan) (margin of error = ±2%).

Model samples were prepared using 2-mm thick plastic boards of ABS (SG 1.03, Sumitomo Bakelite Co., Ltd, Japan) and PVC (SG 1.31, Sekisui seikei, Ltd., Japan) to represent the light and heavy plastics in real samples, respectively. Because ABS and PS have very similar densities, only ABS was used in the experiments using model samples. The plastic boards were crushed by an orient mill (VH16, Seishin Enterprise Co.,Ltd, Japan), sieved to obtain +2.0-10.0 mm size fractions, and then mixed in a one-to-one ratio (total amount = 500 g). A 0.4-mm diameter Cu wire (SG 8.96) was cut to lengths of 10, 30, and 50 mm, which were bent manually to simulate the bending of Cu wires in real samples. The bent Cu wires were mixed with the two types of plastics at varying amounts (0, 5, 10, and 15% of the total weight).

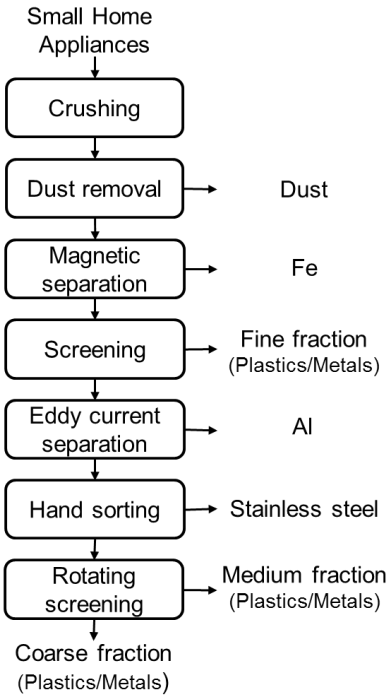

Figure 5-1. The treatment flowchart for discarded small home appliances of a recycling plant in Japan.

5.2.2 Jig separation method

A desktop-type batch-wise RETAC jig with a separation chamber 145 mm long, 155 mm wide, and 320 mm high was used in this study. Jig separation experiments were conducted under the following conditions: displacement of 30 mm, frequency of water pulsation equal to 30 cycles/min, separation time of 3 min and the use of 15 ppm of Di-2-ethylhexyl sodium sulfosuccinate (AOT, $C_{20}H_{37}NaO_7S$, Wako Pure Chemical Industries, Ltd., Japan) as the wetting agent. After jig separation, products were divided into six layers from the top and collected using a vacuum sampling system. An ultrapycnometer (UPY-14, Quantachrome Instruments, Japan) was used to determine the densities of each layer and materials in the layers were separated by hand into three groups: Cu wires, other metals (e.g., Al and Fe), and other materials (e.g., plastics, glasses, wood, and paper) in the case of real samples or into ABS, PVC, and Cu wires in the case of model samples.

5.2.3 Shape separation methods

5.2.3.1 Shape separation using probability of passage

Using the fine fraction of real samples, rod-like materials such as Cu wires were removed by sieving

through a 2-mm aperture screen. The over screen fraction was fed to the RETAC jig.

5.2.3.2 Shape separation using induced entanglement

Real or model samples were treated in a rotating pot at 80% of the critical rotational speed (i.e., calculated from the pot inner diameter of 190 mm and D_{50} of each sample) for 5, 10, and 15 min (Wills and Napier-Munn, 2006). After this, the products were sieved using a 16-mm aperture screen to remove the entangled Cu wires while the under screen fraction was fed to the RETAC jig.

5.3 Results and discussion

5.3.1 Characterization of plastic-dominated residues from an actual recycling plant

The results of sieve analysis showed that D_{50} of the coarse, medium, and fine fractions were 18.5, 8.0, and 2.5 mm, respectively. Fig. 5-2(a) shows that the samples contain 9-18% of floating materials (SG<1.0), 16-55% of light SG fraction (SG 1.0-1.2), 9-10% of medium SG fraction (SG 1.2-1.4), 6-15% of heavy SG fraction (SG 1.4-1.8), and 10-48% of materials containing metals (e.g., printed circuit board (PCB)) (SG > 1.8). The samples are also mainly composed of combustible materials (70-85%) (e.g., PP and PS (Ministry of the Economy, Trade and Industry of Japan, 2017)), non-combustible materials (6-22%) (e.g. glass) and Cu (2-22%) with minor amounts of other metals like Fe (0.2-2.0%) and Al (0.4-1.3%) (Fig. 5-2(b)).

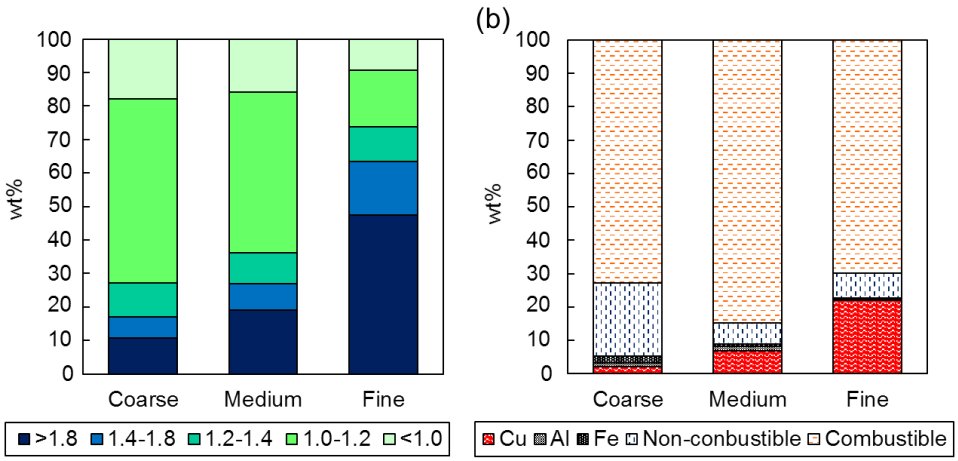

Figure 5-2. (a) Specific gravity distribution, and (b) material compositions of coarse, medium, and fine fractions.

5.3.2 Jig separation of real samples without shape separation

Fig. 5-3(a) shows the results of jig separation of the coarse, medium, and fine fractions. For the coarse (Fig. 5-3(a-1)) and medium fractions (Fig. 5-3(a-2)), Cu wires were recovered in the 6th layer with recovery of 91 and 96%, respectively. For the fine fraction that containing significant amounts of Cu wires (22%) lowered the recovery of Cu wires in the 6th layer (64%) (Fig. 5-3(a-3). Closer inspection showed that Cu wire entanglement occurred in the 5th layer (Fig. 5-3(b)), which created a sort of barrier that prevented the upward motion of plastics and the downward motion of metals, so 2 and 34% of Cu wires remained in the 4th and 5th, respectively and plastics were trapped in the 6th layer. To investigate how this entrapment phenomenon occurred, jig separation of model samples (i.e., mixtures of pure plastic and Cu wires) was carried out.

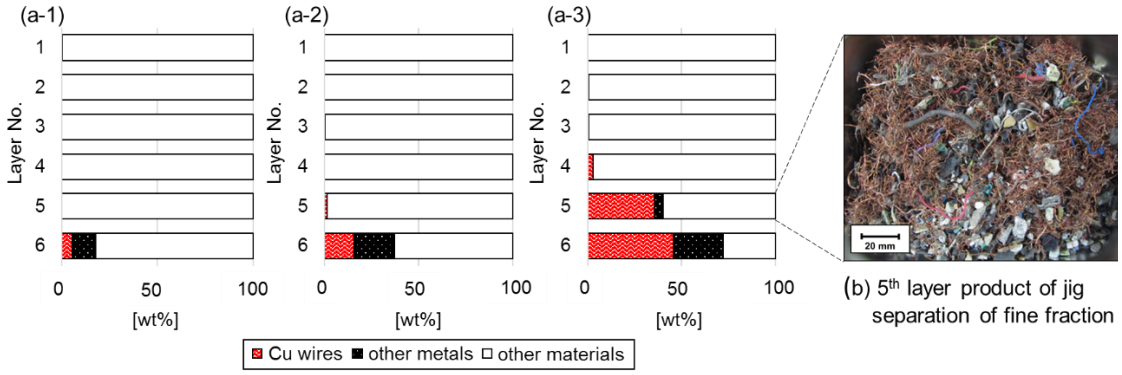

Figure 5-3. (a) The proportion of Cu wires, other metals, and other materials in each layer with the jig separation of real samples at different size fraction; (a-1) coarse, (a-2) medium, (a-3) fine and (b) 5th layer product of jig separation of the fine fraction.

5.3.3 Effects of copper wires on jig separation of model samples

Jig separation of model samples containing ABS, PVC (ABS: PVC, 1: 1) and Cu wires of various amounts (0, 5, 10, and 15%) and length (10, 30, and 50 mm) was carried out for 1, 2, and 3 min, and the results are shown in Fig. 5-4. Without Cu wires (Fig. 5-4(a)), 3 min was sufficient to separate pure ABS and PVC. Fig. 5-4(b) shows the results of jig separation of model samples with 10% Cu wires 30-mm long at various separation times (1, 2, and 3 min). Fig. 5-5(b-3) illustrates that although separation of ABS and PVC in the 1st to 4th layers was almost perfect after 3 min, the 5th and 6th layers still contain ABS with the 5th layer also containing Cu wires. These results replicated those observed in the real sample; that is, entangled Cu wire created a barrier-like layer that clogged the separation chamber and prevented the upward motion of higher plastics, so ABS was trapped in the 5th and 6th layer.

Fig. 5-4(c)&(d) show the effects of Cu wire content and length on jig separation after 3 min. When the Cu wire content was 5% (Fig. 5-4(c-1)), perfect separation of ABS and PVC was obtained with most of the Cu wires recovered in the 6th layer (98%). The recovery of Cu wires in the 6th layer and the separation efficiency of ABS and PVC decreased when the Cu wire content increased (78% recovery at 10% Cu wire content and 32% recovery at 15% Cu wire content). When the Cu wire content was fixed at 10% and short Cu wires were used (10 mm), separation of ABS and PVC was almost perfect and Cu wires could be recovered in the 6th layer (100%). At longer Cu wire length, however, the recovery of Cu wires in the 6th layer and separation efficiency of ABS and PVC decreased (78% recovery with 30-mm long wires and 52% recovery with 50-mm long wires). These results show that both the Cu wire content and length strongly affect the efficiency of jig separation. Based on these results, novel shape separation methods are proposed, and the results are shown in next section.

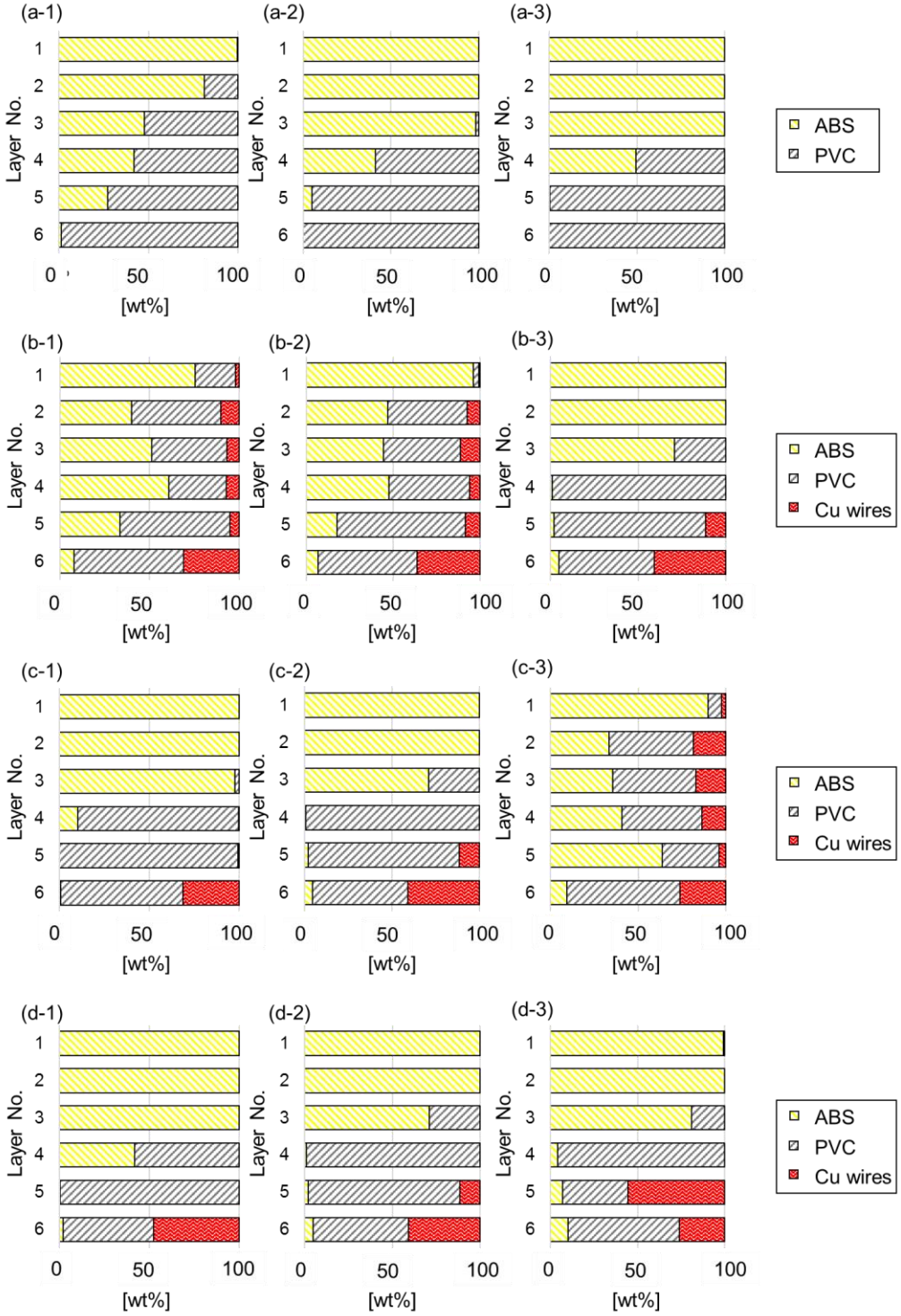

Figure 5-4. The proportion of ABS, PVC and Cu wires in each layer after the jig separation of model samples: (a) without Cu wires at separation time of (a-1) 1 min, (a-2) 2 min, and (a-3) 3 min; (b) with 10% Cu wires of 30-mm long at separation time (b-1) 1 min, (b-2) 2 min, and (b-3) 3 min; (c) with 30-mm Cu wires at Cu wire content of (c-1) 5%, (c-2) 10%, and (c-3) 15% (separation time 3 min); (d) with 10% Cu wires at Cu wire length of (d-1) 10 mm, (d-2) 30 mm, and (d-3) 50 mm (separation time 3 min).

5.3.4 Shape separation

When Cu wires are short and their content is low, separation of ABS and PVC was perfect because Cu wire entanglement was negligible. However, entanglement was more extensive as the length and amounts of Cu wires increased, which resulted in lower separation efficiency. Improvement of jig separation efficiency could be done using two methods: (1) crushing of Cu wires to <10 mm, and (2) reducing the Cu wire content by pre-treatment (e.g., screening). In the first method, shorter Cu wires due to crushing could dramatically limit entanglement, but further crushing may lower the separation efficiency because jig separation of fine particles is more difficult. This means that the second option is the more appropriate method to improve jig separation efficiency of samples containing a lot of Cu wires. To reduce the Cu wire content by pre-treatment before jig separation, shape separations using simple screening method and a novel combination method were applied.

5.3.4.1 Shape separation using probability of passage

Real samples (fine fraction: +1-16 mm, D_{50} = 2.5 mm) were used for the shape separation experiments. Preliminary experimental results show that Cu wires could pass through a 2-mm aperture screen. Thus, screening using a 2-mm opening was carried out to remove Cu wires before the jig separation.

Fig. 5-5 illustrates some examples of probability of passage of a rod-like particle like Cu wires. In the screening of non-spherical particles, probability of passage is a function not only of particle size but also of particle orientation relative to the screen opening (Beunder, 2000; Beunder and Rem, 1999). Non-spherical particles could pass through the screen if they have at least one orientation smaller than the screen opening (Koyanaka et al, 1995; Yamamota et al, 2009). The probability of passage is affected by particle shape, especially for rod-like particles like Cu wires. Fig. 5-5(a) shows that rod-like particles could pass through the screen aperture in cases (a-1), (a-2), and (a-3) but not in case (a-4) (Beunder, 2000). This means that short Cu wires could pass through the opening using the probability of passage and reduction of Cu wire content was possible.

The probability of passage of rod-like particles also depend on their length. Because the screen is not perfectly flat, its vertical movement could make the particles roll, turn over, and pass through if the center of mass and edge of the particle are within the opening as shown in Fig. 5-5(b) (Beunder, 2000; Beunder and Rem, 1999).

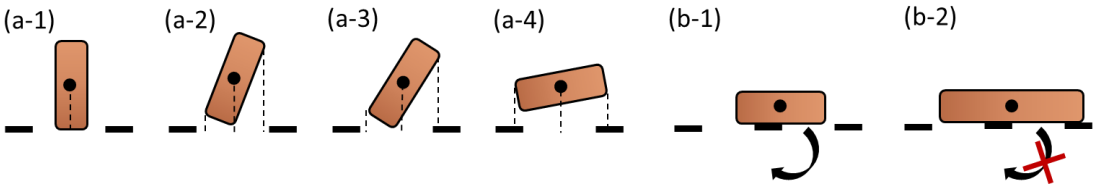

Figure 5-5. A schematic diagram of probability of passage of rod-like particle (a) particle orientations during screening; (a-1, a-2, and a-3) can pass through screen and (a-4) cannot and (b) rolling during screening; (b-1) can turn over and pass through screen and (b-2) cannot (Beunder, 2000; Beunder and Rem, 1999).

5.3.4.2 Shape separation using induced entanglement

As described in previous section, longer Cu wires lowered the efficiency of jig separation. To remove long Cu wires, entanglement was induced in a rotating pot before screening since long Cu wires are easier to entangle with each other by a rotating motion. Before the treatment of real samples, model samples of ABS, PVC, and Cu wires were treated in a rotating pot at 80% of the critical rotational speed for 5, 10, and 15 min, after which, the samples were sieved using a 16-mm aperture screen to recover the entangled Cu wires.

The size and volume of entangled materials in the cases of 10- and 30-mm Cu wires were smaller than that of the 50-mm Cu wires. The removal (i.e., recovery in unwanted fraction) of Cu wires 50-mm in lengths for 5, 10, and 15 min were 48, 79, and 75%, respectively (purities, i.e., concentrations, of Cu wires in the over screen products were more than 95%), which means that 10 min of treatment was enough.

For real samples (i.e. fine fraction), 11% of Cu wires with 93% purity were removed as over screen product (Table 5-1). Cu wire removal using the first method (probability of passage) and second method (induced entanglement) were 61 and 11%, respectively. The average lengths of Cu wires removed by these two methods were 12 mm (probability of passage) and 36 mm (induced entanglement), indicating that the second method could remove longer Cu wires.

Table 5-1. Cu wire removal by shape separation.

Shape separation method	Cu wires removal (%)	Purity of Cu wires (%)	Average length (mm)
Probability of passage (under screen product)	61	49	12
Induced entanglement (over screen product)	11	93	36

5.3.5 Jig separation of real samples after shape separation

The results of jig separation of real samples (fine fraction) with and without shape separation are shown in Fig. 5-6. Table 5-2 shows that the recovery of Cu wires in the 6th layer after jig separation without shape separation (64%) dramatically improved with shape separation using probability of passage (92%) and induced entanglement (98%). Fig. 5-7 shows the SG of other material fractions (e.g., plastics, glass, wood, paper) of jig products. The slope of trendline was 13.72 (without shape separation), 7.56 (with shape separation using probability of passage), and 6.89 (with shape separation using induced entanglement). These results show that shape separation could improve the efficiency of jig separation.

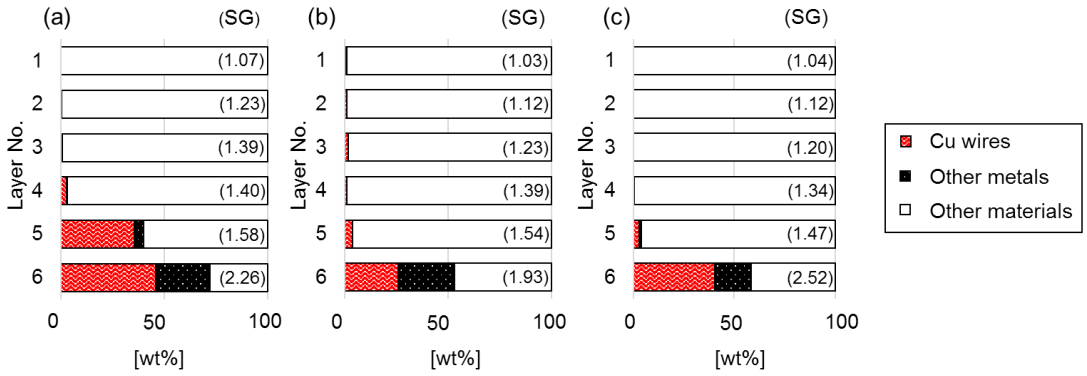

Figure 5-6. The proportion of Cu wires, other metals, and other materials including the specific gravity of other materials fraction (e.g. plastics, glasses, wood, and paper) in each layer after the jig separation of real samples (fine fraction) (a) without shape separation, (b) with shape separation using probability of passage, and (c) with shape separation using induced entanglement.

Table 5-2. Purity and recovery of Cu wires in the 6th layer of jig product with and without shape separation.

Method	**Purity of Cu wires (%)**	**Recovery of Cu wires (%)**
Jig separation w/o shape separation	46	64
Jig separation w/ shape separation (probability of passage)	26	92
Jig separation w/ shape separation (induced entanglement)	40	98

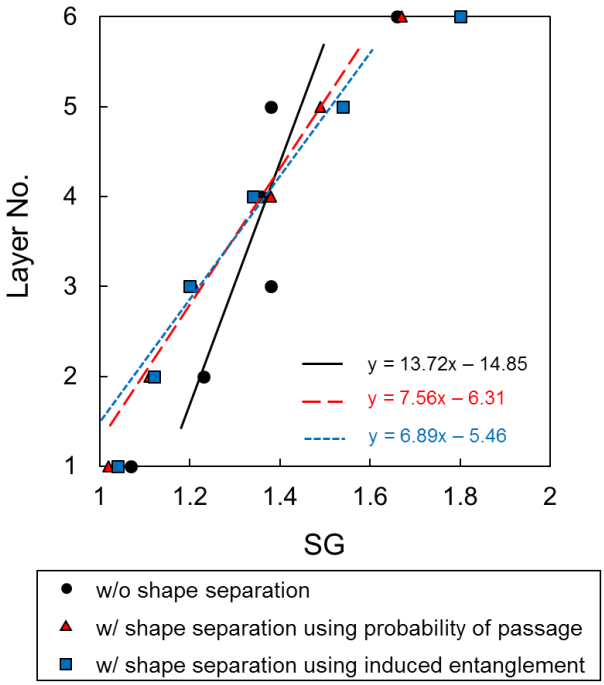

Figure 5-7. Specific gravity of other materials fractions (e.g. plastics, glasses, woods and papers) of products in each layer after jig separation.

Fig. 5-8 shows a proposed flowchart to treat plastic-dominated residues with Cu wires including shape separation. Cu concentrate from shape separation and the 6th layer of jig separation could be sent to Cu smelters while low-chloride plastics fraction could be sent to thermal recovery plants. Table 5-3 shows the purity and recovery of Cu wires in Cu concentrate of Fig. 5-8. Recovery of Cu concentrate was 64% (without shape separation), 97% (with shape separation using probability of passage), and 95% (with shape separation using induced entanglement), indicating that shape separation could dramatically improve the recovery of Cu wires. However, purity of Cu concentrates of jig separation with shape separation using induced entanglement (97%) was higher than that jig separation with shape separation using probability of passage (44%), indicating that shape separation using induced entanglement could improve both purity and recovery.

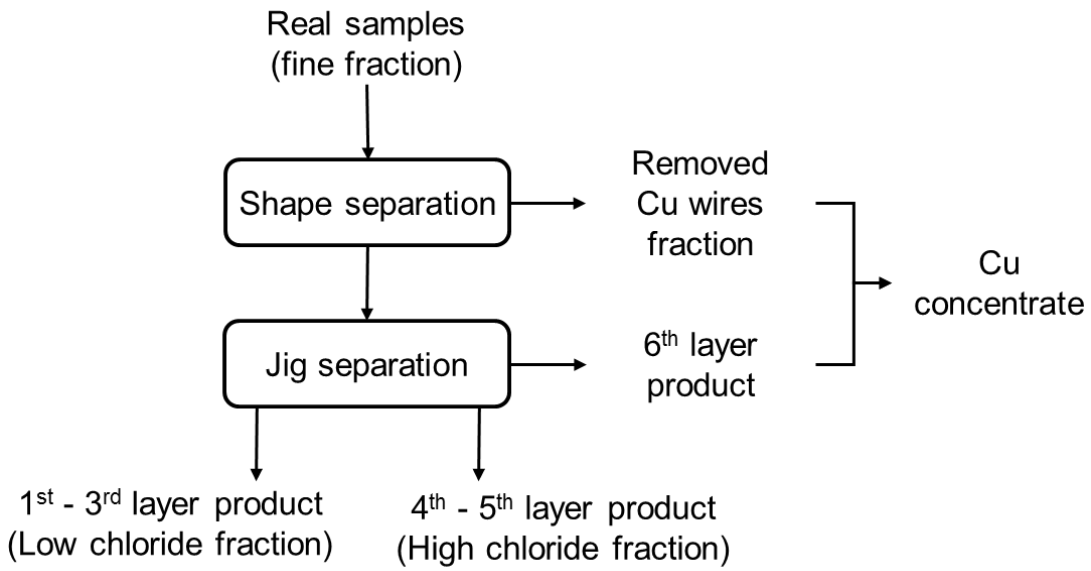

Figure 5-8. Proposed treatment flowchart including shape separation for plastic-dominated residues with Cu wires.

Table 5-3. Purity and recovery of Cu wires in Cu concentrate of Fig. 5-8.

Method	**Purity of Cu wires (%)**	**Recovery of Cu wires (%)**
Jig separation w/o shape separation	46	64
Jig separation w/ shape separation (probability of passage)	44	97
Jig separation w/ shape separation (induced entanglement)	97	95

In commercial scale operations, a rotating pot is not commonly used in recycling plants, so a modified rotating screen could be used instead. A schematic diagram of this modified screen is shown in Fig. 5-9. The feed-end should be covered to induce entanglement of long Cu wires while the discharge-end is composed of a normal screen, which could separate undersize materials for jig separation and entangled Cu wires as over screen product.

Although both recovery and purity were improved by combining shape separation and jig treatment, the entanglement phenomenon during jig separation still remains unclear. To investigate this interesting phenomenon further, the evaluation of bending behavior and entanglement factor of Cu wires were carried out.

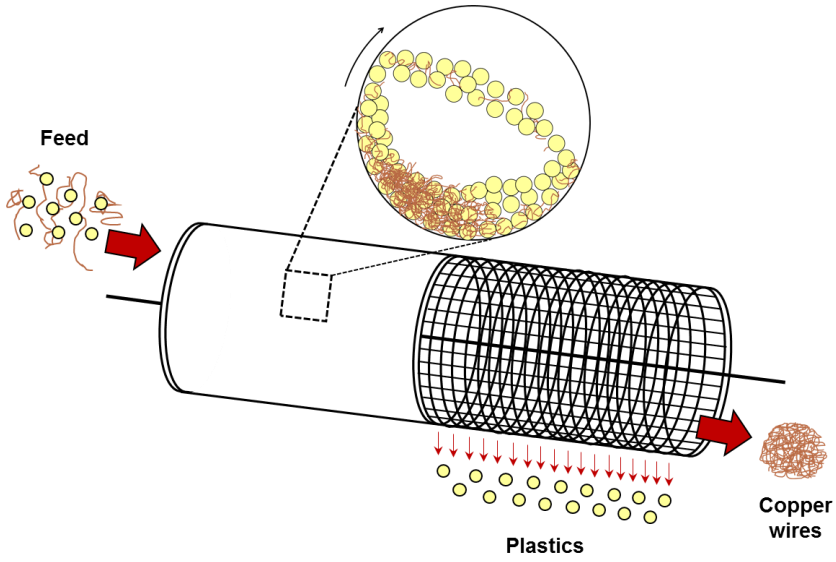

Figure 5-9. A schematic diagram of a modified rotating screen.

5.3.6 Evaluation of bending behavior of flexible rod-like materials

Flexible rod-like materials such as Cu wires are bent easily, and the folded parts become hook-like appendages that induce entanglement. To evaluate the bending behaviors of the Cu wires, a 0.4-mm diameter wire was cut to 10, 30, 50 mm length (L_s) and bent manually to simulate their bending Cu wires in real samples. Absolute maximum lengths of bent Cu wires (L_b) were measured by image analysis (WinRoof, Mitani Corporation, Japan) and the degree of flexion was calculated by Eq. (5-1).

$$Degree\ of\ flexion\ = \frac{L_s}{L_b} \tag{5-1}$$

L_s: Real length of straight Cu wires (mm)

L_b: Absolute maximum length of bent Cu wires (mm)

Fig. 5-10(a) shows the relationship between L_s and the average degree of flexion from 50 measurements. The results showed that increasing of L_s resulted in larger values of the degree of flexion. Fig. 5-10(b), shows that wires with a degree of flexion equal to 3 has 2 folding points, which made them more prone to entangle because of two hook-like appendages. The number of folding points was calculated by Eq. (5-2).

$$Number\ of\ folding\ points = Degree\ of\ flexion - 1 \tag{5-2}$$

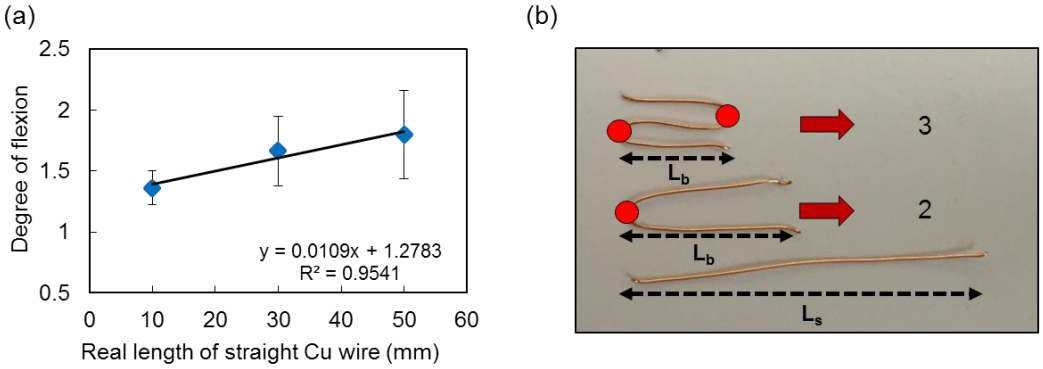

Figure 5-10. (a) The relationship between real length of straight Cu wire (L_s) and average degree of flexion, and (b) real length of straight Cu wire (L_s) and absolute maximum length of bent Cu wire (L_b).

5.3.7 Estimation of separation efficiency using "entanglement factor"

Because folding points resembled hooks, they could easily entangle with each other. This means that although long straight Cu wires do not affect jig separation, their longer lengths could create more folding points that increase the probability of entanglement. Jig separation results on model samples showed that the recovery of Cu wires in the 6th layer was affected by the length and relative amounts of Cu wires. Thus, an entanglement factor (Eq. 5-3) is proposed.

$$Entanglement\ factor = L_s(mm) \times Copper\ content(\%) \times Number\ of\ folding\ points \quad (5\text{-}3)$$

The relationship between the entanglement factor and recovery of Cu wires in the 6th layer is shown in Fig. 5-11. The results showed that at higher values of the entanglement factor, the recovery of Cu wires in the 6th layer became lower. The results also showed that 10% of 30-mm long Cu wires and 5% of 50-mm long Cu wires have similar values of entanglement factor and recovery of Cu wires, indicating that both length and relative abundance have strong effects on the Cu wire recovery. Based on these results, the entanglement factor could be used to estimate the jig separation efficiency of real samples containing Cu wires.

Fig. 5-12 shows the relationship between entanglement factor and recovery of Cu wires in the 6th layer of real samples with the trendline from Fig. 5-11. The results of real samples (coarse, medium, and fine fraction) without shape separation and real samples (fine fraction) with shape separation showed similar trends with model samples, which could be estimated by Eq. (5-4).

$$y = \beta x + \alpha \quad (5\text{-}4)$$

x : Entanglement factor

y : Recovery of Cu wires in 6th layer (%)

α : the vertical intercept of linear regression line =103.85 ± 13.20

β : Slope of linear regression line = -13.015

These results confirmed that both the length and relative abundance of Cu wires affect the recovery of Cu wires in the 6th layer of jig separation. Moreover, the entanglement factor calculated using Cu wire length and amount could estimate the recovery of Cu wires in the 6th layer after jig separation.

Comparing the two shape separation processes, Cu wire removal using probability of passage (61%) was higher than that of induced entanglement (11%). The average length of Cu wires removed by the former was about 12 mm, which was shorter than the latter (about 36 mm). Shape separation using probability of passage removed only short Cu wires while the longer wires remained, albeit in low amount indicating that the entanglement factor was low. In comparison, shape separation using induced entanglement could remove long Cu wires but amounts of short Cu wires still remained that also gave a low value of the entanglement factor. This means that the separation efficiency, could be improved by reduction of the entanglement factor but perfect Cu wire removal is not required.

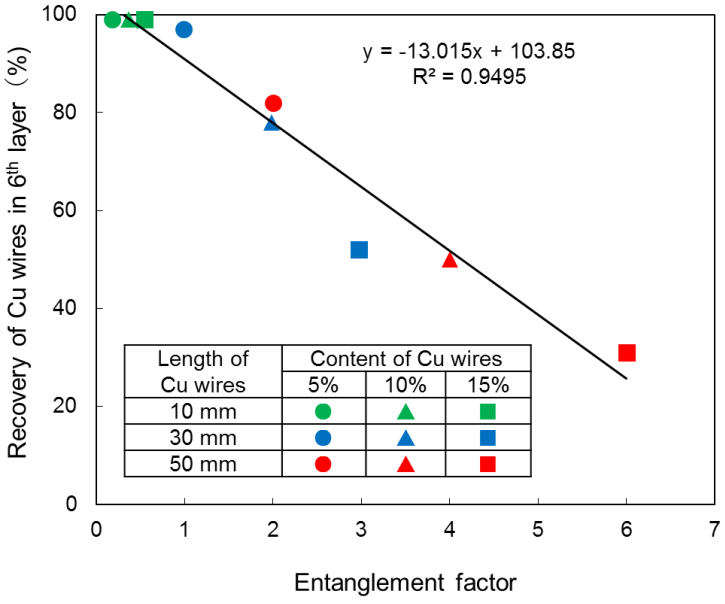

Figure 5-11. Relationship between entanglement factor and recovery of Cu wires in 6th layer of model samples.

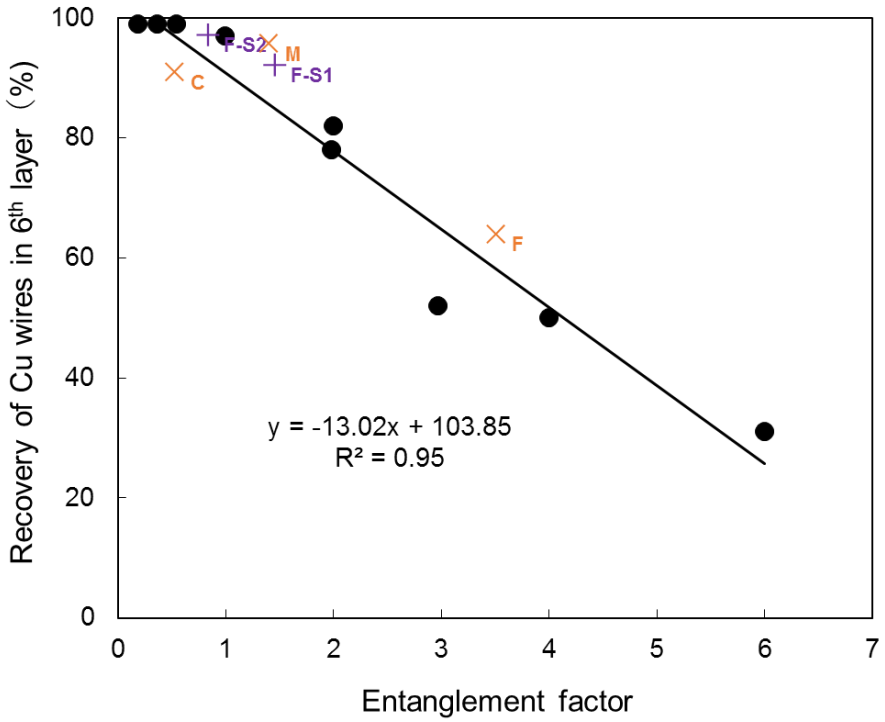

Symbol	Description
●	Model samples
×C	Real samples (coarse fraction) w/o shape separation
×M	Real samples (medium fraction) w/o shape separation
×F	Real samples (fine fraction) w/o shape separation
+F-S1	Real samples (fine fraction) w/ shape separation using probability of passage
+F-S2	Real samples (fine fraction) w/o shape separation using induced entanglement

Figure 5-12. Relationship between entanglement factor and recovery of Cu wires in 6th layer of real samples with trendline from Fig. 5-11.

5.4 Conclusions

Valuable materials recovery from plastic-dominated residues of a recycling plant for small home appliances was investigated using a RETAC jig. The presence of Cu wires in the fine fraction (+1.0-16 mm, D_{50} = 2.5 mm) of the residues resulted in low separation efficiency due to the entanglement of Cu wires in the separation chamber. Jig separation of pure ABS and PVC with bent Cu wires as model samples showed that higher Cu wire content and longer wires (i.e. high entanglement factor) lowered the efficiency of separation.

Two different methods of shape separation, probability of passage and induced entanglement, were used to pre-treat of residues containing Cu wires before being fed to the jig to reduce the entanglement factor and improve jig separation. Shape separation using probability of passage could remove shorter Cu wires (12 mm) with higher Cu wire removal (61%) while shape separation using

induced entanglement can remove longer Cu wires (36 mm) but at lower removal (11%). This suggests that both shape separation techniques could reduce the entanglement factor. The two shape separation methods increased the recovery of Cu wires in the 6th layer of jig separation from 64% (without shape separation) to 92% (with shape separation using probability of passage) and 98% (with shape separation using induced entanglement). This means that the reduction of entanglement factor could improve the separation efficiency even without perfect removal of Cu wires.

This chapter is modified from "Phengsaart et al.,2018. Improvement of jig efficiency by shape separation, and a novel method to estimate the separation efficiency of metal wires in crushed electronic wastes using bending behavior and "entanglement factor". Miner. Eng. 129, 54-62".

References

Beunder, E.M., 2000. Influence of shape on particle behaviour in recycling techniques. https://www.env.go.jp/en/recycle/smcs/attach/hcswm.pdf (accessed 25 December 2017)

Beunder, E.M., Rem, P.C., 1999. Screening kinetics of cylindrical particles. Int. J. Miner. Process. 57, 73-81. https://doi.org/10.1016/S0301-7516(99)00007-1.

Gupta, A., Yan, D.S., 2006. Mineral Processing Design and Operation – An Introduction, Perth, Australia.

Koyanaka, S., Endoh, S., Iwata, H., 1995. The recovery of printed wiring board scraps using a shape sorting techniques - Recovering copper components by inclined vibrating method -. J. Soc. Powder Technol. 32, 385-391. https://doi.org/10.4164/sptj.32.385

Ministry of Economy, Trade and Industry of Japan, 2017. Enforcement status of the small home appliances recycling law and recycling statistics for manufacturers and Importers. http://www.meti.go.jp/committee/sankoushin/sangyougijutsu/haiki_recycle/kogata_kaden/pdf/003_02_00.pdf (accessed 4 July 2018)

Ministry of the Environment of Japan, 2014. History and current state of waste management in Japan. https://www.env.go.jp/en/recycle/smcs/attach/hcswm.pdf (accessed 25 December 2017)

Wills, B.A., Napier-Munn, T.J., 2006. Mineral Processing Technology, seventh ed. Pergamon press, Oxford.

Yamamoto, K., Shiraiwa, M., Honda, Y., Sugimoto, M., 2009. Continuous separation of differently shape particles in a horizontal flowing wet settler. J. Soc. Powder Technol. 46, 688-697. https://doi.org/10.4164/sptj.46.688

CHAPTER 6 –DEVELOPMENT OF A DISCHARGE SYSTEM FOR CONTINUOUS JIG SEPARATION OF PLASTICS USING A RESTRAINING WALL

6.1 Introduction

A continuous-type jig is commonly used in commercial scale application than that of batch-type jig that preferred for laboratory experiments. In case of the BATAC jig for coal cleaning, a gate system is used to recover the bottom layer product for high SG materials such as rocks that can be removed easily with gravity (MBE Coal&Minerals Technology GMBH, 2011). This type of gravity-based recovery system is, however, unsuitable for the RETAC jig because it treats plastics having low SGs and low settling velocities. Because of this, mechanical extractors (e.g., screw-type extractor) are preferred in continuous-type RETAC jig to recover the bottom layer products at an adjustable rate while the top layer products are recovered from the overflow launder. However, when the ratio of heavy particles in feed was low, the purity of bottom layer products is low because of the entrainment of light particles caused by the disturbances in water and particles flow regimes due to a screw-type extractor movement.

In a previous study, a new discharge system using a vertical restraining wall was developed to improve the purity of bottom layer product (Tsunekawa et al., 2012), but because a mechanic extractor was not used, the product recovery rate cannot be controlled in this system. In this chapter, the combined effects of a vertical restraining wall and a screw-type extractor on the purity of bottom layer products were investigated. In addition, an estimation procedure based on multi-step treatment using separation curves is proposed to achieve the target purity of bottom layer products.

6.2 Materials and methods

6.2.1 Samples

The plastic pellets of acrylonitrile butadiene styrene (ABS) with cylindrical shape and polyacetal (polyoxymethylene, POM) with oblate spheroid shape, and the 2-mm thick plastic boards of polyethylene terephthalate (PET) and polyvinylchloride (PVC) were used in this chapter, and brief descriptions of properties as well as specific gravity (SG) are listed in Table 6-1. The plastic boards were crushed by an orient mill (VH16, Seishin Enterprise Co. Ltd, Japan) and screened to obtain suitable size fractions for the jig separation experiments.

Table 6-1. Plastic samples used in this study.

Samples	Abbreviated name	SG	CC	Size fraction [mm]
Acrylonitrile butadiene styrene	ABS	1.27	1.56	+2.0-4.0
Polyacetal or polyoxymethylene	POM	1.42		
Polyethylene terephthalate	PET	1.31	1.23	+2.0-8.0
Polyvinylchloride	PVC	1.38		

6.2.2 Continuous-type jig experiments

Fig. 6-1 shows the schematic diagrams of a continuous-type jig (a) without, and (b) with a vertical restraining wall. Feed materials are fed at an adjustable rate using a vibrating feeder in to a continuous-type RETAC jig and bottom layer products were recovered by a screw-type extractor while the top layer products were recovered from the overflow launder when the restraining was not installed (Fig. 6-1(a)) or manually at a constants rate in the presence of a restraining wall (Fig. 6-1(b)).

In a previous study (Tsunekawa et al., 2012), it was shown that the purity of bottom layer products can be improved when bottom layer is relatively thick, indicating that thickness of the bottom layer effects the purity of bottom layer products. One method to increase the thickness of bottom layer is through the installation of a vertical restraining wall close to the product-end (a screw-type extractor). The restraining wall was installed to divide the separation chamber into two regions and particles can transfer from one region to the other only through a narrow channel below the wall (Fig. 6-2(b)).

The effects of material ratio in feed on the separation efficiency of a continuous-type jig were investigated, two kinds of plastic mixtures (Table. 6-1) at different mass ratio of light and heavy (*L/H*) particles (75:25, 70:30, 65:35, 60:40, 55:45, and 50:50) were fed at a constant rate using a vibrating feeder into a continuous-type RETAC jig with a separation chamber with 445 mm long, 150 mm wide, and 550 mm high (thickness of particle layer was controlled to 135 mm). Continuous-type jig separations were conducted under the following conditions: displacement and frequency of water pulsation equal to 30 mm and 30 cycles/min, and 15 ppm of Di-2-ethylhexyl sodium sulfosuccinate (AOT, $C_{20}H_{37}NaO_7S$, Wako Pure Chemical Industries, Ltd., Japan) as a wetting agent for ABS/POM mixtures and 50 ppm of calcium ligninsulfonate (CaLS, Sigma-Aldrich Co. LLC, USA) as a wetting agent of PET/PVC mixtures. The continuous-type jig experiments were conducted with and without the restraining wall as shown in Figs. 6-1, 6-2, and Table 6-2. After jig separation, the particle remained in jig separation chamber were divided into three zone from feed-end and into six layers from the top (as described later in Fig. 6-4). After recovery of products, hand picking was carried out to determine

the purity of jig products. Particle motion during jig separation were recorded by a video camera and analyzed by 2D motion analysis software (DIPP-MotionV, Ditect Co., Ltd., Japan), and particle image velocimetry (Flownizer2D) using particle tracking velocimetry (PTV) method.

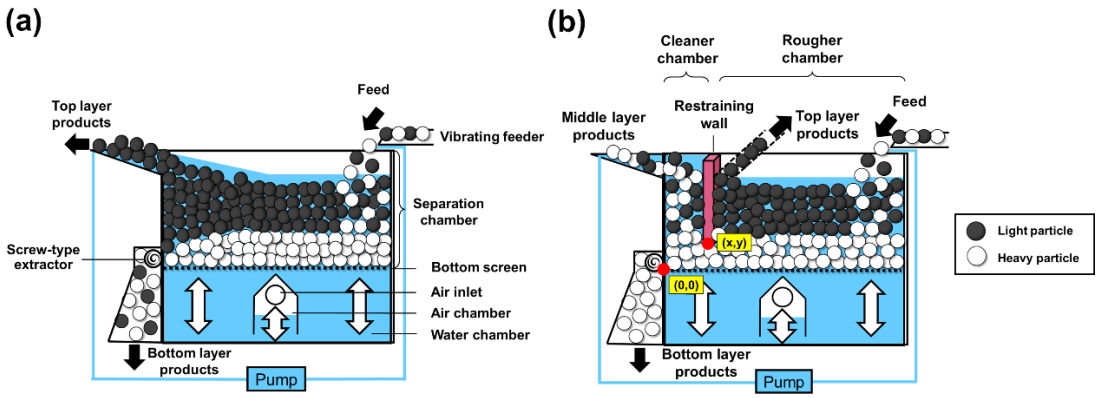

Figure 6-1. Schematic diagrams of a continuous-type jig (a) without, and (b) with a vertical restraining wall.

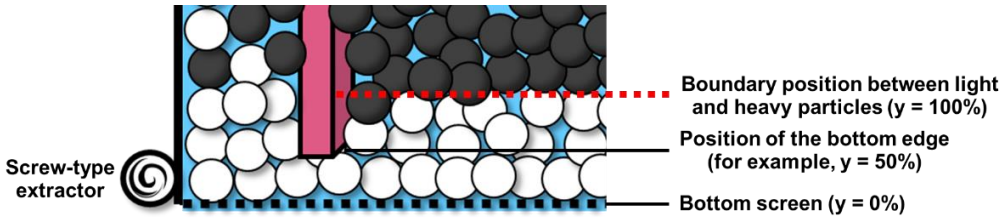

Figure 6-2. Wall position with the relation of boundary position between light and heavy particles.

Table 6-2. Wall position used in this study.

Run No.	ABS/POM		PET/PVC	
	(*x*,*y*) [%]	(*x*,*y*) [mm]	(*x*,*y*) [%]	(*x*,*y*) [mm]
0	-	-	-	-
1	(50, 25)	(65, 50)	(50, 25)	(50, 100)
2	(100, 25)	(130, 50)	(100, 25)	(100, 100)
3	(50, 50)	(65, 100)	(50, 50)	(50, 200)
4	(100, 50)	(130, 100)	(100, 50)	(100, 200)

Note: "–" means without restraining wall. "*x*" was decided from the distance that particle layer start to change the porosity due to the presence of wall (100% indicates that 50 times of D_{50} (Mehta and Hawley, 1969)), and "*y*" was decided from the boundary position between light and heavy particles (100% indicates that bottom edge of restraining wall and the boundary position are same).

6.2.3 Batch-type jig experiments

To elucidate the effects of material ratio of ABS/POM and PET/PVC mixtures in feed without the effects of a screw-type extractor, batch-type jig experiments without restraining wall were investigated. Total 1 kg of feed samples at different *L/H* ratio (75:25, 70:30, 65:35, 60:40, 55:45, and 50:50) (thickness of particle layer was controlled to around 135 mm, so that it is the similar as the continuous-type jig experiments) with different mass ratios (the same as the continuous-type jig experiments) were fed into a batch-type RETAC jig with a separation chamber (145 mm long, 155 mm wide, and 320 mm high). Batch-type jig experiments were conducted under the same condition as continuous-type jig. After 10 min of jig separation, products were divided into six layers from the top and hand picking was carried out to determine the purity of jig products.

In addition, to investigate the effects of a restraining wall on water and particles flow without the effects of a screw-type extractor, a vertical restraining wall was installed in the separation chamber of batch-type RETAC jig (Fig. 6-3) and batch-type jig experiments with restraining wall were carried out using the total 2 kg of ABS/PS at *L/H* ratio of 65:35, 100:0, and 0:100. Particle motion during jig separation were recorded by a video camera.

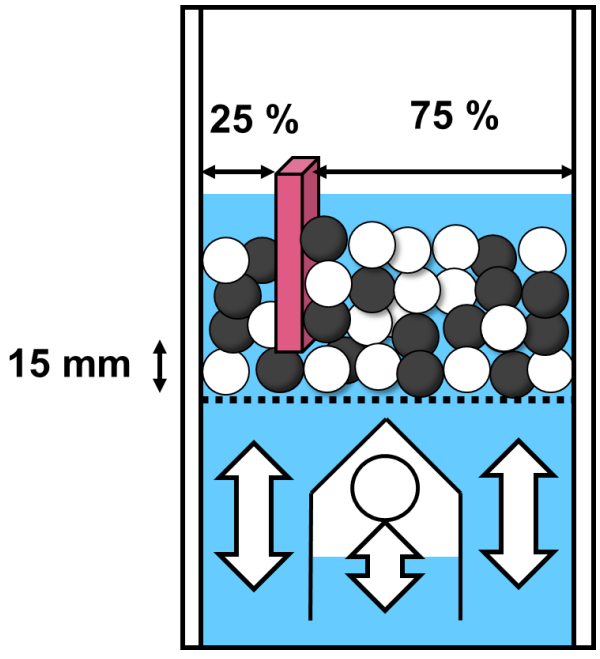

Figure 6-3. Schematic diagrams of a batch-type jig with a vertical restraining wall.

6.3 Results and discussion

6.3.1 Continuous-type jig experiments with and without restraining wall

Fig. 6-4 shows the examples of sample distribution (i.e., 65:35 *L/H* ratio of ABS(*L*)/POM(*H*)) in each zone (A, B, and C) and layer (1-6) after continuous-type jig experiments (a) without and (b) with a restraining wall (at wall position (*x, y*) of (65, 100)). The results of A zone that closed to the feed side showed that the POM that is the heavy particles remained in the top layer because feed materials are fed from a vibrating feeder that located at the upper side of separation chamber (Fig. 6-1). However, in the case of a continuous-type jig experiments without a restraining wall (Fig. 6-4(b)), both of purity of ABS in 1st layer and POM in 6th layer in B Zone were very high (>99%) indicating that the separation time is enough. C zone also showed the similar results as B zone, however, the bottom layer products recovered by a screw-type extractor was low (83%) and this confirmed that jig separation by water pulsation can obtain very high purity of top and bottom layer (>99%) but recovered products by a screw- type extractor caused the entrainment of light particles and development of recovery method is needed. In the case of the results of a continuous-type jig experiments with a restraining wall (Fig. 6-4(b)), due to the presence of a vertical restraining wall, the particles only pass through the small channel under the restraining wall between the chamber close to feed side (rougher chamber) to the chamber close to product-end (cleaner chamber) (Fig. 6-1(b)) and since the POM was located at the bottom layer so, mostly POM could pass this channel and distribution ratio of POM in C zone increased and the purity of bottom layer products recovered by a screw-type extractor increased (90%). These results suggest that material ratio affect to the purity of recovered products. In next section, the effects of material ratio in feed on the purity were investigated.

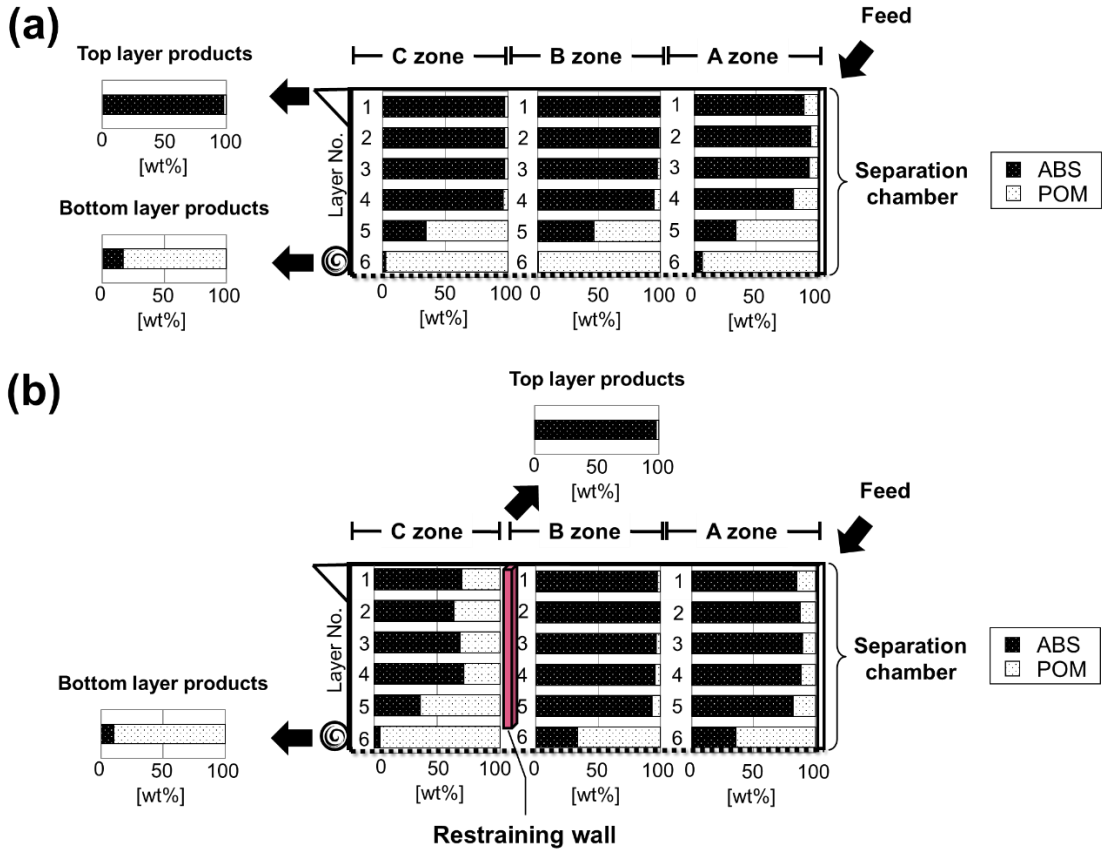

Figure 6-4. Distributions of ABS and POM in in top and bottom layer products, and particles remained in each zone and layer after the equilibrium state of continuous-type jig experiments (a) without, and (b) with a vertical restraining wall.

6.3.2 Effects of material ratio in feed on the purity

The effects of material ratio in feed on the separation efficiency of batch and continuous-type jig were investigated, two kinds of plastic mixtures (Table 6-1) at different *L/H* ratio (75:25, 70:30, 65:35, 60:40, 55:45, and 50:50) were used in this section.

Fig. 6-5(a) shows the purity of light particles (ABS or PET) in top layer products of continuous-type jig experiments at different L/H ratios in feed. The results showed that the purity of light particles in top layer products increased with the increasing of light particles ratio in feed and these results confirmed that materials ratio in feed affect the purity of products. When compared the different CC of plastic mixtures, ABS/POM (CC of 1.56) showed higher purity than that of PET/PVC (CC of 1.23). Fig. 6-5(b) shows the purity of light particles in 1st layer products of batch-type jig experiments at different *L/H* ratios in feed under the same condition of continuous-type jig experiments. These results were in line with the results of continuous-type jig. However, the value of purity of batch-type was lower than that of continuous-type under this condition. This lower purity may be caused by imperfect fluidization in batch-type jig. In continuous-type jig, fluidization is caused by not only the water

pulsation in vertical direction but also water and particles flows in horizontal direction that was introduced by a screw-type extractor so, the fluidization in this condition was enough for continuous-type jig, however, enough fluidization could not be obtained for batch-type jig under the same condition with continuous-type jig.

Fig. 6-6(a) shows the purity of heavy particles (POM or PVC) in bottom layer products recovered by a screw-type extractor of continuous-type jig tests at different ratios between light and heavy materials in feed. The results showed that the purity of heavy particles in bottom layer products increased with the increasing of heavy particles ratio in feed and these results were in line with the results of batch-type jig (Fig. 6-6(b)). However, the value of purity of continuous-type was lower than that of batch-type because of the entrainment of light particles occurred by a screw-type extractor.

Improvement of bottom layer products purity could be done using two methods: (1) multiple step treatment (bottom layer products jig of first step jig are fed to next step jig, as the cleaning separation), and (2) increasing of materials ratio of heavy particles near the screw-type extractor using a vertical restraining wall (Figs. 6-1(b) & 6-4(b)). Separation of both methods are carried out with high materials ratio of heavy particles. Fig. 6-7 shows the relation of materials ratio of heavy particles in feed (horizontal axis) and purity of heavy particles in bottom layer products (vertical axis) from the experimental results of continuous-type-jig separation without restraining wall (ABS/POM: CC of 1.56 and PET/PVC: CC of 1.23), and these curves are called as the “separation curves”. These separation curves showed that at same materials ratio of heavy particles in feed, the purity of heavy particles in bottom layer products of ABS/POM mixtures was higher than that of PET/PVC since higher separation efficiency could be obtained with higher CC as described in Chapter 4. Using these separation curves, required cleaning treatment to achieve the target purity of bottom layer products can be estimated. For examples, when the materials ratio of heavy particles in feed of ABS/POM mixture is 25%, expected purity of bottom layer products is 40%, after that this product (40% purity) is fed to next cleaning step, and 90% of bottom layer products purity can be obtained. As described in section 6.3.1, since the high separation efficiency was obtained even in B zone thus, a vertical restraining was installed between B and C zones. This C zone that close to the product-end can become the “cleaner chamber” and the material ratio in C zone is increased that resulted to the increasing of purity of heavy particles in bottom layer products (Fig. 6-3(b)). This system is better than that of multiple step treatment jig separation since both of separation time and cost can be reduced.

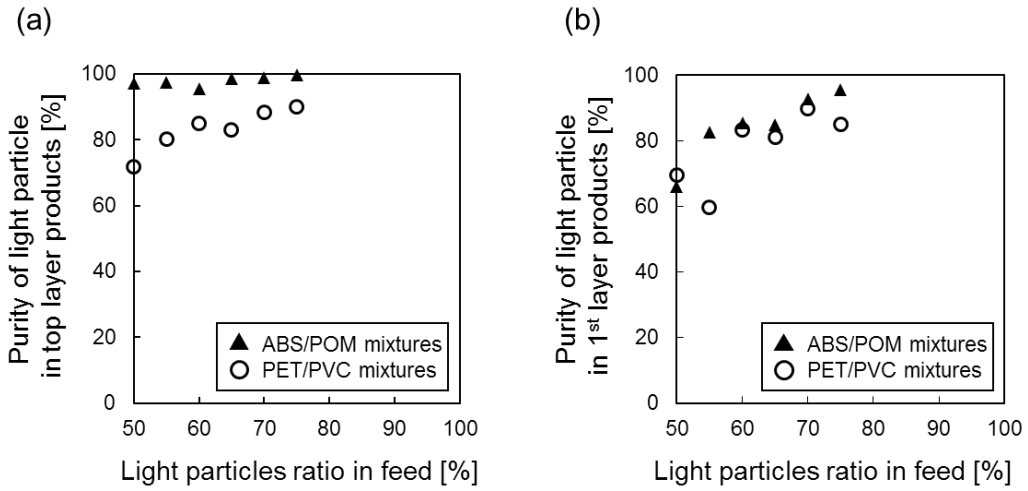

Figure 6-5. Relation between the light particles ratio in feed and (a) purity of light particles in top layer products from continuous-type jig experiments and (b) purity of light particles in 1st layer products from batch-type jig experiments.

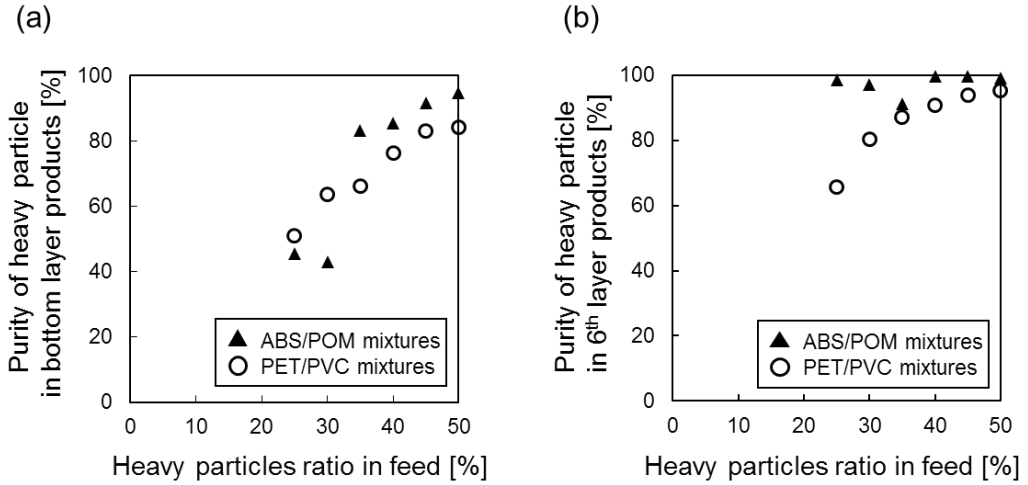

Figure 6-6. Relation between the heavy particles ratio in feed and (a) purity of heavy particles in bottom products from continuous-type jig test and (b) purity of heavy particles in 6th layer products from batch-type jig test

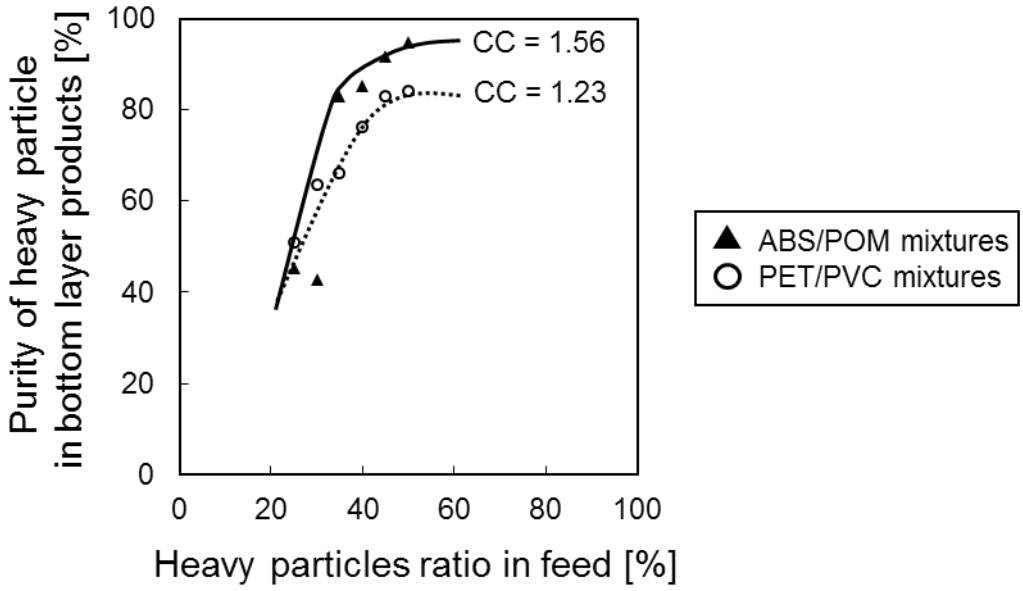

Figure 6-7. Separation curves of ABS/POM (CC of 1.56) and PET/PVC (CC of 1.23)

6.3.3 Effects of wall position on the purity of heavy particles in bottom layer products

If light particles cannot pass through the channel under the restraining wall, almost 100% of purity of heavy particles in bottom layer products can be obtained. In this section, effects of wall position on the purity of heavy particles in bottom layer products were investigated. Position of bottom edge of restraining wall (y) (Figs. 6-1(b) and 6-3) was decided based on the boundary position between light and heavy particles (100% indicates that bottom edge of restraining wall and the boundary position are same and 50% indicates bottom edge of restraining wall places under the boundary position). The distance between a restraining wall and product-end (x) may also affect the purity of bottom layer products. Mehta and Hawley (1969) reported that, porosity of particle layer increases when the length of two walls is lower than the 50 times of D_{50} of the particles (100% indicates that 50 times of D_{50}) and 50% indicates distance between a restraining wall and product-end is narrow rather than 100%) (Fig. 6-1(b)).

Table 6-3 shows the purity of bottom layer products at different wall positions shown in Table 6-2 when the material ratio of PET/PVC mixture was 50:50. The results showed that the restraining wall installation could improve the purity of PVC in bottom layer products. Effects of (x: 50% and 100%) position was negligible (95 and 96%, for run 1 (x: 50%) and run 2 (x: 100%), respectively and 93 and 93%, for run 3 (x: 50%) and run 4 (x: 100%), respectively) while the purity of heavy particles in bottom layer products were higher when the (y: 25% and 50%) position was low (95 and 96%, for run 1 (y: 50%) and run 2 (y: 50%), respectively and 93 and 93%, for run 3 (y: 25%) and run 4 (y: 25%), respectively) indicating narrower channel (y: 25%) caused lower purity even the bottom edge of

restraining wall placed lower than another (*y*: 50%) (Fig. 6-3). Since the narrower channel under the wall caused the higher velocity of particle and water flow so, the light and heavy particles could be mixed due to this higher velocity. These can be suggested that wall position of (*x*) is not important while position of (*y*) is important to obtain high purity. In addition, from the visual observation showed that particle movement along the wall was faster than other areas since the change of water and materials flow so, effects of a restraining wall on the water and materials flow were investigated in next section. Especially, in the batch-type jig experiments with restraining wall without the effects of a screw-type extractor.

Table 6-4 shows the purity of bottom products at different wall positions shown in Table 6-2 when the material ratio of ABS/POM mixture was 50:50. The results showed that the restraining wall installation cannot improved POM purity. This may be caused by the value of CC of ABS/POM mixtures was higher than that of PET/PVC so, the separation of ABS/POM is better with the same mixture ratio (50:50) and this condition already reached the highest purity of heavy particles in bottom layer products limit indicating that CC also affect to this discharge system as described earlier.

Table 6-3. Purity of in top and bottom layer products of continuous-type jig experiments of PET/PVC mixtures (with and without wall).

Run No.	**0**	**1**	**2**	**3**	**4**
Wall position (*x*,*y*)[%, %]	-	**(50, 50)**	**(100, 50)**	**(50, 25)**	**(100, 25)**
Purity of PET in top layer products [%]	86	98	98	98	93
Purity of PVC in bottom layer products [%]	87	96	95	93	93

Note: "–" means without restraining wall.

Table 6-4. Purity of in top and bottom layer products of continuous-type jig experiments of ABS/POM mixtures (with and without wall)).

Run No.	**0**	**1**	**2**	**3**	**4**
Wall position (*x*,*y*)[%, %]	**-**	**(50, 50)**	**(100, 50)**	**(50, 25)**	**(100, 25)**
Purity of ABS in top layer products [%]	97	95	95	99	99
Purity of POM in bottom layer products [%]	95	85	96	98	97

Note: "–" means without restraining wall.

6.3.4 Effects of material ratio in feed on the purity of heavy particles in bottom layer products of continuous-type jig separation with a vertical restrain wall

To investigate the materials ratio on the improvement using a restraining wall especially for ABS/POM, the continuous-type jig test at different materials ratio of ABS/POM with a vertical restraining wall at wall position (*x, y*: 65, 50 mm) were carried out. Fig. 6-8 shows the relation between the ratio of POM in feed and purity of POM in bottom layer products of continuous-type jig test with and without restraining wall. The results showed that when ratio of POM was low, the restraining wall could enhance the purity of bottom products since the ratio of POM in cleaner chamber was increased. However, not only heavy particles (POM) could pass through the small channel below the wall but also light particles (ABS). This phenomenon may occur due to the water and particles flows that was affected by both of a screw-type extractor and a restraining wall. Fig. 6-9 shows the relation between the ratio of POM in the cleaner chamber (C zone) and purity of POM in bottom layer products recovered by a screw-type extractor of continuous-type jig test with restraining wall fitted with the separation curve of ABS/POM in Fig. 6-7 when "cleaner (2-step)" is the ratio of POM in the cleaner chamber (C zone) of the continuous-type jig experiments with a restraining wall and "rougher (1-step)" is the ratio of POM in the feed of the continuous-type jig experiments without restraining wall (horizontal axis) and purity of POM in bottom layer products recovered by a screw-extractor is a vertical axis. These results indicate that the separation curve made from the results of continuous-type jig without restraining wall could also be used to estimate the results of continuous-type jig with restraining wall (cleaning step).

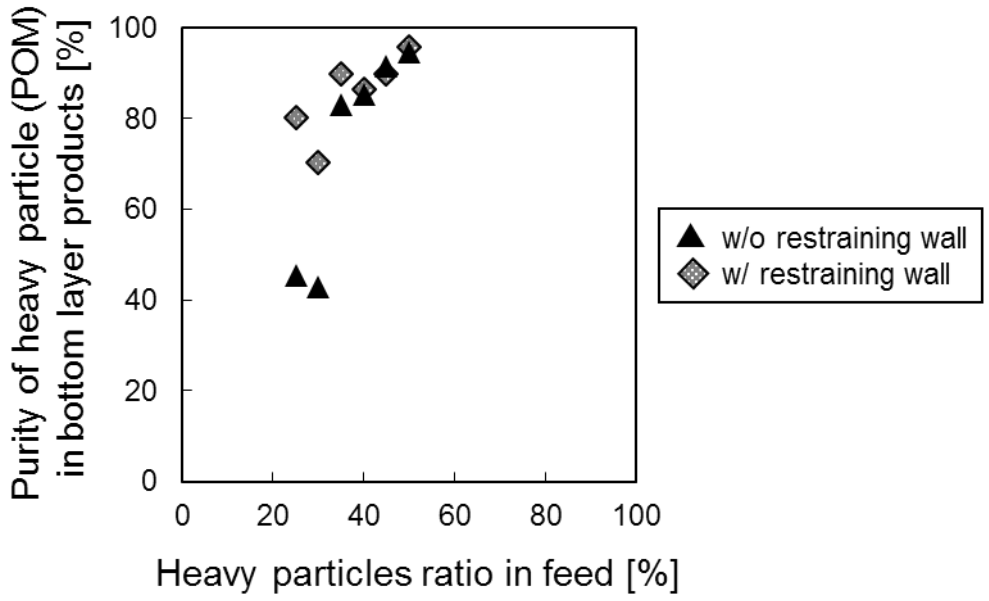

Figure 6-8. Relation between the heavy particle ratio in feed and purity of heavy particles purity of heavy particles in bottom products from continuous-type jig experiments of ABS/POM mixtures with and without restraining wall.

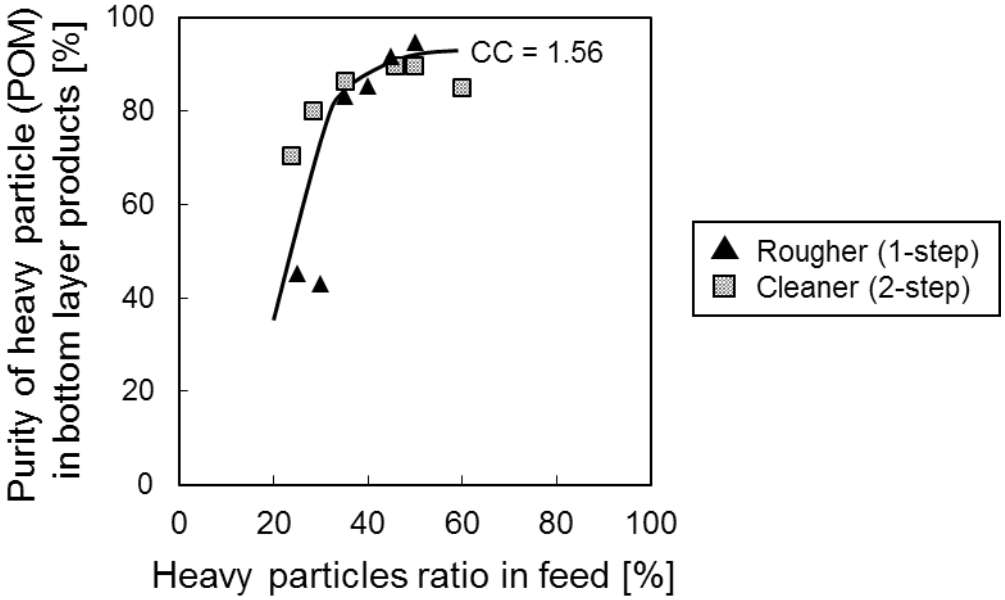

Figure 6-9. Relation between the ratio of POM in the cleaner chamber (C zone) and purity of POM in bottom layer products recovered by a screw-type extractor of continuous-type jig test with restraining wall fitted with the separation curve of ABS/POM (CC of 1.56) in Fig. 6-7.

6.3.5 Effects of a vertical restrain wall on the materials and water flow in continuous-type jig separation

Fig. 6-10(a) showed the flow velocities of particles during the upward flow (Fig. 6-10(a-1)) and downward flow (Fig. 6-10(a-2)) periods of continuous-type jig separation without restraining wall using particle image velocimetry (Flownizer2D). The results showed that the light particles moved downward to a screw-type extractor during the downward flow periods of continuous-type jig separation without restraining wall due to the movement of water and particles flows caused by a screw-type extractor (Fig. 6-10(a-2)).

Fig. 6-10(b) showed the flow velocities of particles during the upward flow (Fig. 6-10(b-1)) and downward flow (Fig. 6-10(b-2)) periods of continuous-type jig separation with restraining wall using particle image velocimetry (Flownizer2D). The results showed that most particle moved to a screw-type extractor was heavy particles since the boundary of light and heavy particles became higher due to the presence of restraining wall. This confirmed that a vertical restraining wall could improve the purity of heavy particles in bottom layer products recovered by a screw-type extractor. However, from the visual observation showed that particle movement along the wall was faster than other areas since the change of water and particles flow. To confirm these phenomena, particle motion along the wall during continuous-type jig separation (with a screw-type extractor) was analyzed using 2D motion analysis software (DIPP-MotionV). The results showed that the light particles that move from the rougher (wider) chamber to the cleaner (narrower) chamber moved upward to the overflow launder (middle layer products) so, the entrainment of light particles in the bottom layer products was prevented and purity of heavy particles in bottom layer products was increased.

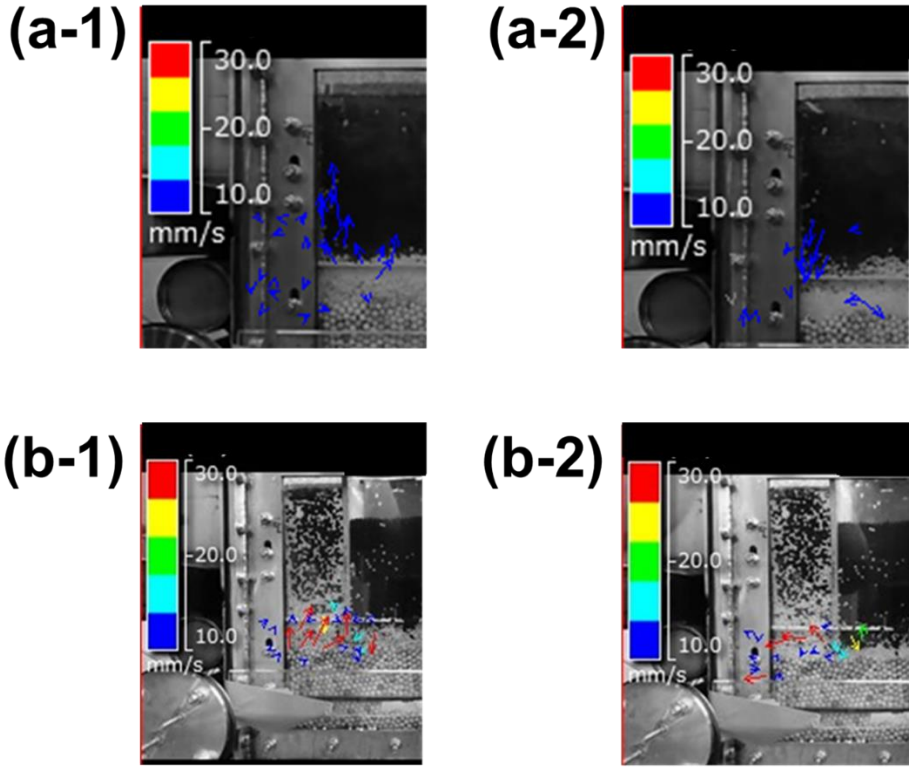

Figure 6-10. Particle flow velocities during continuous-type separations without a vertical restraining wall: (a-1) upward flow period, and (a-2) downward flow period, and with a vertical restraining wall: (b-1) upward flow period, and (b-2) downward flow period.

6.3.6 Effects of a vertical restrain wall on the materials and water flow in batch-type jig separation

To investigate the effects of a restraining wall on water and particles flows without the effects of a screw-type extractor, a vertical restraining wall was installed in the separation chamber of batch-type RETAC jig.

Fig. 6-11 shows the photograph of batch-type jig test of 65:35 *L/H* ratio with a restraining wall, before and after 10 min of separation. The results showed that after the water pulsation was introduced, the particle transferred to the narrower chamber (left) through the small channel below a restraining wall and after separation finished, the top surface position of light particles (ABS) in narrower chamber became higher than wider chamber (right) while the boundary between the light and heavy in both chamber showed same level indicating that light particles moved from the wider chamber to narrower chamber even without the presence of a screw-type extractor indicating that a restraining wall could be affected the water and particles flows.

To investigate the effects of a restraining wall on water and one kind of particle flow, the water pulsation of single-type materials (ABS or POM) were carried out. Fig. 6-12 shows the photograph before (Fig. 6-12(a)) and after (Fig. 6-12(b)) of batch-type jig test of ABS (light) with a restraining

wall. The result showed that after the water pulsation was introduced, the ABS transferred to the narrower chamber through the small channel below a restraining wall so, the top surface position of light particles (ABS) in narrower chamber became higher than wider chamber that same as the results of ABS/PS mixtures, indicating that light particles could move from the wider chamber to narrower chamber even without the presence of a screw-type extractor that same as the results of ABS/POM mixture. However, in the case of heavy particles like POM, the top surface position was not change (Fig. 6-13) that also same as the results on the boundary layer position of ABS/POM mixtures, indicating that SG could affect to these phenomena.

These results could be discussed using the effects of permeability difference of particle layer. According to theory of the permeability of fluid in packed bed, Kozeny-Carman (McCabe et al., 2004.) equation is shown in Eq. 6-1 (this equation is only valid for laminar flow, particle Reynolds numbers up to approximately 1.0).

$$u = \frac{\Psi^2 \varepsilon^3 D^{*2}}{180(1-\varepsilon)^2} \frac{\Delta P}{\mu L} \tag{6-1}$$

where ΔP is the pressure drop [Pa],

L is the total height (top surface position) of particle layer [m],

u is the water velocity [m/s],

μ is the viscosity of the fluid [Pa·s],

ε is the porosity of particle layer [-],

Ψ is the sphericity of the particles [-],

D^* is the equivalent volume diameter of the particles [m]

This equation can be expressed as “flow is proportional to the pressure drop (ΔP) and inversely proportional to the fluid viscosity (μ)”, which is known as Darcy's law (Eq. 6-2)

$$u = \kappa \frac{\Delta P}{\mu L} \tag{6-2}$$

where κ is absolute (i.e., single phase) permeability [mD = millidarcy]

Combining Eqs. 6-1&2 gives the final Kozeny equation for absolute permeability (κ) (Eq. 6-3)

$$\kappa = a \frac{\varepsilon^3 D_{50}^2}{(1-\varepsilon)^2} \tag{6-3}$$

where a is the proportionality and unity factor [mD / mm^2]

The visual observation showed that top surface of water in narrower chambers (L_n) and wider chambers (L_w) were almost same. In this case, velocity of water in wider chamber and narrower chamber were also same, and using Eqs. 6-1 to 6-3, the balance of water velocity (u) can be expressed as (Eq. 6-4):

$$\kappa_n \frac{\Delta P_n}{\mu L_n} = \kappa_w \frac{\Delta P_w}{\mu L_w} \tag{6-4}$$

where κ_n is absolute permeability of narrower chamber [mD]

κ_w is absolute permeability of wider chamber [mD]

ΔP_n is the pressure drop of narrower chamber [Pa],

ΔP_w is the pressure drop of wider chamber [Pa],

L_n is top surface position of particle layer in narrower chamber [m],

L_w is top surface position of particle layer in wider chamber [m]

At first (before the water pulsation was introduce), the top layer position of both chambers is same ($L_n = L_w$), however, the porosity in narrower chamber was larger due to the effects of wall on the packed bed ($\varepsilon_n > \varepsilon_w$) (Mehta and Hawley, 1969). Because of this, κ_n is larger than κ_w, and the pressure loss of wider chamber is higher than that of narrower chamber ($\Delta P_n < \Delta P_w$). With the introduction of water pulsation, the water flow from wider chamber to narrower chamber due to the pressure difference that causes the particle flow to the narrower chamber resulting in the increasing of top surface position ($L_n > L_w$). From these discussions the ratio of top surface position of particle layer in both chambers can be estimated by the absolute permeability (κ) as shown in Eq. 6-5, where absolute permeability (κ) is the function of porosity (ε) (Eq. 6-3).

$$\frac{L_n}{L_w} = \frac{\kappa_w}{\kappa_n} \tag{6-5}$$

These indicates that difference in the porosity of two chambers caused the difference in top surface position of particle layer.

The discussion using permeability difference can be concluded that water flow from wider chamber to narrower chamber resulting in the increase in top surface position of particle layer in narrower chamber. So, if we compare the water rising velocity in the upward motion in both chambers, the water rising velocity in narrower chamber is higher because of the water flow from wider chamber.

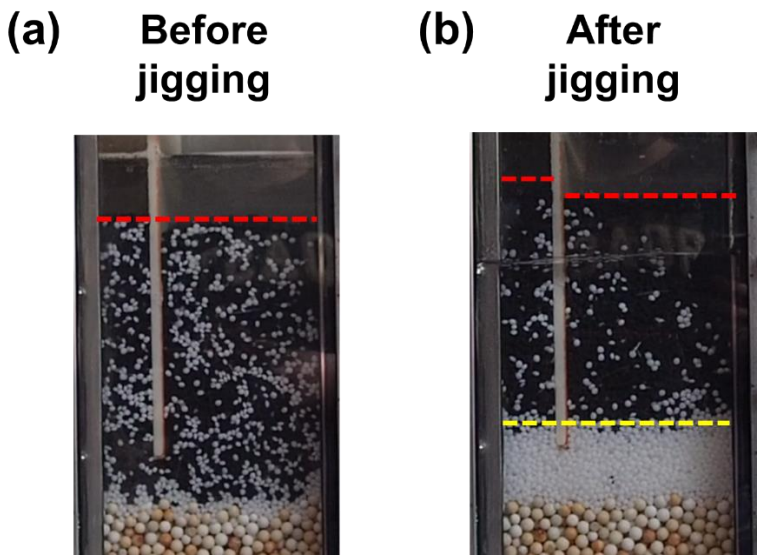

Figure 6-11. Photographs of batch-type jig experiment of ABS/POM at *L/H* ratio of 65:35 with a vertical restraining wall; (a) before and (b) after jigging.

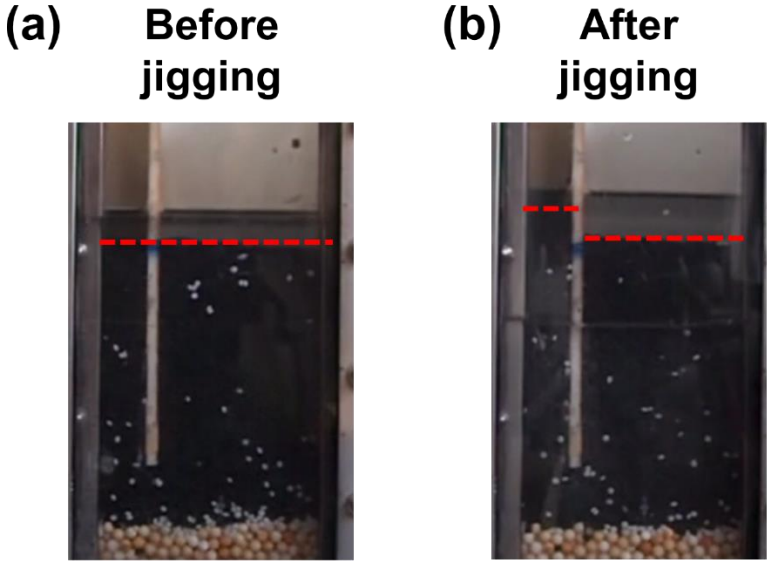

Figure 6-12. Photographs of batch-type jig experiment of ABS with a vertical restraining wall; (a) before and (b) after jigging.

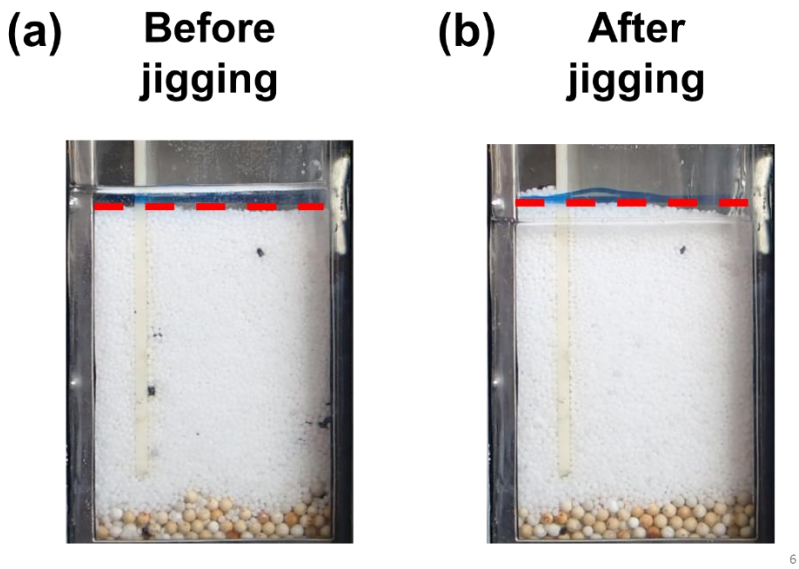

Figure 6-13. Photographs of batch-type jig experiment of POM with a vertical restraining wall; (a) before and (b) after jigging.

6.4 Conclusions

Discharge systems for continuous jig separation of plastics are discussed. The purity of bottom layer products becomes lower when the heavy particles ratio in feed is low, because entrainment of light particles by a screw-type extractor occurs. To suppress the entrainment, a new discharge system using a vertical restraining wall was developed. The restraining wall was installed to separate a chamber into two and particles can transfer from one to another through the channel under the wall. These results showed that the discharge system using a vertical restraining wall proposed in this chapter could improve the purity of heavy particles in bottom layer products due to the increasing of material ratio closed to product-end and the change of water and particles flow.

References

MBE Coal& Minerals Technology GMBH, 2011. BATAC□ & ROM Jig□ jigging technology. http://www.mbe-cmt.com/fileadmin/user_upload/Download_Produktflyer/mbe_Jigging_e_RZ_120305.pdf (accessed 20 June 2018)

McCabe, W., Smith, J., Harriott, P., 2004. Unit Operations of Chemical Engineering, seventh ed. McGraw Hill.

Mehta, D., Hawley, M.C., 1969. Wall Effect in Packed Columns. Ind. Eng. Chem. Proc. Des. Dev. 8, 280–282. https://doi.org/10.1021/i260030a021

Tsunekawa, M., Kobayashi, R., Hori, K., Okada, H., Abe, N., Hiroyoshi, N., Ito, M., 2012. Newly developed discharge device for jig separation of plastics to recover higher grade bottom layer product. Int. J. Miner. Process. 114-117, 27-29. https://doi.org/10.1016/j.minpro.2012.09.003.

CHAPTER 7 – GENERAL CONCLUSION

Recycling is an important trend of our modern society due to a global concern about demand for natural resources and waste generation. Among of the generated wastes, plastic is one of big amount waste rather than traditional materials like glass, metals and wood, especially when compared in volume-based due to their low specific gravity (SG). There are two common types of plastic recycling: (1) material recycling wherein plastics are recovered and reused, and (2) thermal recycling whereby plastics are used as fuel for power generation. Among the two, material recycling is a more sustainable and profitable approach, but different types of plastics must be separated to obtain very high purities. Most separation techniques for recycling were modified from techniques developed for mineral processing. Among of these techniques, jig separation, one of the oldest techniques that separates particles based on density differences, that widely used in mineral processing especially in coal cleaning because of its simplicity, low cost, and high efficiency, was also applied for resources recycling. However, there is a critical challenge in the use of jig separation for secondary resources because of the wide variety of shapes formed after crushing, which is very different from the more uniform and sphere-like particles traditionally treated in mineral processing. In jig separation, the separation efficiency is dependent on particle motion, which is also a function of geometrical properties like size and shape. This means that understanding the effects of particle shape is important in the design of suitable jig separation process. This study investigated the effects of particle shape (disk-like plastics and rod-like metals wires) on the jig separation and identified the reasons why the particles shape affects to their behaviors and jig separation efficiency. Moreover, novel methods to estimate the jig separation efficiency using shape factors were proposed, and modified waveform and shape separation methods to improve jig separation efficiency were developed. Finally, a discharge system for continuous jig separation of plastics using a restraining wall was developed.

Chapter 1 describes the background and objectives of the study.

In Chapter 2, previous studies on “the effects of particle geometry on physical separation” and “the application of gravity separation for coal cleaning and resources recycling” are reviewed.

In Chapter 3, effects of particle geometry (size and shape) on jig separation efficiency of crushed plastics are investigated. Plastic boards with 2-mm and 3-mm thicknesses of acrylonitrile butadiene styrene (ABS, specific gravity (SG) = 1.03) and polystyrene (PS, SG = 1.06) were crushed to obtain a size fraction of +2.0−8.0 mm. The shape factors (flatness ratio etc.) and settling velocity of crushed plastics containing various size and shape were measured. The shape distribution in each size fraction (+2.0−2.8, +2.8−4.0, +4.0−5.6, and +5.6−8.0 mm) showed the strong effects of crushing on particle shape; that is, particles are more disk-like (low flatness ratio) at coarser size fraction while the fine

fraction is dominated by sphere-like (high flatness ratio) particles. Settling velocity of sphere-like PS increased with increasing particle size while those of disk-like ABS had similar values regardless of the size, which were consistent with the results of jig separation of single-type plastics. The results of jig separation of mixed plastics showed that separation efficiency was higher for the mixture of light, disk-like particles and heavy, sphere-like particles that was in line with the results of settling velocity experiments. These results indicate that settling velocity and jig separation are affected by both size and shape.

In Chapter 4, empirical equation to calculate settling velocity of non-spherical particles using flatness ratio and projection area was developed, and a modified concentration criterion (CC_s) is proposed to estimate jig separation efficiency of non-spherical particles. ABS boards 2-mm and 5-mm thick and PS boards 2-mm and 3-mm thick were cut into square prism with same equivalent volume diameter but different flatness ratios. The particles motion under static and water pulsation conditions were recorded using a video camera and analyzed by image analysis. The results showed that disk-like particles (low flatness ratios) settled down slower than sphere-like particles (high flatness ratios). These results were in line with the jig separation results that separation efficiency was higher for the mixture of disk-like light plastic and sphere-like heavy plastic than that for sphere-like light plastic and disk-like heavy plastic mixture. This could be attributed to the differences in settling velocities of disk-like and sphere-like particles. The experimental results showed that sharpness index decreased with increasing CC_s calculated from the velocity of non-spherical particles. This result indicates that CC_s can be used to estimate jig separation efficiency of non-spherical particles. For particle motion during water pulsation (step 1), the results showed that disk-like particles rose faster than sphere-like particles during water rising step, while motion of disk-like particles and sphere-like particles was almost the same in other steps indicating that jig separation efficiency may be affected by particles motion of step 1. Using these results, modification of water pulsation to reduce the effects of particle shape on jig separation was proposed.

In Chapter 5, improvement of jig efficiency by shape separation, and a novel method to estimate the separation efficiency of metal wires in crushed electronic wastes using bending behavior and "entanglement factor" were proposed. Jig separation was applied to separate plastics and metals including copper (Cu) wires obtained from a recycling plant. The results showed that separation efficiency was low because of Cu wire entanglement that prevents particle motion in the separation chamber. The results of model experiments showed that the separation efficiency decreased with increasing the amount and length of Cu wires (high entanglement factor). To limit the effects of wire entanglement, two methods of shape separation were investigated. These shape separation techniques increased the recovery of Cu wires in the Cu concentrate from 64% (without shape separation) to 97% (with shape separation using probability of passage) and 95% (with shape separation using induced entanglement). In addition, estimation of jig separation efficiency using the entanglement factor of

rod-like particles is proposed.

In Chapter 6, development of discharge systems for bottom layer products are proposed. Batch and continuous jig results were compared using plastic mixtures with various mixing ratios. The purities of bottom products of continuous jig were lower than that of batch jig and when the heavy material ratio was low, the purity of bottom product was lower than that of higher ratios, because entrainment of light particles by a screw-extractor occurs. To suppress the entrainment, a new discharge system using a vertical restraining wall was developed. The restraining wall was installed to separate a chamber into two and particles can transfer from one to another through the channel under the wall. The results showed that purity of bottom layer products was improved with a restraining wall.

Finally, Chapter 7 gives the general conclusions of this study.

ACKNOWLEDGMENT

Foremost, I would like to acknowledge to my supervisor, Assoc. Prof. Mayumi Ito, for her kindness and all the support since I was an internship student during my bachelor's program, when I was an exchange student during my master's program, and now during my doctoral program. She gave me a lot of constructive advice to succeed in my research. She also guided me to walk through the path of a professor. I will never forget your enthusiasm to do your best to inspire not only me but also all the students. I feel really happy to work under your guidance.

Beside this, I would like to express my gratitude to Prof. Naoki Hiroyoshi, for the recommendation of this study. Your valuable advice and critical comments for the improvements of my research are gratefully appreciated.

My sincere thanks are extended to Asst. Prof. Carlito Baltazar Tabelin, for his kind suggestion on the paper writing as well as daily life in Japan. Thank you very much for your time and effort.

Special appreciation goes to Prof. Toshifumi Igarashi and Assoc. Prof. Yasumasa Tojo, who served as examiners of my dissertation. Thanks to their efforts and advice, this dissertation could have improved considerably.

It is difficult to overstate my appreciation to Assoc. Prof. Pinyo Meechumna, Assoc. Prof. Quanchai Leepowpanth, Assoc. Prof. Dawan Wiwattanadate, and Assoc. Prof. Somsak Saisinchai from Department of Mining and Petroleum Engineering, Faculty of Engineering, Chulalongkorn University, Thailand, for teaching me the knowledge background on Mineral Processing and Resources Recycling during my bachelor's and master's programs.

Special thanks are extended to Ms. Arisa Azuma, Mr. Daiki Kitayama, Ms. Shoko Kimura, and other members in the Plastics Research Group, for assistance on this research. I would like to say thank you for putting your trust in me and for always helping me in academic and university matters.

Many thanks are extended to all members in Laboratory of Mineral Processing and Resources Engineering, Graduate School of Engineering, Hokkaido University, Japan, and Department of Mining and Petroleum Engineering, Faculty of Engineering, Chulalongkorn University, Thailand, whose friendship and support are beyond a place of study.

I am deeply grateful to the JICA: AUN/Seed-Net for giving me the scholarship for study in Japan. I am indebted to Eriez Magnetic, Japan, for your valuable advice.

Finally, I am forever grateful my parent and my family who have always supported and encouraged me to do my best in all matters of life.